# Understanding the Interactions Between Maternal PBDE Exposure and the Functional Gut Microbiome in Developing Mouse Offspring

Sarah Kim

A dissertation

submitted in partial fulfillment of the

requirements for the degree of

Doctor of Philosophy

University of Washington

2025

Reading Committee:

Julia Cui, Chair

Judit Marsillach

Yijie Geng

Program Authorized to Offer Degree:

Environmental and Occupational Health Sciences

University of Washington

**Abstract**

# Understanding the Interactions Between Maternal PBDE Exposure and the Functional Gut Microbiome in Developing Mouse Offspring

Sarah Kim

Chair of the Supervisory Committee:

Julia Cui

Environmental and Occupational Health Sciences

Persistent organic pollutants (POPs), such as polybrominated diphenyl ethers (PBDEs), are ubiquitously detected in the environment despite being banned from commercial and industrial use. Due to their lipophilic nature, PBDEs bioaccumulate in the human environment, including food (e.g. milk, meat, seafood), soil, and water. In humans, such exposures have been linked to inflammation and metabolic disorders. The liver is a vital organ responsible for xenobiotic metabolism and nutrient homeostasis. It functions as a central hub for digestive and systemic regulation, playing crucial roles in the metabolism of carbohydrates, amino acids, nucleotides, fatty acids, cholesterol, hormones, and especially, xenobiotics including drugs and toxicants present in our environment such as PBDEs. In close interactions with the liver, the gut microbiome can influence the host's xenobiotic biotransformation capacity. Disruption of the microbial ecosystem–gut dysbiosis–is now recognized as a critical factor influencing disease susceptibility by modulating host metabolism, immunity, and response to environmental exposures. However,

very little is known regarding how maternal exposure to PBDEs modulate the metabolic signatures involved in obesity/diabetes and inflammation later in life, and how microbial metabolites, such as indole-3-propionic acid (IPA) could modify the effect of PBDEs during the interplay between endogenous versus toxicological pregnane X receptor (PXR) activation, an important nuclear receptor for xenobiotic biotransformation. Therefore the goal of my dissertation is to investigate how developmental PBDE exposure disrupts the gut microbiome and microbial metabolism of tryptophan (Aim 1), as well as to investigate whether microbial indole metabolites and indole derivatives reduce inflammation and improve diabetic- or inflammation-related phenotype following developmental PBDE exposure (Aim 2), and lastly to determine whether targeting gut microbiome mechanistically contributes to developmental PBDE exposure-mediated disruption of PXR signaling and delayed onset of obesity and inflammation (Aim 3). I hypothesized that maternal PBDE exposure induces acute and persistent gut dysbiosis, disrupting the interplay between endogenous PXR activation (by indoles) and xenobiotic PXR activation (by PBDEs), ultimately contributing to the delayed onset of obesity and inflammation. To achieve Aim 1, breeders of conventional (CV) humanized PXR-transgenic (hPXR-TG) mice were exposed to vehicle, 0.1 mg/kg/day DE-71 via diet, DE-71+IPA (20 mg/kg/day via drinking water), or IPA from 4 weeks preconception until end of lactation, whereas weaned pups were fed standard chow with no DE-71 with or without IPA supplementation via drinking water. Organs were collected at postnatal day (PND) 21, 3 months, and 6 months of age. Targeted and untargeted metabolomic responses were analyzed with metagenomic shotgun sequencing to identify differentially abundant bacterial taxa and predict microbial functional changes associated with PBDE exposure. For Aim 2, serum immunoassays, cytokine and chemokine levels in the intestine and liver, and liver histopathological analysis were assessed in PND21, 3 months, and 6 months of age. Overall, the

maternal DE-71 exposure on the gut microbiome of pups were amplified over time. The regulation of hepatic cytokines and prototypical xenobiotic-sensing transcription factor target genes by DE-71 and IPA was age- and sex-dependent, where DE-71-induced mRNA increased selected cytokines (*Il10*, *Il12p40*, *Il1β* [both sexes]). The hepatic mRNA of the aryl hydrocarbon receptor (AhR) target gene *Cyp1a2* was increased by maternal DE-71 and DE-71+IPA exposure at PND 21 but intestinal *Cyp1a1* was not altered by any of the exposures and ages. In addition, maternal DE-71 exposure increased serum indole, a known AhR ligand, in age- and sex-dependent manner. To achieve Aim 3, 3 months- and 6 months-old germ-free (GF) hPXR-TG mice were used for fecal microbiota transplantation (FMT) using fecal donors from CV control and DE-71-exposed mice were utilized. To investigate whether gut microbiome perturbations contribute to PBDE-mediated disruption of PXR signaling and delayed-onset inflammation, analysis of inflammatory signaling in metabolic organs, xenobiotic-sensing transcription factor-target gene expression, RNA sequencing, metagenomic shotgun sequencing, and targeted and untargeted metabolomics were assessed across multiple tissues. Overall, the microbiome from DE-71 exposed donors produced more pronounced changes in the hepatic transcriptomes of the female recipients than males, with enriched pathways linked to sterol and cholesterol metabolism and stress-activated protein kinase signaling cascades. Interestingly, exposed GF male recipients exhibited enrichment of pathways related to xenobiotic metabolism and fatty acid metabolic processes. In the large intestinal tissues, transcripts of tight junction genes *Tjp1* and *Tjp2* were consistently downregulated, indicative of compromised intestinal barrier integrity, or "leaky gut," likely driven by DE-71-induced gut microbiome dysbiosis. Furthermore, hepatic inflammatory markers were more pronounced in female recipients compared to males, suggesting sex-specific susceptibility to inflammation following microbial transfer. In conclusion, my findings demonstrate that

maternal PBDE exposure induces a proinflammatory signature along the gut-liver axis, characterized by gut dysbiosis, disrupted tryptophan metabolism, and attenuated PXR signaling in postweaned hPXR-TG offspring over time. Notably, these effects were partially mitigated by IPA supplementation, highlighting the potential of microbiome-derived metabolites in counteracting environmentally-induced metabolic dysfunction.

**List of Abbreviations**

| | |
|---|---|
| ACN | acetonitrile |
| AhR | aryl hydrocarbon receptor |
| ANOVA | analysis of variance |
| BAs | bile acids |
| BDE | brominated diphenyl ether |
| CAR | constitutive androstane receptor |
| cDNA | complementary DNA |
| CV | conventional |
| Cyps | cytochrome P450s |
| DE-71 | industrial PBDE mixture |
| DOHaD | Developmental Origins Of Health and Disease |
| EI | electron ionization |
| ESI | electrospray ionization |
| EPA | Environmental Protection Agency |
| FMT | fecal microbiota transplant |
| FXR | farnesoid x receptor |
| Gapdh | glyceraldehyde 3-phosphate dehydrogenase |
| GC-MS | gas chromatography-mass spectrometry |
| GF | germ-free |
| GO | gene ontology |
| H&E | hematoxylin and eosin |
| HFD | high-fat diet |
| hPXR-TG | humanized pregnane X receptor transgenic |
| IACUC | Institutional Animal Care and Use Committee |
| IFNγ | interferon gamma |
| IPA | indole-3-propionic acid |
| KEGG | Kyoto Encyclopedia of Genes and Genomes |
| LC-MS/MS | liquid chromatography-tandem mass spectrometry |
| LIC | large intestinal contents |
| LXR | liver X receptor |
| MFA | metabolic flux analysis |
| MCP1 | monocyte chemoattractant protein-1 |
| MRM | multiple-reaction monitoring |
| mRNA | messenger RNA |
| NF-κB | nuclear factor kappa-light-chain-enhancer of activated B cells |
| Nrf2 | nuclear factor erythroid 2-related factor 2 |
| OTUs | operational taxonomic units |
| PBDEs | polybrominated diphenyl ethers |
| PCN | pregnenolone 16α-carbonitrile |
| PCA | principal component analysis |
| PND | postnatal day |
| POPs | persistent organic pollutants |
| Pparα | peroxisome proliferator activated receptor alpha |
| PXR | pregnane X receptor |

| | |
|---|---|
| qPCR | quantitative polymerase chain reaction |
| RT-qPCR | reverse transcription quantitative PCR |
| SCFAs | short chain fatty acids |
| SPSS | Statistical Package for the Social Sciences |
| SULT | sulfotransferase |
| TCA cycle | tricarboxylic acid cycle |
| Tjp1, Tjp2 | tight junction proteins 1 and 2 |
| TNFα | tumor necrosis factor alpha |
| UGT | UDP-glucuronosyltransferase |
| UPLC | ultra performance liquid chromatography |
| WT | wild type |

**Acknowledgments**

First and foremost, I would like to express my deepest gratitude to my mentor, Dr. Julia Cui, for her unwavering support and guidance throughout my Ph.D. journey. Her encouragement has been instrumental in shaping my growth as a researcher and as a female scientist. She has been more than just a mentor—she has been my science mom, friend, and role model. During the most challenging moments of my Ph.D., she stood by me, offering support and never losing faith in me.

I also sincerely thank Drs. Judit Marsillach, Yijie Geng, Haiwei Gu, and Libin Xu for serving on my Doctoral Advisory Committee and for their invaluable feedback. Their insights and expertise have greatly enriched my work. A special thank you to Drs. Julia Cui, Judit Marsillach, and Yijie Geng for serving on my Reading Committee, and to Dr. Libin Xu for serving as my Graduate School Representative.

I am deeply appreciative of my current and past lab members for their support, friendship, and assistance in my research. This work would not have been possible without your collaboration, encouragement, and willingness to help. A heartfelt thank you to Dr. Moumita Dutta and Jasmine Armad for their contributions and support.

I am also grateful to my collaborators who have provided their expertise in different aspects of this work. Thank you to Dr. Haiwei Gu for his contributions to metabolomics, Dr. Sridhar Mani for academic research support and guidance, Dr. Maxwell Gyamfi for his work on liver inflammation, the University of Washington Gnotobiotic Core staff, and the University of Washington IT support team.

To my family, I am beyond thankful. My parents have selflessly supported me for 29 years, and their unwavering encouragement has been my foundation. To my little sister, your creativity, board game nights, and endless support have been a source of joy and motivation. To my family in Canada, your constant encouragement helped me push forward in my research. I want to express my gratitude to my fiancé, who has stood by my side, offering inspiration, love, and support throughout this final phase of my Ph.D. I also thank God for His guidance and for making this journey possible—I would not have been able to accomplish this without Him.

Finally, I want to acknowledge the funding and financial support from the National Institutes of Health (R01 ES025708, R01 ES030197, R01 ES031098), University of Washington (UW) Center for Exposures, Diseases, Genomics, and Environment (NIH P30 ES0007033), UW DEOHS Environmental Pathology/Toxicology Training Program (T32ES007032), UW Sheldon D. Murphy Endowment, and UW DEOHS Environmental Health and Microbiome Research Center (EHMBRACE).

## Table of Contents

# CHAPTER 1. Introduction

## Persistent organic pollutants: polybrominated diphenyl ethers (PBDEs)

Environmental chemicals such as persistent organic pollutants (POPs) are widespread in the environment and are known to exert endocrine-disrupting effects, contributing to a range of adverse health outcomes including metabolic disorders, reproductive and developmental toxicity, and immune dysfunction (Chiu et al. 2021). Among these, polybrominated diphenyl ethers (PBDEs) are a class of flame retardants previously used in plastics, furniture, electronics, and other household products (Vojta et al. 2016; J. Xu et al. 2019; Xue et al. 2023). Due to their lipophilic nature, PBDEs persist in the environment and bioaccumulate in the food chain, commonly detected in meat, seafood, dairy products, human breast milk, and household dust (Babalola and Adeyi 2018; Cade, Kuo, and Schultz 2018; Pietron et al. 2019; Xue et al. 2023). Developmental exposure to PBDEs has been linked to an increased risk of diabetes in both humans and rodent models (Zhang et al. 2016). DE-71, a human health-relevant industrial PBDE mixture with BDE-47 and BDE-99 as its major congeners, is commonly used to study the toxicological effects of PBDEs. In a previous study, maternal exposure to DE-71 resulted in diabetic-like phenotype and disrupted the regulation of glucose homeostasis and hepatic lipid metabolism in adult female mouse offspring (Kozlova et al. 2020). Additionally, neonatal oral exposure to BDE-99 led to the emergence of cancer-prone hepatic transcriptomic signatures at 60 days old young adulthood pups (Lim et al. 2021). However, little is known about how maternal PBDE exposure modulates metabolic signatures associated with inflammation and metabolic disorders later in life. Therefore, the goal of the present study was to test the hypothesis that maternal PBDE exposure leads to persistent dysregulation of metabolic pathways linked to obesity, diabetes, and inflammation.

## Gut microbiome

The gut microbiome, comprising an estimated over 3 million unique genes, exhibits considerable variability influenced by host genetics, diet, xenobiotic exposure, and anatomical location. It plays a critical role in xenobiotic biotransformation, nutrient acquisition, energy harvest, and the regulation of host metabolic pathways–all of which are intricately linked to pathogenesis of metabolic syndrome (Koppel, Maini Rekdal, and Balskus 2017; Spanogiannopoulos et al. 2016; S. F. Clarke et al. 2012). Disruption of the gut microbiome through dietary changes or environmental toxicant exposure can impair physiological and metabolic homeostasis, potentially leading to the development of metabolic diseases later in life (Bassols et al. 2016; Kalliomäki et al. 2008; Martinez and Guerra 2018). For instance, acute exposure to BDE-47 and BDE-99 has been shown to induce gut dysbiosis, including enrichment of obesity-associated microbes in male mice (Scoville et al. 2019). Similarly, neonatal oral exposure to BDE-99 resulted in persistent alterations to the gut microbiome detectable in young adult male offspring (Lim et al. 2021). Collectively, these findings support the concept that gut microbiome alterations may serve as novel biomarkers of metabolic toxicity following developmental PBDE exposure.

**Xenobiotic-sensing nuclear receptor: pregnane X receptor (PXR)**

Pregnane X receptor (PXR) is a xenobiotic-sensing nuclear receptor that regulates the inducible expression of genes involved in xenobiotic metabolism, including biotransformation enzymes and drug transporters. Through this regulation, PXR enhances drug metabolism, reduces inflammation, and plays a critical role in lipid, glucose, and energy homeostasis (Kliewer, Goodwin, and Willson 2002; Xie and Chiang 2013). Notably, PXR gene polymorphisms have been linked to disease severity in metabolic syndrome (Sookoian et al. 2010). Upon ligand activation, PXR induces a broad spectrum of drug-metabolizing enzymes and efflux transporters

as a compensatory mechanism for xenobiotic detoxification (Aleksunes and Klaassen 2012; Kliewer, Goodwin, and Willson 2002; Xie and Chiang 2013). Indole-3-propionic acid (IPA), a gut microbiota-derived tryptophan metabolite, is a well-characterized endogenous ligand for PXR. IPA has been shown to protect intestinal barrier function and attenuate inflammation in a PXR-dependent manner (Venkatesh et al. 2014a; Wikoff et al. 2009). Moreover, IPA is increasingly recognized as a protective biomarker associated with lower risk of obesity, type 2 diabetes (T2D), and systemic inflammation (Chen et al. 2022; Tuomainen et al. 2018; B. Zhang et al. 2022). Importantly, neonatal activation of PXR not only increases the expression of PXR target genes but also suppresses PPARα target gene expression, suggesting potential cross-talk between these pathways (Giebel et al. 2016). In addition, age-dependent epigenetic regulation at the Cyp3a locus has been observed in mice, where PXR activation enhances permissive histone methylation, promoting gene transcription. Similar epigenetic remodeling has been reported in human liver cells, further supporting Cyp3a transcriptional activation following PXR stimulation (Yan et al. 2017). Taken together, combining microbial and metabolomic data in the context of toxic exposures can enhance our understanding of the mechanistic pathways underlying toxicity and dysbiosis-associated diseases.

**Dissertation Outline**

The overall goal of this dissertation is to elucidate the maternal impact of environmental contaminant exposure, specifically PBDEs, on the gut-liver axis and to characterize persistent metabolic and inflammatory responses triggered by these toxicants. By understanding these mechanisms, this research aims to identify novel therapeutic strategies to prevent or mitigate disease in vulnerable populations, including underserved communities. The objective of this research is to utilize a multi-omics approach to investigate gut microbiome-mediated and age-dependent mechanisms underlying metabolic disorders, such as obesity, diabetes, and inflammation arising from maternal PBDE exposure. Additionally, this work explores how indole-3-propionic acid (IPA) modulates PBDE-induced effects by influencing the balance between endogenous and toxicological PXR activation. My central hypothesis is that early-life PBDE exposure induces acute and persistent gut dysbiosis, disrupting the interplay between endogenous PXR activation (by indoles) and xenobiotic PXR activation (by PBDEs), ultimately contributing to the delayed onset of obesity and inflammation.

**Chapter 1.** Introduction

**Chapter 2**. Polybrominated diphenyl ethers (PBDEs) are previously used flame retardants that persist in the environment due to their lipophilic nature and have been implicated in metabolic disorders. The gut microbiome is increasingly recognized as a key regulator of disease susceptibility and metabolic health. However, the mechanisms by which maternal PBDE exposure modulates metabolic signatures linked to obesity, diabetes, and inflammation later in life remain poorly understood. In this chapter, to investigate the basal role of the gut microbiome in PBDE-

induced alterations in serum and liver gene expression and metabolism over time, I analyzed liver and serum targeted and untargeted metabolomic responses in conventional (CV) mice exposed to PBDEs at three time points: Day 21, 3 months, and 6 months. Additionally, I conducted metagenomic shotgun sequencing to identify differentially abundant bacterial taxa and predict microbial functional changes associated with PBDE exposure, providing insights into microbiome-mediated metabolic regulation.

**Chapter 3.** Indole-3-propionic acid (IPA) is a microbial tryptophan metabolite and a known pregnane X receptor (PXR) ligand that plays a crucial role in protecting mucosal barrier function and reducing inflammation in a PXR-dependent manner. Additionally, IPA has been identified as a protective biomarker against obesity, type 2 diabetes, and inflammation. However, the mechanisms by which IPA modulates PBDE-induced effects remain poorly understood. In this chapter, to determine whether microbial indole metabolites and derivatives mitigate inflammation following developmental PBDE exposure, I performed serum immunoassays, quantified cytokine and chemokine levels in the intestine and liver, and conducted liver histopathological analysis to assess inflammatory responses and tissue alterations.

**Chapter 4.** Metabolic flux analysis (MFA) is a robust quantitative technique used to measure the rates of metabolic reactions within cells via *in vitro*. This approach yields valuable insights into cellular metabolism, revealing essential regulatory control points and rate-limiting steps. However, there is lack of physiological complexity, especially the absence of multi-organ interactions that critically influence systemic metabolic flux when doing *in vitro*. Therefore, in this chapter, I applied MFA in an *in vivo* system to trace metabolites across multiple bio-compartments using

$^{13}C_{11}$-L-tryptophan in CV and germ-free (GF) mice. This approach was designed to investigate tissue-specific metabolic responses associated with gut microbiome-dependent tryptophan metabolism. To evaluate these effects, I conducted both targeted and untargeted metabolomics analyses across various tissues to assess differential metabolic outcomes.

**Chapter 5.** Targeting gut microbiota and their metabolites has emerged as a critical strategy for regulating host metabolism. Alterations in the gut microbiome have been linked to inflammatory diseases, including metabolic disorders. However, the mechanistic role of the gut microbiome in mediating developmental PBDE-induced metabolic disruptions remains unclear. In this chapter, I utilized GF mice for fecal microbiota transplantation (FMT) using fecal donors from CV control and DE-71-exposed mice to determine whether gut microbiome perturbations contribute to PBDE-mediated disruption of PXR signaling and delayed-onset inflammation. To assess these effects, I conducted inflammatory signaling analysis in metabolic organs, xenobiotic-sensing transcription factor-target gene expression, RNA sequencing, and targeted and untargeted metabolomics across multiple tissues. Additionally, I performed metagenomic shotgun sequencing to identify differentially abundant bacterial taxa, comparing these profiles with those of CV mice to better understand the microbiome's role in PBDE-induced metabolic dysregulation.

**Chapter 6.** Conclusion and future work

**Specific Aims and Hypotheses**

**Chapter 2.**

**Specific Aim:** To determine that developmental PBDE exposure disrupts the gut microbiome and microbial metabolism of tryptophan.

**Hypothesis:** PBDE exposure will disrupt the gut microbiome and microbial indole metabolites of tryptophan, such as IPA, will decrease in PBDE-exposed mice at certain developmental stages, whereas indole-supplement diet will increase the indole levels in PBDE-exposed mice.

**Chapter 3.**

**Specific Aim:** To determine whether microbial indole metabolites and indole derivatives reduce inflammation and improve diabetic- or inflammation-related phenotype following developmental PBDE exposure.

**Hypothesis:** PBDE-exposed hPXR-TG mice will have more pro-inflammatory and diabetic status when compared to vehicle-treated mice and indole supplementation will at least partially protect against PBDE-mediated inflammation and diabetic phenotype.

**Chapter 4.**

**Specific Aim:** To investigate the role of tryptophan metabolism within multiple bio-compartments using metabolic flux analysis (MFA) into the *in vivo* system using $^{13}C_{11}$-L-tryptophan.

**Hypothesis:** Gut microbiome's presence or absence will uniquely influence how tryptophan-derived carbons are incorporated into host metabolic pathways, with effects

varying across various tissues in a tissue-specific manner.

**Chapter 5.**

**Specific Aim:** To determine that targeting the gut microbiome mechanistically contributes to developmental PBDE exposure to delayed onset of obesity and inflammation.

**Hypothesis:** GF mice with fecal microbiome transplant and without developmental PBDE exposure will develop a certain degree of inflammation and obesity-related genotype in adulthood.

**Chapter 2 & Chapter 3**

**Maternal PBDE exposure disrupts gut microbiome and promotes hepatic proinflammatory signaling in humanized PXR-transgenic mouse offspring over time**

*These chapters were published in Toxicological Sciences on 6/2023.*

**Kim S**, Li H, Jin Y, Gu H, Mani S, Cui JY. Maternal PBDE exposure disrupts gut microbiome and promotes hepatic pro-inflammatory signaling in humanized PXR-transgenic mouse offspring over time. *Toxicol Sci*. 2023 Jun 2. doi:10.1093/toxic/kfad056. **PMID: 37267213**

**ABSTRACT**

Developmental exposure to polybrominated diphenyl ethers (PBDEs), a persistent environmental pollutant, has been linked to increased diabetes prevalence. The microbial tryptophan metabolite, indole-3-propionic acid (IPA), is associated with lower inflammation, reduced type 2 diabetes risk, and pregnane X receptor (PXR) activation. To investigate IPA's role in modifying PBDE developmental toxicity, we exposed humanized PXR-transgenic (hPXR-TG) mouse dams to vehicle, DE-71 (0.1 mg/kg/day, an industrial PBDE mixture), DE-71+IPA (20 mg/kg/day), or IPA alone from four weeks preconception through lactation. Pups were weaned at postnatal day 21, with IPA supplementation continuing in designated groups. Tissues were collected at multiple time points up to six months (n=5 per group). Maternal DE-71 exposure persistently altered gut microbiome composition, with effects amplifying over time. Hepatic cytokine expression and xenobiotic-sensing transcription factor target gene regulation were age- and sex-dependent, with DE-71 exposure increasing *Il10*, *Il12p40*, and *Il1β* mRNA (both sexes), and additional cytokines in males. Aryl hydrocarbon receptor (AhR) signaling was activated by DE-71 exposure, as indicated by increased hepatic *Cyp1a2* expression at postnatal day 21, though intestinal *Cyp1a1* expression remained unchanged. Serum indole levels, a known AhR ligand, were elevated in an age- and sex-dependent manner following maternal DE-71 exposure. In conclusion, maternal DE-71 exposure induced a pro-inflammatory signature along the gut-liver axis, characterized by gut dysbiosis, disrupted microbial tryptophan metabolism, attenuated PXR signaling, and elevated AhR activation in hPXR-TG pups post-weaning. Notably, IPA supplementation partially mitigated these effects, suggesting a potential microbiome-targeted intervention for PBDE-induced metabolic dysfunction.

## INTRODUCTION

Polybrominated diphenyl ethers (PBDEs), previously used as flame retardants, persist in the environment due to their lipophilic nature, leading to continued detection in breast milk, blood, and fatty foods. Developmental PBDE exposure is linked to increased diabetes prevalence in humans and animal models (Zhang et al. 2016). DE-71, a human health-relevant PBDE mixture, contains BDE-47 and BDE-99 as dominant congeners. Maternal DE-71 exposure disrupts glucose homeostasis, alters hepatic lipid metabolism, and induces a diabetic phenotype in female adult offspring (Kozlova et al. 2020). Additionally, our previous study demonstrated that neonatal oral BDE-99 exposure led to cancer-prone hepatic transcriptomic signatures in young adult mice (Lim et al. 2021).

The gut microbiome plays a pivotal role in host xenobiotic metabolism (Koppel, Maini Rekdal, and Balskus 2017; Spanogiannopoulos et al. 2016), as well as in obesity and diabetes (S. F. Clarke et al. 2012; Drissi et al. 2014). Early-life gut dysbiosis has been linked to the onset of immune and metabolic disorders (Bassols et al. 2016; Kalliomäki et al. 2008; Martinez and Guerra 2018). In response to environmental insults, increased bacterial swarming activity and associated enzyme production serve as biomarkers of intestinal stress in mice and humans (De et al. 2021). Our previous work showed that acute BDE-47 and BDE-99 exposure induced gut dysbiosis, including obesity-associated microbes in male mice (Scoville et al. 2019), while neonatal oral BDE-99 exposure led to persistent gut microbiome disruption in young adult males (Lim et al. 2021). These findings support the concept that altered gut microbiome composition serves as a biomarker of metabolic toxicity following developmental PBDE exposure.

The pregnane X receptor (PXR) is a xenobiotic-sensing nuclear receptor essential for xenobiotic metabolism and an energy receptor essential for xenobiotic metabolism and energy

regulation (Kliewer, Goodwin, and Willson 2002; Xie and Chiang 2013). The aryl hydrocarbon receptor (AhR), a ligand-dependent transcription factor, regulates the xenobiotic response (Flaveny, Murray, and Perdew 2010). Serum AhR ligand activity has been linked to insulin resistance and type 2 diabetes (T2D) in humans (Roh et al. 2015). Upon ligand activation, PXR and AhR regulate drug-metabolizing enzymes and efflux transporters, facilitating xenobiotic detoxification (Aleksunes and Klaassen 2012; Kliewer, Goodwin, and Willson 2002; Xie and Chiang 2013). However, PXR-AhR crosstalk is complex, as AhR activation can suppress PXR-mediated gene expression, and vice versa, which may influence ligand specificity and activity.

The role of PXR in metabolic syndrome is species- and context-dependent. In terms of species differences, humanized PXR transgenic (hPXR-TG) mice exhibit resistance to high-fat diet (HFD)-induced weight gain but display impaired glucose and insulin signaling (Spruiell et al. 2014). Conversely, PXR-null mice are protected from HFD-induced hepatic steatosis and inflammation, with an associated attenuation of the HFD-induced Firmicutes/Bacteroidetes ratio shift (a hallmark of obesity) and reduction in proinflammatory microbes (Kim et al. 2021). Given these, hPXR-TG mice provide a relevant model for studying the role of human PXR in metabolic syndrome and diabetes risk. Regarding context specificity, pharmacological PXR activation exerts anti-inflammatory effects in inflammatory bowel disease (Cheng, Shah, and Gonzalez 2012). However, pathophysiological PXR activation by HFD promotes hepatic inflammation and induces an obese- and proinflammatory gut microbiome profile (Kim et al. 2021). The endogenous PXR ligand, indole-3-propionic acid (IPA), a microbial metabolite of tryptophan, is known to protect the intestinal barrier and reduce inflammation via PXR activation (Venkatesh et al. 2014a; Wikoff et al. 2009). Additionally, IPA is a protective biomarker against obesity, T2D, and inflammation (Chen et al. 2022; Tuomainen et al. 2018; B. Zhang et al. 2022).

Our previous study demonstrated that acute exposure to BDE-47 and BDE-99, known PXR activators in mouse liver (Pacyniak et al. 2007), led to reduced serum IPA levels in male mice (Scoville et al. 2019). However, how maternal PBDE exposure influences metabolic signatures linked to obesity, diabetes, and inflammation in the offspring later in life remains unclear, as does the role of IPA in modulating PBDE-induced effects through endogenous versus toxicological PXR activation. Therefore, the goal of our study is to delineate this potential relationship and we hypothesize that maternal PBDE exposure induces persistent gut dysbiosis, including altered microbial tryptophan metabolism, leading to disrupted PXR signaling and increased biomarkers of obesity, diabetes, and inflammation. Furthermore, we propose that IPA supplementation will partially mitigate these effects, protecting against DE-71-induced metabolic dysfunction.

## MATERIALS AND METHODS

### Chemical preparation

Individual components of the PBDE commercial mixture (DE-71) were purchased from AccuStandard, Inc. (New Haven, Connecticut) and prepared according to the ratio of each component (Konstantinov et al. 2008). Briefly, DE-71 mixture was prepared in corn oil (1 mg DE-71/g corn oil). The mixture was then evaporated with a vacuum overnight and then dissolved DE-71 mixture was used in the study upon successful congener-specific analysis. The corn oil (vehicle) and DE-71 mixture were then supplied to Envigo (Indianapolis, Indiana) and mixed each into the rodent chow. The final concentration of DE-71 was 625 µg/kg rodent chow. The food dyes Yellow No. 5 and Blue No. 1 were mixed into the control diet (LabDiet No. 5021) and DE-71-containing diet, respectively, for easy differentiation by the laboratory personnel. Indole propionic acid (IPA) was purchased from Sigma Aldrich (St. Louis, Missouri, Catalog No.: 57410-25G-F). All other

chemicals, unless otherwise noted, were purchased from Sigma Aldrich. The overall experimental design is summarized in Figure 1.

**Animals and chemical exposures**

The hPXR-TG mice were generously provided by Dr. Frank Gonzalez (National Cancer Institute, Bethesda, Maryland), as previously described (Ma et al. 2007). The original breeder pairs were acclimated to the University of Washington animal facility and bred for at least two generations before experimental use. All mice were housed in accordance with the Association of Assessment and Accreditation of Laboratory Animal Care International (AAALAC) guidelines, and all procedures were approved by the Institutional Animal Care and Use Committee (IACUC) at the University of Washington. Mice were housed in standard air-filtered cages with autoclaved Enrich-N'Pure bedding (Andersons, Maumee, Ohio) and given ad libitum access to non-acidified autoclaved water. hPXR-TG breeders were exposed to vehicle, DE-71 (0.1 mg/kg/day via diet), DE-71+IPA (20 mg/kg/day via drinking water), or IPA alone from four weeks preconception through lactation. Weaned pups were placed on a standard LabDiet No. 5010 (St. Louis, Missouri) with no direct DE-71 exposure. In the present study, an IPA dose of 20 mg/kg/day administered via drinking water was selected based on prior evidence demonstrating that IPA at this dosage effectively prevented gut dysbiosis, reduced endotoxin leakage, and attenuated hepatic inflammation and steatohepatitis in rats (Z.-H. Zhao et al. 2019). Additionally, IPA at the same dose for five days (Z.-B. Huang et al. 2022) protected against sepsis-related mortality, reducing bacterial burden and organ damage in mice. Clinical correlations with septic patients revealed significantly lower fecal IPA levels, which were associated with worse clinical outcomes. Based on these findings, this IPA dose was selected for the present study.

**Tissue collection**

Tissues were harvested at postnatal day (PND) 21, 3 months, and 6 months of age. Whole blood was collected via cardiac puncture and transferred to a MiniCollect serum separator (Greiner Bio-One, Kremsmünster, Austria), and was kept on ice for at least 30 min to allow sufficient time for blood coagulation. Serum was collected by centrifugation at 4000 rpm (1503 × g) at 4°C for 20 min and stored at −80°C until analysis. Large intestinal contents (LICs) were flushed with 10 mL of ice-cold phosphate-buffered saline (PBS) containing 0.1% dithiothreitol (Sigma Aldrich), immediately frozen on dry ice, and stored at −80°C. Liver samples were rapidly frozen in liquid nitrogen and stored at −80°C for subsequent analysis.

**Metagenomic shotgun sequencing and data analysis**

Bacterial DNA was isolated from large intestinal content (LIC) pellets using the OMEGA E.N.Z.A. Stool DNA Kit (OMEGA Biotech, Inc., Norcross, GA) following the manufacturer's protocol. DNA concentration was quantified using a Qubit fluorometer (Thermo Fisher Scientific, Waltham, MA). Metagenomic shotgun sequencing (Diversigen, New Brighton, MN) was conducted to assess gut microbiome composition and functional changes over time. DNA sequences were aligned to a curated database comprising all bacterial genomes from RefSeq, along with manually curated, high-quality metagenomically assembled and cell-cultured mouse-specific genomes. Alignments were performed at 97% identity against all reference genomes. Samples with >10,000 sequences were retained for downstream analysis, and operational taxonomic unit (OTU) counts were normalized to genome length. Functional microbiome changes were predicted by comparing aligned reads to the Kyoto Encyclopedia of Genes and Genomes (KEGG) Orthology

(KO) groups.

**Large-scale targeted LC-MS/MS metabolomics**

The large-scale targeted LC-MS/MS method utilized in this study was adapted from established protocols previously applied in numerous studies (Carroll et al. 2015a; Eghlimi et al. 2020; Gu et al. 2015a; 2016; Jasbi et al. 2019; 2021; Shi et al. 2019). All LC-MS/MS experiments were conducted using an Agilent 1290 UPLC-6490 QQQ-MS system (Santa Clara, CA). Tissue samples (~20 mg) were homogenized in 200 µL methanol (MeOH):PBS (4:1, v/v) containing 1810.5 µM $^{13}C_3$-lactate and 142 µM $^{13}C_5$-glutamic acid using a Bullet Blender homogenizer (Next Advance, Averill Park, NY). These internal standards were used to assess MS signal stability but were not used for indole quantification, consistent with previous studies (Carroll et al. 2015a; Eghlimi et al. 2020; Gu et al. 2015a; 2016; Jasbi et al. 2019; 2021; Shi et al. 2019). An additional 800 µL MeOH:PBS (4:1, v/v, containing internal standards) was added, and samples were vortexed for 10 s, then stored at −20°C for 30 min. After 30 min of ice bath sonication, samples were centrifuged at 14,000 rpm for 10 min (4°C), and 800 µL of supernatant was transferred to a new tube. Samples were then vacuum-dried using a CentriVap Concentrator (Labconco, Fort Scott, KS). Before LC-MS/MS analysis, dried residues were reconstituted in 150 µL of 40% PBS/60% acetonitrile (ACN). A quality control (QC) sample was pooled from all study samples. Each sample was injected twice into the LC-MS/MS system, 10 µL for analysis using negative ionization mode and 4 µL for analysis using positive ionization mode. Both chromatographic separations were performed in hydrophilic interaction chromatography mode on a Waters XBridge BEH Amide column (150 × 2.1 mm, 2.5 µm particle size, Waters Corporation, Milford, Massachusetts). The flow rate was 0.3 mL/min, auto-sampler temperature was kept at 4°C, and the

column compartment was set at 40°C. The mobile phase was composed of Solvents A (10 mM ammonium acetate, 10 mM ammonium hydroxide in 95% $H_2O$/5% ACN) and B (10 mM ammonium acetate, 10 mM ammonium hydroxide in 95% ACN/5% $H_2O$). After the initial 1 min isocratic elution of 90% B, the percentage of Solvent B decreased to 40% at t = 11 min. The composition of Solvent B was maintained at 40% for 4 min (t = 15 min), and then the percentage of B gradually went back to 90%, to prepare for the next injection.

The mass spectrometer utilized an electrospray ionization (ESI) source, and targeted data acquisition was performed in multiple-reaction-monitoring (MRM) mode. The entire LC-MS system was controlled using Agilent MassHunter Workstation software, with extracted MRM peaks integrated using Agilent MassHunter Quantitative Data Analysis (Santa Clara, CA).

**Untargeted LC-MS metabolomics**

The untargeted LC-MS metabolomics method used in this study was adapted from previously established protocols (Gu et al. 2015b; Qi et al. 2013; Y. Wei et al. 2021; Yao et al. 2014). LC-MS experiments were conducted using a Thermo Vanquish UPLC-Exploris 240 Orbitrap MS system (Waltham, MA). Leftover samples from targeted LC-MS/MS metabolomics were analyzed using this high-resolution mass spectrometer equipped with an ESI source. Untargeted data were collected over a mass range of 70–1050 m/z. Peak identification was performed using a combination of in-house chemical standards (~600 aqueous metabolites) and spectral searches against multiple metabolomics databases, including HMDB, LipidMaps, METLIN, mzCloud, Metabolika, and ChemSpider. For MS data extraction, the absolute intensity threshold was set at 1000, with a mass accuracy limit of 5 ppm. Metabolite identification and annotation were based on retention time (RT), exact mass, MS/MS fragmentation patterns, and

isotopic distributions. Thermo Compound Discoverer 3.3 was used for aqueous metabolomics data processing, including peak picking, alignment, and normalization. To ensure data quality and reproducibility, only signals/peaks with a coefficient of variation < 20% across QC pools, and the signals showing up in > 80% of all the samples were included for further analysis.

**Gas Chromatography- Mass Spectrometry (GC-MS)**

GC-MS experiments were performed using an Agilent 7820A GC system coupled to an Agilent 5977B mass spectrometer (Agilent Technologies, Santa Clara, CA). Sample separation was achieved using an HP-5ms capillary column (30 m x 250 µm i.d., 0.25 µm film thickness) coated with 5% phenyl-95% methylpolysiloxane (Agilent Technologies). A 1 µL sample was injected, with a solvent delay time of 5 min. The oven temperature program was set as follows: initial hold at 60°C for 1 min, ramped to 325°C at a rate of 10°C/min, and held at 325°C for 10 min. Helium was used as the carrier gas at a constant flow rate of 20 mL/min. The inlet, transfer line, and electron impact (EI) ion source temperatures were set to 250°C, 290°C, and 230°C, respectively. The electron energy was maintained at −70 eV, and mass spectral data were collected in full scan mode (m/z 30–600).

Data processing was performed using Agilent MassHunter Workstation Software Quantitative Analysis (B.09.00). Peak identification, integration, and quantification were carried out with a signal-to-noise (S/N) ratio threshold of 3. The RT and quantification masses for BDE-47 and BDE-99 were determined using chemical standards.

**RNA isolation**

Total RNA was extracted from frozen liver samples using RNA-Bee reagent (Tel-Test Inc.,

Friendswood, TX) following the manufacturer's protocol. RNA concentration was determined by measuring absorbance at 260 nm using a NanoDrop 1000 Spectrophotometer (Thermo Scientific, Waltham, MA). RNA integrity was assessed by formaldehyde-agarose gel electrophoresis, with visualization of 18S and 28S rRNA bands under UV light. The quality of total RNA was further confirmed using an Agilent 2100 Bioanalyzer (Agilent Technologies Inc.).

**RT-qPCR quantification of liver and data analysis**

Total RNA was extracted from liver and intestinal tissues (n = 5 per group) at postnatal day (PND) 21, 3 months, and 6 months of age. RNA was reverse-transcribed into complementary DNA (cDNA) using the High-Capacity cDNA Reverse Transcription Kit (Life Technologies, CA). Quantitative PCR (qPCR) was performed using Sso Advanced Universal SYBR Green Supermix on a Bio-Rad CFX384 Real-Time PCR Detection System (Bio-Rad, Hercules, CA). Gene expression data were normalized to the geometric mean of the housekeeping genes *Gapdh* and *β-actin* using the ΔΔCq method and expressed as a percentage of housekeeping gene expression.

**H&E staining of liver sections**

Liver tissues were fixed in 10% neutral-buffered formalin, embedded in OCT, sectioned , and stained with hematoxylin and eosin (H&E) for blinded evaluation. Histopathological signs of necrosis included pyknosis, karyolysis, karyorrhexis, cytoplasmic hyper-eosinophilia, membrane disruption, and cell loss. Inflammatory markers were assessed based on edema and leukocyte accumulation. Fibrosis was identified by the replacement of damaged tissue with angiogenic connective tissue. Apoptosis features included chromatin condensation, cell shrinkage, and cytoplasmic bleb formation.

**Statistical analysis**

A three-way analysis of variance (ANOVA) was initially performed to assess the effects of sex, age, and chemical exposure on microbiome composition, metabolite levels, and host gene expression. For each sex and age group, one-way ANOVA was used to evaluate chemical exposure effects, followed by Duncan's post-hot test, with adjusted p-values $< 0.05$. Statistical analyses were conducted using SPSS Version 29.0.1.0 (IBM, Armonk, NY).

## RESULTS

**Effects of maternal PBDE exposure on gut microbiome**

To determine the effects of maternal PBDE exposure on the gut microbiome composition and predicted functions in hPXR-TG mouse pups, DNA was extracted from LIC, and metagenomic shotgun sequencing was performed as described in the Materials and Methods section. At the phylum and class levels, microbial composition remained largely unchanged across exposures, with a moderate DE-71-induced decrease in the *Deferribacteres* phylum and *Bacilli* class and an IPA-mediated increase in *Clostridia* class in 21-day-old male pups and 6-month-old female pups (Supplementary Figures 1 and 2). Notably, *Clostridia* levels were slightly lower in control female pups compared to control males at PND 21. Interestingly, most DE-71-induced microbial alterations occurred at the species level, with an age-dependent increase in the number of affected taxa, suggesting that DE-71 exposure had a persistent and progressive impact on gut microbiome composition throughout development (Figure 2A).

At PND 21, maternal DE-71 exposure led to an increase in *Lachnoclostridium edouardi*, a known biomarker for hepatic steatosis (Dong et al. 2021), and *Clostridium innocuum*, associated

with proinflammation (Chia et al. 2018; Mefferd et al. 2020), in female pups. Additionally, *Mordavella sp. Marseille P3756*, a microbe known to be increased by antibiotic use and a Western diet in mice (Cabral et al. 2020), was also elevated. Notably, IPA supplementation normalized the abundance of these microbes back to control levels (Figure 2B). A similar trend was observed for *L. edouardi* and *C. innocuum* in male pups, though the changes did not reach statistical significance (Figure 2B). Maternal DE-71 exposure also increased the abundance of microbial genes associated with bacterial swarming activity, including *aroE* (though not statistically significant in male pups), *hyaB*, and *zwf*, which serve as indicators of gastrointestinal stress (De et al. 2021) in both sexes. Unlike its effects on microbial composition, IPA supplementation did not reverse these DE-71-mediated alterations (Figure 2B). Many of these bacterial enzymes are also involved in bacterial stress responses and reactive oxygen species (ROS) regulation, suggesting they may serve as novel biomarkers of maternal DE-71 toxicity (Inoue et al. 2007).

At 3 months of age, maternal DE-71 exposure reduced the DNA abundance of *Eubacterium sp. 14-2*, a known anti-obesity microbe (Jones et al. 2019), in both male and female pups, while IPA supplementation partially restored its levels. In male pups, DE-71 exposure significantly decreased *Lachnospiraceae bacterium M18-1*, which plays a role in regulating microbial metabolites in a rat model of T2D (Mercer et al. 2020), and *Blautia caecimuris*, a microbe associated with anti-inflammatory properties (X. Liu et al. 2021). IPA supplementation partially corrected these reductions, restoring *L. bacterium M18-1* in males and *B. caecimuris* in females. However, DE-71+IPA further reduced *L. bacterium M18-1* in females, while IPA alone decreased *B. caecimuris* in both sexes (Figure 2C). Additionally, *sdhA*, a key bacterial enzyme associated with swarming motility (Zhuang et al. 2016), was reduced by all three exposures (DE-71, DE-71+IPA, and IPA alone), but only in male pups.

At 6 months of age, maternal DE-71 exposure increased *Alistipes shahii* and *Bacteroides faecichinchillae*, microbes associated with anti-obesity effects (Gong et al. 2022; Won et al. 2020), in male and female pups, respectively. Maternal DE-71 exposure also increased *Bacteroides caccae*, a known taxonomic T2D biomarker (Cunningham, Stephens, and Harris 2021; Qin et al. 2012), in female pups. The observed DE-71-induced increases in these potentially protective microbes may reflect a compensatory response to metabolic disruption. IPA supplementation reversed these DE-71-mediated effects (Figure 2D). Maternal DE-71 exposure also reduced *sdhB*, a bacterial swarming-related enzyme, in male pups, whereas the opposite trend was observed in female pups. IPA supplementation partially normalized these DE-71-mediated effects; however, IPA alone also reduced *sdhB* in male pups. In summary, maternal DE-71 exposure induced persistent gut dysbiosis linked to obesity, inflammation, and T2D, with effects that persisted throughout development. IPA supplementation partially mitigated some, but not all, DE-71-induced alterations. In addition, distinct age- and sex-specific regulatory patterns were observed, and IPA itself exhibited baseline effects on certain microbes and microbial enzyme DNA expression.

To further investigate microbial functional pathways associated with maternal DE-71 exposure, predicted changes in microbiome metabolic activity were assessed using metagenomic shotgun sequencing data. At PND 21, maternal DE-71 exposure resulted in a significant increase in microbial DNA encoding oxidoreductases, enzymes involved in glucose metabolism (Hardman and Scopes 1988), in both male and female pups. IPA supplementation had a minimal impact during DE-71+IPA coexposure, although IPA alone increased oxidoreductase gene abundance in female pups (Figure 3A). In male pups, maternal DE-71 exposure also elevated DNA levels encoding cysteine peptidases family C16, which has been linked to obesity and insulin resistance

in adolescents (Elshorbagy et al. 2012). This effect was normalized by IPA supplementation, while IPA alone increased its abundance in female pups (Figure 3A). Additionally, in PND 21 female pups, maternal DE-71 exposure slightly increased the abundance of microbial genes encoding acid-D-ammonia ligases, which are involved in acid-base homeostasis, cell signaling, and cellular proliferation (Chek et al. 2021). IPA supplementation reversed these DE-71-induced changes, while IPA alone and in combination with DE-71 modestly increased the DNA abundance of these enzymes in male pups (Figure 3A).

At 3 months of age, maternal DE-71 exposure slightly reduced microbial DNA encoding ligases involved in the formation of phosphoric-ester bonds in both male and female pups. This DE-71-mediated reduction was partially reversed by IPA supplementation (Figure 3B). In female pups, maternal DE-71 exposure significantly increased the abundance of microbial DNA encoding serine peptidases family S51, enzymes associated with proteolytic processing, while a similar non-significant trend was observed in male pups. Notably, IPA supplementation reversed these DE-71-induced changes in both sexes (Figure 3B). Interestingly, the DNA encoding twitching motility proteins of the pilus system, which is linked to formation of biofilms on gastrointestinal injuries (Zolfaghar, Evans, and Fleiszig 2003), was increased by maternal DE-71 exposure in male pups and IPA supplementation corrected this DE-71-mediated effect. In females, DE-71+IPA coexposure group reduced its DNA abundance (Figure 3B).

At 6 months of age, maternal DE-71 exposure did not alter microbial DNA abundance for oxidoreductases and isomerases-enzymes involved in glucose metabolism (Sierkstra et al. 1993)- in male pups. However, in female pups, DE-71 exposure increased the abundance of these enzymes, and this effect was normalized by IPA supplementation (Figure 3C).

In summary, functional predictions of the microbiome revealed age- and sex-specific

regulatory patterns in response to maternal DE-71 exposure, particularly in pathways related to glucose metabolism, cell signaling, cell proliferation, and biofilm formation-the latter being implicated in gastrointestinal injury. While IPA supplementation was able to reverse some of the DE-71-mediated alterations, it did not fully normalize all affected pathways. In addition, IPA alone induced distinct microbial functional changes, highlighting its independent influence on host-microbiome interactions.

**Differential regulation of other DNA encoding intestinal content bacterial enzymes related to diabetes and obesity in postweaning pups following in response to maternal DE-71 exposure**

As shown in Supplementary Figure 3A, at PND 21, maternal DE-71 exposure upregulated microbial DNA encoding ketoreductase tylD, an enzyme involved in the biosynthesis of 6-deoxy-D-allose, a structural analog of D-glucose (Fouces et al. 1999), and glucose-fructose oxidoreductase (gfo), which plays a role in glucose metabolism (Zachariou and Scopes 1986), in female pups. IPA supplementation partially reversed these DE-71-mediated effects. At 3 months of age, maternal DE-71 exposure increased DNA abundance of limonene hydroxylase (K14732), an enzyme implicated in diabetes-related metabolic changes (Bacanlı et al. 2017), and NADP-reducing hydrogenase subunit hndD, associated with energy metabolism (de Luca et al. 1998), specifically in male pups. IPA supplementation attenuated these elevations, though not completely (Supplementary Figure 3B). At 6 months of age, a broader range of differentially regulated microbial enzymes was observed, many associated with secondary metabolite biosynthesis and xenobiotic biodegradation (Supplementary Figure 3C). Among these, impose isomerase (ioll), involved in carbohydrate metabolism (Bui et al. 2021), was significantly upregulated by DE-71

exposure in female pups, with a similar non-significant trend shown in males and IPA supplementation corrected the DE-71-mediated effect (Supplementary Figure 3C). Interestingly, GTP cyclohydrolase I, previously reported to be elevated in overweight premenopausal women (Wu et al. 2020), was upregulated by DE-71 exposure in both sexes and IPA supplementation reversed this effect (Supplementary Figure 3C).

These results demonstrate that maternal DE-71 exposure modulates the DNA abundance of several microbial enzymes associated with obesity and diabetes, in a sex- and age-specific manner. IPA supplementation was able to reverse a subset of these changes, highlighting its potential as a microbiome-targeted intervention. In conclusion, maternal DE-71 exposure persistently disrupted the gut microbiome composition and predicted metabolic functions across developmental stages, with alterations linked to pathways associated with obesity and diabetes. IPA supplementation partially ameliorated these DE-71-induced dysbiotic effects, supporting its role in mitigating environmentally-driven metabolic disturbances.

**Effects of maternal PBDE exposure on tryptophan microbial metabolites**

Given that microbial metabolism of tryptophan (Figure 4A) is known to influence host xenobiotic-sensing nuclear receptors, such as the PXR and AhR, we hypothesized that early-life DE-71 exposure-mediated gut dysbiosis may contribute to altered host receptor signaling by modulating microbial tryptophan-derived metabolites (Figure 4A). To evaluate this, targeted metabolomic profiling of serum and liver samples from pups at various developmental stages was conducted, as described in the Materials and Methods section. At PND 21, maternal DE-71 exposure led to an increase in serum indole, a known AhR ligand (Hubbard, Murray, and Perdew 2015), in male pups, with a non-significant increase trend in serum of female pups, whereas IPA

supplementation effectively reversed this DE-71-mediated elevation (Figure 4B). In addition, DE-71 exposure increased serum indole-3-lactic acid, another AhR agonist implicated in bifidobacterial host-microbiota interactions (Wong et al. 2020), in both sexes. Again, IPA supplementation reversed this effect, suggesting its potential role in modulating microbial metabolite signaling (Figure 4B).

At 3 months of age, maternal DE-71 exposure increased or tended to increase serum indole levels in both male and female pups, while IPA supplementation reversed these DE-71-mediated changes (Figure 4B). Notably, IPA alone elevated serum indole levels in female pups, but not in males. Serum IPA concentrations were unaffected by maternal DE-71 exposure in either sex; however, DE-71+IPA coexposure showed a non-significant increasing trend, whereas IPA alone had no effect on serum IPA (Figure 4B). In the liver, maternal DE-71 exposure significantly reduced IPA levels in male pups, an effect that was normalized by IPA supplementation. In contrast, female hepatic IPA levels remained unchanged by either DE-71 or IPA exposure (Figure 4C). At 6 months of age, there were no statistical changes in serum or hepatic tryptophan-derived metabolites (data not shown).

In summary, maternal DE-71 exposure persistently altered microbial tryptophan metabolism in an age- and sex-dependent manner. Key changes included increased serum indole at PND 21 and 3 months and reduced hepatic IPA levels at 3 months in male pups, as well as elevated serum indole-3-lactic acid at PND 21 in both sexes. IPA supplementation partially or fully corrected most of these DE-71-induced alterations. Additionally, IPA alone exerted distinct effects, such as an increase in serum indole at 3 months in female pups, highlighting its independent influence on microbial metabolite profiles.

**Expression of prototypical xenobiotic-sensing transcription factor-target genes in pups**

The mRNA expression of *Cyp1a2* (cytochrome P450 family 1 subfamily A member 2, AhR-target) (Flaveny, Murray, and Perdew 2010; Lo and Matthews 2012) and *Cyp3a11* (PXR target) (Cui and Klaassen 2016; Kiyosawa et al. 2008) was assessed in the livers of offspring following maternal DE-71 exposure as shown in Supplementary Figure 4. At PND 21, maternal DE-71 exposure significantly upregulated *Cyp1a2* mRNA expression in the livers of both male and female pups. IPA coexposure normalized *Cyp1a2* expression in female pups but not in male pups. Interestingly, IPA treatment alone increased hepatic *Cyp1a2* expression in females, but had no effect in males (Supplementary Figure 4A). By 3 and 6 months of age, *Cyp1a2* mRNA expression was no longer affected by DE-71 exposure in either sex (data not shown), suggesting that the AhR activation by DE-71 was transient and age-specific.

Regrading *Cyp2b10*, the prototypical target gene of constitutive androstane receptor (CAR) that is responsible for binding to specific protein on cancer cells (P. Wei et al. 2000), at PND 21, maternal DE-71 exposure significantly increased hepatic *Cyp2b10* mRNA expression in both male and female pups, while IPA coexposure further enhanced this upregulation, indicating a potential synergistic effect (Supplementary Figure 4A). At 3 months of age, DE-71 exposure had no significant effect on *Cyp2b10* mRNA expression (data not shown). However, at 6 months of age, *Cyp2b10* mRNA was again upregulated by DE-71 in the livers of both sexes. In male pups, both IPA alone and DE-71+IPA coexposure also increased *Cyp2b10* expression (Supplementary Figures 4B-C), suggesting a persistent and sex-specific modulation of CAR signaling by maternal exposure and microbial metabolites.

Regarding the prototypical PXR target gene *Cyp3a11*, at PND 21, both DE-71 and DE-71+IPA coexposure significantly upregulated *Cyp3a11* mRNA expression in male pups, indicating

early activation of PXR signaling. At 3 months of age, DE-71 exposure continued to elevate *Cyp3a11* mRNA in male livers, whereas in female pups, DE-71 led to a slight reduction in expression. At 6 months of age, IPA treatment alone resulted in a notable increase in hepatic *Cyp3a11* mRNA expression in male pups, suggesting that IPA may independently modulate PXR-regulated pathways in a sex- and age-dependent manner.

Regarding *Cyp4a14*, the prototypical target gene of lipid-sensing nuclear receptor peroxisome proliferator-activated receptor (PPARα) (Patsouris et al. 2006), at PND 21, both DE-71 and DE-71+IPA coexposure significantly increased hepatic *Cyp4a14* mRNA expression in male and female pups, suggesting early activation of PPARα signaling. At 6 months of age, DE-71 exposure continued to elevate *Cyp4a14* expression in both sexes, but IPA coexposure normalized expression levels back to control, indicating a potential corrective effect of IPA on DE-71-induced disruption of hepatic lipid metabolism. Interestingly, IPA alone increased *Cyp4a14* mRNA expression exclusively in the livers of 6 months old female pups, suggesting a sex- and age-specific regulatory role of microbial metabolites on host lipid signaling pathways (Supplementary Figure 4C).

Regarding NAD(P)H quinone dehydrogenase (*Nqo1*), the prototypical target gene of the major sensor for oxidative stress and electrophiles, namely nuclear factor erythroid 2-related factor 2 (*Nrf2*) (F. He, Ru, and Wen 2020), DE-71 exposure did not have effect at 21 days or 3 months of age, however, at 6 months of age, DE-71 significantly increased *Nqo1* expression in the livers of both male and female pups (Supplementary Figure 4). IPA coexposure attenuated this DE-71-induced upregulation, suggesting a potential antioxidant effect of IPA in mitigating oxidative stress-related gene activation.

Interestingly, the host response to maternal DE-71 and IPA exposure was tissue-specific.

At PND 21, the hepatic AhR target gene *Cyp1a2* was significantly upregulated by both DE-71 and DE-71+IPA in both sexes. In contrast, the intestinal AhR target gene *Cyp1a1*–the predominant Cyp1a isoform in the intestine (as *Cyp1a2* was not detectable in intestinal tissue)-remained unchanged across all exposures and time points (Supplementary Figure 5). At PND 21, intestinal *Cyp3a11* mRNA was increased by DE-71 but was normalized by IPA coexposure in male pups; whereas at 6 months of age, all 3 exposures decreased *Cyp3a11* mRNA in intestine of male pups, but DE-71 and IPA increased *Cyp3a11* mRNA in intestine of female pups (Supplementary Figure 5).

In summary, the regulation of prototypical xenobiotic-sensing transcription factor target genes by maternal DE-71 and IPA exposure was highly age-, sex-, and tissue-dependent. DE-71 significantly upregulated hepatic *Cyp1a2* mRNA, a canonical AhR target gene, at PND 21 in both sexes; however, this effect was not sustained at later time points, indicating transient AhR activation. In contrast, persistent DE-71-mediated effects were observed for other nuclear receptors. Specifically, early-life exposure to DE-71 led to sustained upregulation of *Cyp2b10* (CAR target) and *Cyp4a14* (PPARα target) at PND 21 and 6 months, as well as *Nqo1* (Nrf2 target) at 6 months, in both male and female pups. In addition, *Cyp3a11* (PXR target) was upregulated in the livers and intestines of PND 21 male pups, and in the livers of 3-month-old females, indicating activation of PXR signaling across tissues and time points. IPA normalized the DE-71 effect back to control for *Cyp1a2* mRNA in females at PND 21 and 3 months of age, *Cyp2b10* mRNA in females at 6 months of age, as well as *Cyp4a14* and *Nqo1* mRNAs in both sexes at 6 months of age. However, IPA was not able to correct the other DE-71-mediated effect and may have distinct regulatory patterns on its own.

The DE-71-induced increase in hepatic *Cyp1a2* mRNA expression in both sexes at PND

21 was accompanied by a corresponding increase or trend toward increased serum levels of indole, a known AhR ligand. Interestingly, although IPA supplementation normalized serum indole concentrations in both sexes, it only restored hepatic *Cyp1a2* mRNA to control levels in female pups (Figure 4 and Supplementary Figure 4), suggesting potential sex-specific regulation of AhR signaling. At 3 months of age, serum indole remained elevated following DE-71 exposure, particularly in male pups, yet hepatic *Cyp1a2* mRNA levels were unchanged. This apparent dissociation may be attributed to differences in indole tissue distribution, as hepatic indole levels–which directly influence local AhR activation–were not significantly altered (data not shown). Similarly, the DE-71-mediated reduction in hepatic IPA levels in male pups at 3 months did not lead to a decrease in *Cyp3a11* mRNA expression, a canonical PXR target gene. This suggests that DE-71 may directly maintain PXR activity, potentially through receptor interaction or alternative regulatory mechanisms, independent of changes in endogenous ligand levels such as IPA.

**Hepatic gene expression of inflammation markers**

To evaluate the effects of maternal DE-71 exposure on hepatic inflammatory responses, the mRNA expression of inflammation-related cytokines was assessed by RT-qPCR across treatment groups and developmental stages, with a focus on how IPA coexposure modulated DE-71-mediated effects. At PND 21, maternal DE-71 exposure significantly increased hepatic Il1β mRNA in both sexes and *Tnfα* mRNA in male pups. Notably, IPA coexposure did not attenuate these DE-71-mediated upregulation of Il10, an anti-inflammatory cytokine often co-induced with proinflammatory markers during immune activation, and *Il12p40*, a cytokine subunit primarily produced by activated proinflammatory cells in response to pathogenic stimuli (Supplementary Figure 6A). At 3 months of age, DE-71 and DE-71+IPA coexposure increased *Il12p40* mRNA in

the livers of male pups, whereas in female pups, IPA coexposure attenuated the DE-71-induced elevation. Interestingly, DE-71 reduced the expression of certain proinflammatory cytokines in a sex-specific manner, including interferon gamma (*Ifnγ*) in male livers at 3 months and monocyte chemotactic protein-1 (*Mcp-1*) in female livers at 6 months. IPA alone influenced cytokine expression, including downregulation of *Ifnγ* in male pups at 3 months, and upregulation of *Mcp-1* in both sexes at 6 months (Supplementary Figures 5B and 5C).

In summary, the regulation of hepatic cytokine expression by DE-71 and IPA was both age- and sex-dependent. While IPA effectively attenuated the DE-71-induced increase in *Il10* and *Il12p40*, it did not block the upregulation of *Il1β* (in both sexes) or *Tnfα* (in males). In addition, DE-71 appeared to reduce the expression of certain cytokines (*Ifnγ* and *Mcp-1*) in an age- and sex-dependent manner.

**Histopathological examination of livers following early life exposure to DE-71 and effect of IPA exposure**

Representative H&E stained liver sections are shown in Supplementary Figure 7. At PND 21, maternal DE-71 exposure promoted apoptotic features in the livers of both male and female pups with widespread nuclear shrinkage observed morphologically throughout the hepatic lobes, with effects more pronounced in males than females. Notably, this DE-71-induced apoptotic pattern was attenuated by IPA coexposure. At 3 and 6 months of age, DE-71-exposed livers exhibited an increased incidence of immune cell infiltration, again more prominent in males, and IPA treatment did not reverse this effect.

In summary, maternal DE-71 exposure modulated the hepatic proinflammatory cytokines and liver inflammation in an age- and sex-dependent manner, and some but not all of these effects

were partly corrected by IPA treatment.

**Effects of maternal DE-71 exposure on other serum metabolites as determined by untargeted metabolomics**

To determine the unbiased metabolic effects of maternal DE-71 exposure and IPA supplementation on postweaned offspring, untargeted metabolomics was performed on serum and liver samples collected at PND 21 (Figure 5), 3 months (Figure 6), and 6 months of age (Figure 7). At PND 21, maternal DE-71 exposure altered a greater number of serum metabolites in female pups compared to males (Figure 5). In male pups, DE-71 exposure resulted in changes to several metabolites associated with obesity and diabetes, including cytosine and pyruvic acid, which have also been linked to cancer-related pathways (Ehrich et al. 2006; Roudier and Perrin 2009). In female pups, maternal DE-71 exposure significantly impacted a range of metabolites implicated in obesity, diabetes, inflammation, and cancer, Notably, L-pyroglutamic acid, a metabolite elevated in gestational diabetes mellitus (Tian et al. 2021), was strongly upregulated by DE-71 in both sexes, and IPA supplementation effectively attenuated this elevation (Figure 5C). Similarly, L-phenylalanine, known to influence gut hormone secretion and glucose tolerance with potential therapeutic relevance for obesity and T2D (Alamshah et al. 2017), exhibited an upregulation response to DE-71 exposure in both sexes at PND 21, though this change did not reach statistical significance and IPA supplementation partially reversed the DE-71-mediated effect (Figure 5C).

As shown in Figure 6, at 3 months of age, the serum metabolomic profile of female pups exhibited more differentially regulated metabolites in response to maternal DE-71 exposure compared to males. For example, leucine has been shown to modulate dietary amino acid balance and reduce adiposity, therefore protecting organism against obesity (Zhou et al. 2021). In our

study, leucine was slightly upregulated by DE-71 exposure in females 3 months of age, however, IPA was not able to suppress the damage done by DE-71 (Figure 6C).

As shown in Figure 7, at 6 months of age, the serum metabolomic profiles of female pups exhibited more differentially regulated metabolites in response to maternal DE-71 exposure compared to males. Among these, myristic acid was previously shown to improve hyperglycemia and symptoms of T2D mellitus in mice (Takato et al. 2017). In our study, myristic acid was reduced by maternal DE-71 only in females 6 months of age, and IPA supplementation was partially able to reverse the DE-71-mediated effect (Figure 7C). Stearic acid was previously shown to increase apoptosis (programmed cell death) and cytotoxicity in preadipocytes in mice (Shen et al. 2014). In our study, stearic acid was increased in both males (trend was not statistically significant) and females; however, IPA supplementation was not able to correct the DE-71-mediated effects (Figure 7C).

Overall, untargeted metabolomics revealed a clear female-predominant metabolic response to maternal DE-71 exposure and IPA supplementation. Several serum metabolites associated with obesity and diabetes were found to be persistently altered by DE-71 exposure across developmental stages. While IPA supplementation was able to reverse some of these DE-71-induced metabolic disruptions, its effects were metabolic-specific, and not all alterations were corrected, highlighting the partial and selective efficacy of IPA in mitigating environmentally-induced metabolic dysregulation.

As summarized in Figure 8, we have demonstrated that maternal DE-71 exposure induces a constellation of proinflammatory and obesity/diabetes-prone signatures across metagenomic, metabolomic, and hepatic gene expression profiles within the gut-liver axis of postweaned hPXR-TG offspring. Key features include persistent gut dysbiosis, disrupted microbial tryptophan

metabolism, attenuated PXR signaling, and elevated AhR activation, observed in an age- and sex-dependent manner over the developmental time course. Importantly, IPA supplementation was able to partially mitigate several of these DE-71-induced alterations, though its corrective effects were selective and not universally observed, highlighting the complex and context-specific nature of the host-microbiome-environment interaction.

## DISCUSSION

Our study demonstrated that PBDEs modulate the gut-liver axis in a sex- and age-dependent manner. Untargeted metabolomics revealed that maternal PBDE exposure dysregulated more circulating intermediary metabolites in female offspring than in males at all three developmental stages examined (Figures 5-7). At PND 21, female pups also exhibited a greater increase in obesity- and inflammation-associated microbial taxa in response to DE-71 exposure compared to males (Figure 2), suggesting a female-predominant metabolic susceptibility. While most existing literature on sex-specific PBDE toxicity focuses on neurodevelopmental and cognitive outcomes in both humans (Azar et al. 2021) and animal models (Viberg, Fredriksson, and Eriksson 2004), recent evidence supports sex-specific metabolic disturbances. A recent study showed that DE-71-exposed female offspring displayed more lipid disorders including hypercholesterolemia and elevated lipids than the male offspring, associated with female-specific downregulation of the expression of various hypothalamic genes involving energy regulation circuits that control lipid homeostasis (Kozlova et al. 2022). These findings suggest that PBDEs, as endocrine-disrupting chemicals (EDCs), may exert sex-dependent effects via the hypothalamus-liver axis. In addition, thyroid hormones–another known target of PBDE toxicity–may contribute to the observed female-biased metabolic changes, particularly in the gut-liver axis, as thyroid

hormone-related disorders and transcriptomic alterations are more prevalent in females than males (Cho et al. 2018; Morganti et al. 2005). Furthermore, baseline sex differences in the gut microbiome composition between control males and females may predispose offspring to sex-specific microbiome and metabolic responses following PBDE exposure. Regarding the age effect, we observed an age-dependent increase in the number of DE-71-regulated microbial species, persisting well beyond the cessation of exposure (Figure 2A). This suggests that maternal DE-71 exposure induces long-lasting and progressively amplified alterations in the intestinal microenvironment, potentially disrupting microbial colonization dynamics and influencing the developmental trajectory of the gut microbiome over time.

Previous epidemiologic studies showed that PBDE exposure led to childhood obesity and pathogenesis of metabolic syndrome (J.-S. Lim, Lee, and Jacobs 2008; Turyk et al. 2010; Windham et al. 2010). A recent study showed that maternal DE-71 exposure produced distinct serum metabolite profiles related to metabolism of amino acids, lipids, and carbohydrates on rats (H. Gao et al. 2021). Consistent with these findings, our study showed that maternal DE-71 exposure in hPXR-TG mice produced unique untargeted serum metabolomic signatures reflective of disruptions in lipid and carbohydrate metabolism. Furthermore, our functional metagenomic predictions revealed numerous DE-71-regulated microbial enzymes and KEGG pathways associated with amino acid, lipid, and carbohydrate metabolism. These findings highlight novel molecular and microbial targets through which maternal PBDE exposure may influence metabolic programming, offering new mechanistic insights into the delayed onset of obesity and diabetes observed in later life.

Our study showed that maternal DE-71 exposure led to sustained dysregulation of the gut microbiome in offspring, consistent with previous findings (Gomez et al. 2021; Laue et al. 2019;

Lim et al. 2021; Scoville et al. 2019). Alterations in the gut microbial community are known to influence the production of microbial metabolites, which can enter the systemic circulation and interact with host receptors across multiple organs–including the liver–to modulate xenobiotic metabolism and immune response (Flannigan et al. 2023; Fu and Cui 2017; Sittipo, Shim, and Lee 2019; Spanogiannopoulos et al. 2016). To assess the potential for direct chemical contribution, we quantified BDE-47 and BDE-99 levels in liver tissue using GC-MS and found no or minimal detectable concentrations (Supplementary Figure 8). These results suggest that the persistent effects observed in the gut-liver axis are primarily driven by persistent dysbiosis of the gut microbiome and not the direct chemical effect.

Given that inflammation plays a central role in the development of obesity and diabetes (Rohm et al. 2022), our findings highlight IPA as a promising microbiome-derived therapeutic candidate to mitigate maternal DE-71-induced toxicity. We showed that IPA supplementation partially reversed DE-71-mediated effects across multiple proinflammatory and prediabetic parameters in an age- and sex-dependent manner, supporting its potential in modulating long-term metabolic health outcomes. Our results further substantiate the anti-inflammatory properties of IPA, aligning with previous studies demonstrating its ability to alleviate sepsis-associated acute liver injury and suppress dextran sulfate sodium (DSS)-induced intestinal inflammation and fibrosis, both of which are mediated through PXR activation (Flannigan et al. 2023; Wang et al. 2023). Interestingly, tissue-specific host response to DE-71 and IP was also observed in our study regarding both PXR and AhR target gene expression, with liver being more responsive than intestine. This finding aligns with a previous report showing that IPA does not alter the expression of PXR target gene *Mdr1* or AhR target gene *Cyp1a1* in mouse colonic spheroid cultures (Wlodarska et al. 2017), further emphasizing the tissue-specific context in which microbiome-

derived metabolites like IPA exert their effects.

In our study, we observed that IPA modulates multiple nuclear receptors and transcription factors beyond PXR, as indicated by its regulation of prototypical target gents including *Cyp1a1*, *Cyp2b10*, *Cyp4a14*, and *Nqo1*. Previously, using nuclear receptor reporter assays demonstrated that IPA and indole mixtures robustly activate PXR, with additional moderate activity toward CAR, PPARγ, LXR, and FXR (Venkatesh et al. 2014a). Our findings further support the multifaceted role of IPA in regulating these pathways. However, unlike their cooperative activation of PXR, IPA and indole do not synergize in activating AhR, suggesting that in vivo–where multiple microbial metabolites coexist–IPA's influence on AhR is limited or unpredictable (Vrzalová et al. 2022). Thus, AhR activation observed in our model is more likely driven by other tryptophan-derived microbial metabolites, rather than IPA itself. Regarding oxidative stress, IPA has been previously shown to exhibit antioxidant properties, including attenuation of oxidative injury in the ischemic hippocampus (Hwang et al. 2009), protection of hepatic microsomal membranes from iron-induced damage (Karbownik et al. 2001), and reduction of lipid peroxidation in skin membranes (Rynkowska, Stępniak, and Karbownik-Lewińska 2021). In our study, DE-71 exposure upregulated *Nqo1* mRNA, a canonical target of the oxidative stress sensor Nrf2, while IPA supplementation attenuated this effect, indicating a protective antioxidant response likely independent of PXR activation. Taken together, these data suggest that IPA's beneficial effects may be mediated through both PXR-dependent and -independent mechanisms, including anti-inflammatory and antioxidant pathways. While IPA-PXR signaling is associated with protection against inflammation and lower metabolic disease risk (Cheng, Shah, and Gonzalez 2012; Tuomainen et al. 2018; Venkatesh et al. 2014a), indole-AhR signaling is also linked to reduced obesity, inflammation, and metabolic dysfunction (Kahalehili et al. 2020; X. Xu

et al. 2021). Therefore, AhR-PXR crosstalk, modulated by altered tryptophan microbial metabolism, may contribute to DE-71-induced inflammation and metabolic dysfunction. Additionally, we hypothesize that there is a yin-yang balance between PXR activation by xenobiotics versus endobiotics; the exogenous PXR activation by environmental toxicants upsets the gut microbiome, attenuating the endogenous PXR activation through reduced IPA levels. While xenobiotic-induced PXR activation supports detoxification, this competition with endogenous ligands may impair homeostasis functions, contributing to inflammation and increased susceptibility to metabolic syndrome.

The present study has certain limitations. First, our findings regarding the role of the gut-liver axis in maternal DE-71 exposure and IPA supplementation in hPXR-TG mice remain associative. Future studies utilizing germ-free (GF) mice with fecal microbiota transplantation (FMT) or antibiotic-treated mice on an hPXR-TG background would be valuable to establish causality and further define the role of the gut microbiome in modulating proinflammatory responses and metabolic outcomes. Second, we did not include PXR-null mice in the current experimental design, nor did we use polychlorinated naphthalene (PCN) as a pharmacological positive control for PXR activation. However, we recently published a separate study comparing PXR-null mice, PCN-treated mice, and DE-71-exposed mice, which identified both overlapping and distinct microbial alterations between pharmacologic and toxicologic PXR activation (Little et al. 2022). These findings suggest that some effects of DE-71 may occur independently of PXR signaling, and that PCN may not fully represent the endogenous role of PXR in regulating microbiome function. In contrast, IPA serves as well-established endogenous microbial ligand for PXR, with prior evidence demonstrating that IPA-induced *Mdr1* expression is abolished in the intestines of PXR-null mice (Venkatesh et al. 2014b). Therefore, the inclusion of IPA in our study

provides a more physiologically-relevant approach to investigate endogenous PXR signaling. Nevertheless, as shown in both our study (Supplementary Figure 4) and previous literature (Morgan et al. 2018), IPA does not robustly induce *Cyp3a11* in the liver, indicating that its hepatic effects may be mediated indirectly through gut PXR activation. Future work using PXR-null mice in the FVB background is needed to confirm this mechanism. In addition, we did not assess fecal metabolites, as the primary focus of this study was the gut-liver axis, and thus we focused on internal metabolites such as serum and liver-derived tryptophan metabolites. However, we recognize that excreted microbial metabolites may differ from biologically active circulating metabolites. Given that many clinical studies use fecal metabolites as indirect biomarkers of host-microbiome interactions, future research should include fecal metabolomic profiling to better connect microbial output with systemic metabolic outcomes.

Despite the limitations, our study provided the first evidence that maternal DE-71 exposure induced a proinflammatory signature within the gut-liver axis associated with dysregulated tryptophan microbial metabolism and elevated AhR signaling in a sex-dependent manner. More interestingly, several of the toxicological and molecular effects triggered by DE-71 were partially attenuated by IPA supplementation, highlighting the potential of microbiome-derived metabolites as therapeutic modulators. These findings underscore the importance of host-microbiome interactions in shaping the long-term metabolic consequences of early-life environmental exposures. Future studies should further explore the role of human PXR activation in mediating these effects, with the goal of identifying novel therapeutic strategies to mitigate metabolic diseases associated with developmental exposure to environmental toxicants.

## FUNDING STATEMENT

Supported by the National Institutes of Health (grants R01 ES030197, ES025708, and ES031098); the University of Washington Interdisciplinary Center for Exposures, Diseases, Genomics, and Environment (NIH P30 ES007033); the University of Washington (Sheldon D. Murphy Endowment); UW Environmental Health and Microbiome Research Center (EHMBRACE); the University of Washington Sheldon Murphy Endowment (J.Y.C.); as well as the graduate student fellowship from the UW Provost funds (S.K.).

## ACKNOWLEDGEMENTS

The authors would like to thank the members of Dr. Cui's laboratory for their help in tissue collection and Drs. Gu and Mani laboratories for helping with manuscript revision.

## Figure legends

**Figure 1.** Experimental design of the study. Humanized PXR-transgenic (hPXR-TG) dams were exposed to one of the following: (1) standard rodent chow, (2) DE-71 (an industrial PBDE mixture) via diet, (3) indole propionic acid (IPA) supplementation via drinking water; or (4) DE-71 via diet + IPA via drinking water; from 4 weeks preconception until lactation. The pups were weaned at

postnatal day (PND) 21, when the DE-71 exposure stopped; whereas the IPA supplementation continued in the 2 corresponding groups (3 and 4). Tissues were collected at PND 21, 3 months, and 6 months of age. Intestinal contents were subjected to metagenomic shotgun sequencing. Serum tryptophan metabolites were quantified using LC-MS. Untargeted metabolomics was also performed in serum. RT-qPCR was performed to quantify the mRNA expression of distinct liver genes in these pups. Three-way analysis of variance (ANOVA) was first performed to determine the effect of sex, age, and chemicals, as well as their potential interactions. Because the primary focus of the study is the effect of chemicals, at each sex and age, 1-way ANOVA was then performed followed by Duncan's post hoc test. Statistically significant differences were considered at $p < 0.05$.

**Figure 2.** Differentially regulated intestinal bacteria at the species level in 3 ages of the pups (PND 21, 3 months, and 6 months of age; $n = 5$ per group). **A**. Number of species significantly changed by DE-71 exposure over time points. **B.** Examples of differentially regulated microbial species (top row), as well as differentially regulated microbial DNA encoding swarming-related enzymes (bottom row) at PND 21. **C.** Bacteria species level at 3 months of age where maternal DE-71 exposure reduced the anti-obesity and anti-inflammatory species in both sexes (top row) and the differentially regulated microbial DNA encoding swarming-related enzymes (bottom row) at 3 months of age. **D.** Bacteria species level (top row) and the differentially regulated microbial DNA encoding swarming-related enzymes (bottom row) at 6 months of age. To determine the chemical effect, statistical analysis was done by 1-way ANOVA followed by Duncan's post hoc test with $p$-value < 0.05 being statistically significant. Groups a, b, and ab represent different post hoc groups.

**Figure 3.** Differentially regulated intestinal bacterial KEGG pathway related to obesity and/or diabetes at PND 21 **(A)**, 3 months of age **(B)**, and 6 months of age **(C)**. To determine the chemical effect, at each age and sex, statistical analysis was done by 1-way ANOVA followed by Duncan's post hoc test, $p$-value < 0.05. Groups a, b, ab, bc, and c represent different post hoc groups.

**Figure 4.** Tryptophan metabolites in serum and livers of mouse pups of the 4 exposure groups at various postnatal ages (PND 21, 3 months, and 6 months; $n$ = 5 per group). **A.** Diagram of microbial tryptophan metabolism. **B.** Statistically significant tryptophan metabolites in serum at PND 21 (top row) and 3 months of age (bottom row). **C.** Statistically significant tryptophan metabolite in the liver of pups at 3 months of age. Statistical analysis was done by 1-way ANOVA followed by Duncan's post hoc test, $p$-value < .05. Groups a, b, and ab represent different post hoc groups. Tryptophan metabolites in serum and livers of pups at 6 months of age were not included because they were not statistically significant.

**Figure 5.** Two-way hierarchical clustering of differentially regulated untargeted metabolites in serums of PND 21 pups ($n$ = 5 per group). **A.** Differentially regulated untargeted metabolites in the male serums of PND 21 pups. **B.** Differentially regulated untargeted metabolites in the female serums of PND 21 pups. **C.** Bar plots of statistically significant untargeted metabolites related to obesity and diabetes of 21-days old pups. Statistical analysis was done by 1-way ANOVA followed by Duncan's post hoc test; asterisks on Figures 5A and 5B: $p$-value < 0.05. Groups a, b, and ab represent different post hoc groups.

**Figure 6.** Two-way hierarchical clustering of differentially regulated untargeted metabolites in serums of 3 months old pups of the 4 exposure groups ($n$ = 5 per group). **A.** Differentially regulated untargeted metabolites in the male serums of 3 months old pups. **B.** Differentially regulated untargeted metabolites in the female serums of 3 months of pups. **C.** Bar plot of untargeted metabolite related to obesity of 3 months old pups. Statistical analysis was done by 1-way ANOVA followed by Duncan's post hoc test; asterisks on Figures 6A and 6B: $p$-value < 0.05. Groups a, b, and ab represent different post hoc groups.

**Figure 7.** Two-way hierarchical clustering of differentially regulated untargeted metabolites in serums of 6 months old pups of the 4 exposure groups ($n$ = 5 per group). **A.** Differentially regulated untargeted metabolites in the male serums of 6 months old pups. **B.** Differentially regulated untargeted metabolites in the female serums of 6 months of pups. **C.** Bar plot of untargeted metabolite related to obesity of 6 months old pups. Statistical analysis was done by 1-way ANOVA followed by Duncan's post hoc test; asterisks on Figures 7A and 7B: $p$-value < 0.05. Groups a, b, and ab represent different post hoc groups.

**Figure 8.** Summary diagram of the major findings of this study. Overall, the effect of maternal DE-71 exposure on hPXR-TG mice produced a proinflammatory signatures within the gut-liver axis associated with dysregulated tryptophan microbial metabolism, attenuated PXR signaling, and elevated AhR signaling in an age- and sex-dependent, and some but not all of these effects can be at least partially corrected y IPA supplementation.

# Figure 1

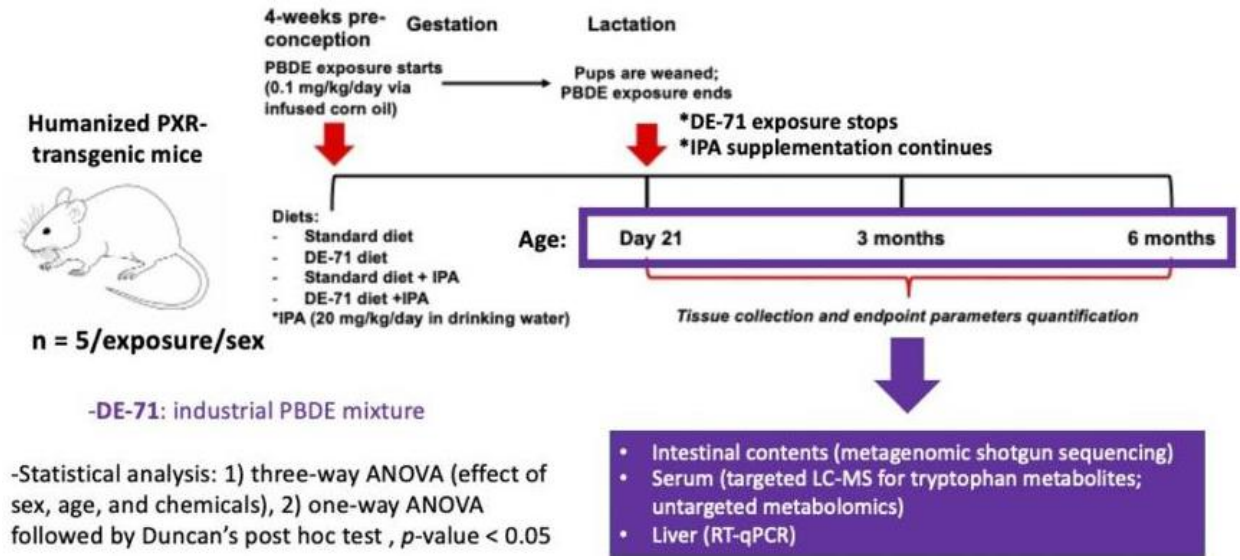
4-weeks pre-conception
Gestation
Lactation
PBDE exposure starts (0.1 mg/kg/day via infused corn oil)
Pups are weaned; PBDE exposure ends
*DE-71 exposure stops
*IPA supplementation continues
Humanized PXR-transgenic mice
Diets:
- Standard diet
- DE-71 diet
- Standard diet + IPA
- DE-71 diet +IPA
*IPA (20 mg/kg/day in drinking water)
Age:
Day 21
3 months
6 months
Tissue collection and endpoint parameters quantification
n = 5/exposure/sex
-DE-71: industrial PBDE mixture
-Statistical analysis: 1) three-way ANOVA (effect of sex, age, and chemicals), 2) one-way ANOVA followed by Duncan's post hoc test , p-value < 0.05
• Intestinal contents (metagenomic shotgun sequencing)
• Serum (targeted LC-MS for tryptophan metabolites; untargeted metabolomics)
• Liver (RT-qPCR)

# Figure 2

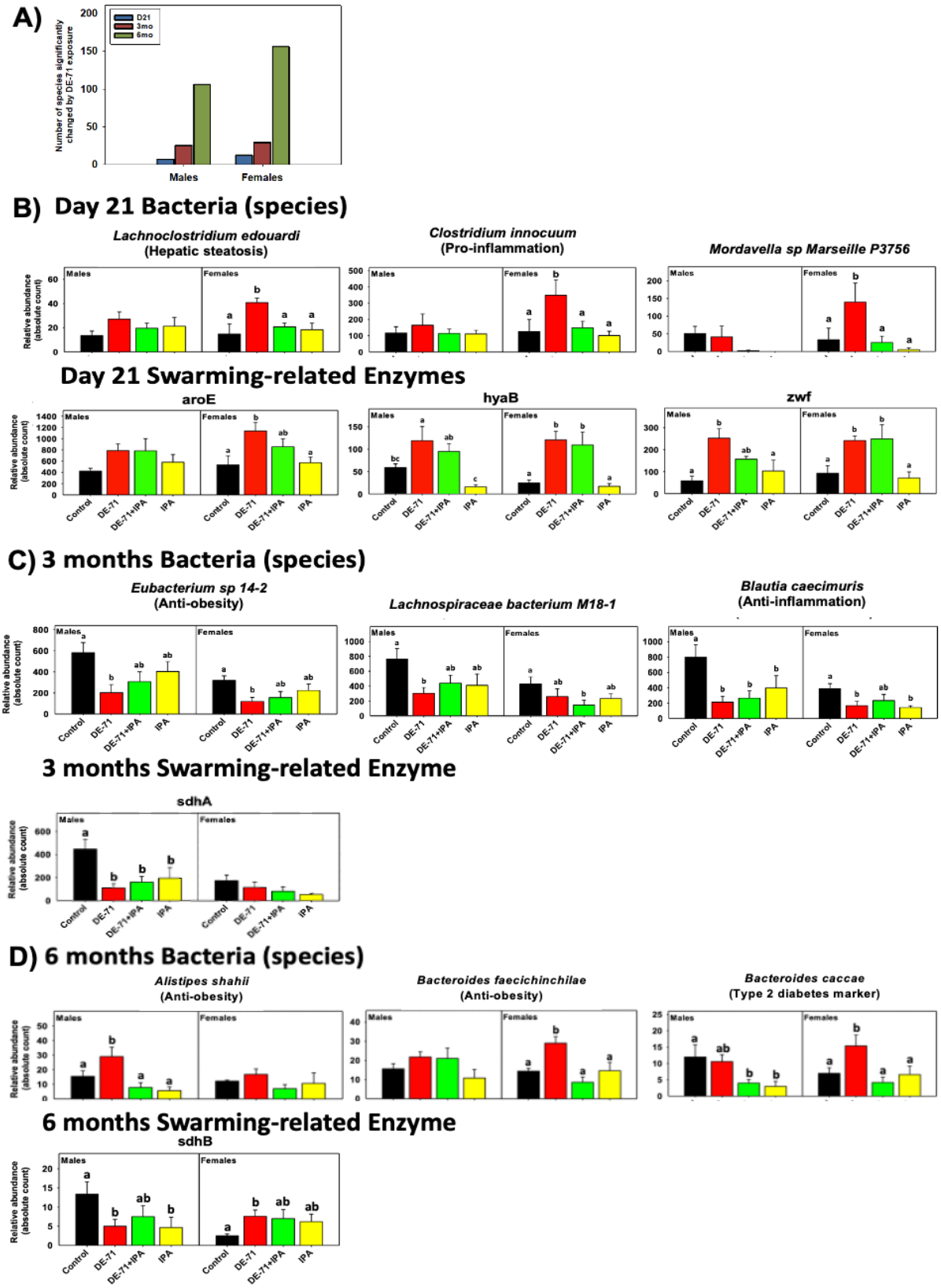
A)
Number of species significantly changed by DE-71 exposure
D21
3mo
6mo
Males
Females
B) Day 21 Bacteria (species)
Lachnoclostridium edouardi
(Hepatic steatosis)
Clostridium innocuum
(Pro-inflammation)
Mordavella sp Marseille P3756
Day 21 Swarming-related Enzymes
aroE
hyaB
zwf
C) 3 months Bacteria (species)
Eubacterium sp 14-2
(Anti-obesity)
Lachnospiraceae bacterium M18-1
Blautia caecimuris
(Anti-inflammation)
3 months Swarming-related Enzyme
sdhA
D) 6 months Bacteria (species)
Alistipes shahii
(Anti-obesity)
Bacteroides faecichinchilae
(Anti-obesity)
Bacteroides caccae
(Type 2 diabetes marker)
6 months Swarming-related Enzyme
sdhB
Relative abundance (absolute count)
Control
DE-71
DE-71+IPA
IPA

# Figure 3

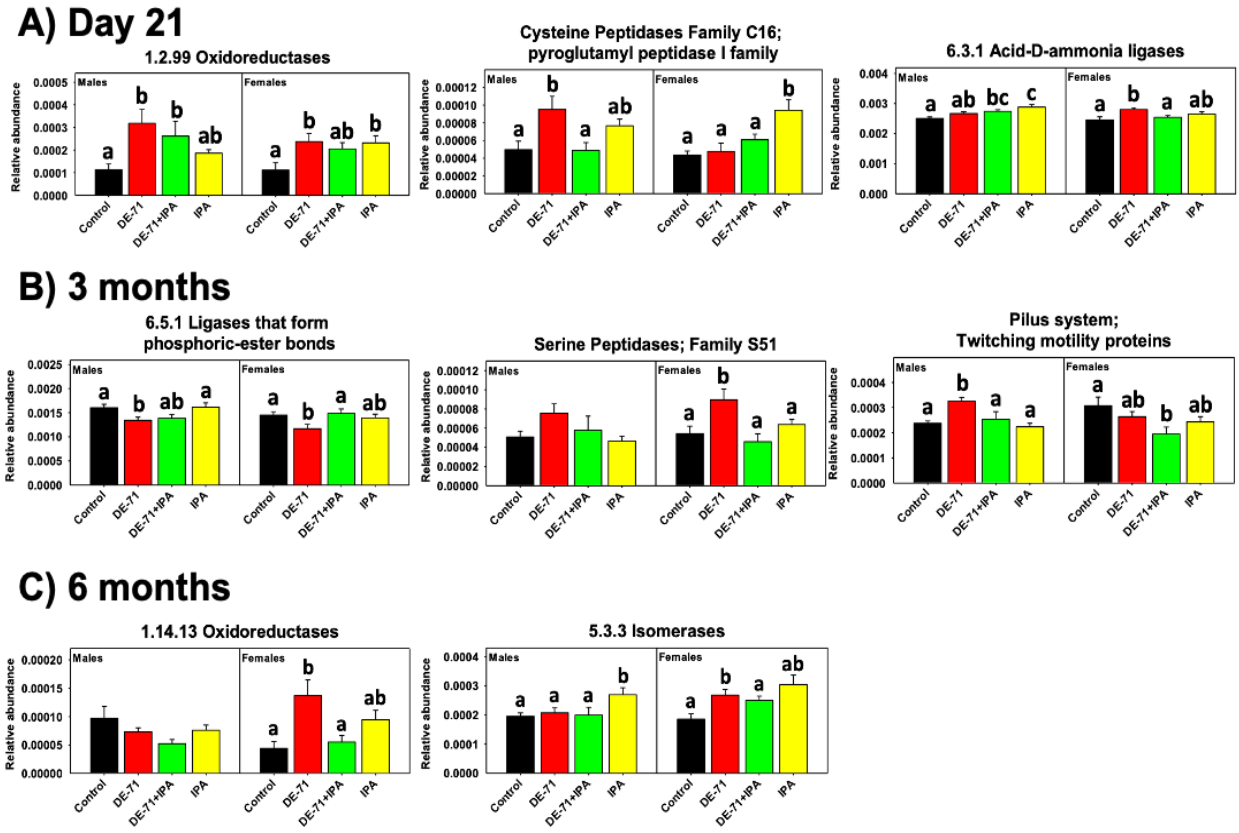
A) Day 21
1.2.99 Oxidoreductases
Cysteine Peptidases Family C16; pyroglutamyl peptidase I family
6.3.1 Acid-D-ammonia ligases
B) 3 months
6.5.1 Ligases that form phosphoric-ester bonds
Serine Peptidases; Family S51
Pilus system; Twitching motility proteins
C) 6 months
1.14.13 Oxidoreductases
5.3.3 Isomerases
Males
Females
Relative abundance
Control
DE-71
DE-71+IPA
IPA

# Figure 4

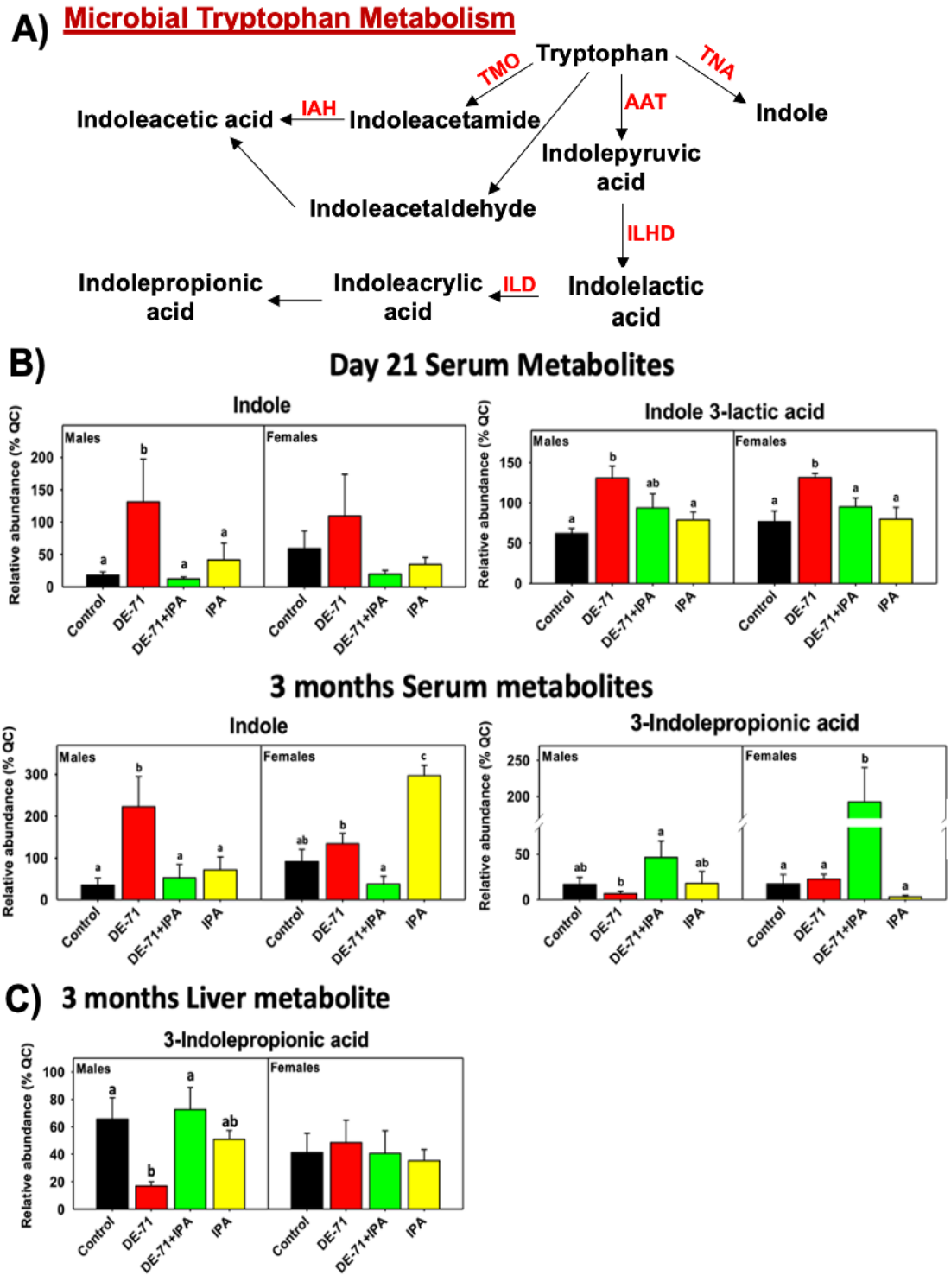
A)
Microbial Tryptophan Metabolism
Tryptophan
TMO
TNA
AAT
Indole
Indoleacetamide
IAH
Indoleacetic acid
Indolepyruvic acid
Indoleacetaldehyde
ILHD
Indolelactic acid
ILD
Indoleacrylic acid
Indolepropionic acid
B)
Day 21 Serum Metabolites
Indole
Indole 3-lactic acid
Males
Females
Relative abundance (% QC)
Control
DE-71
DE-71+IPA
IPA
3 months Serum metabolites
Indole
3-Indolepropionic acid
C)
3 months Liver metabolite
3-Indolepropionic acid

# Figure 5

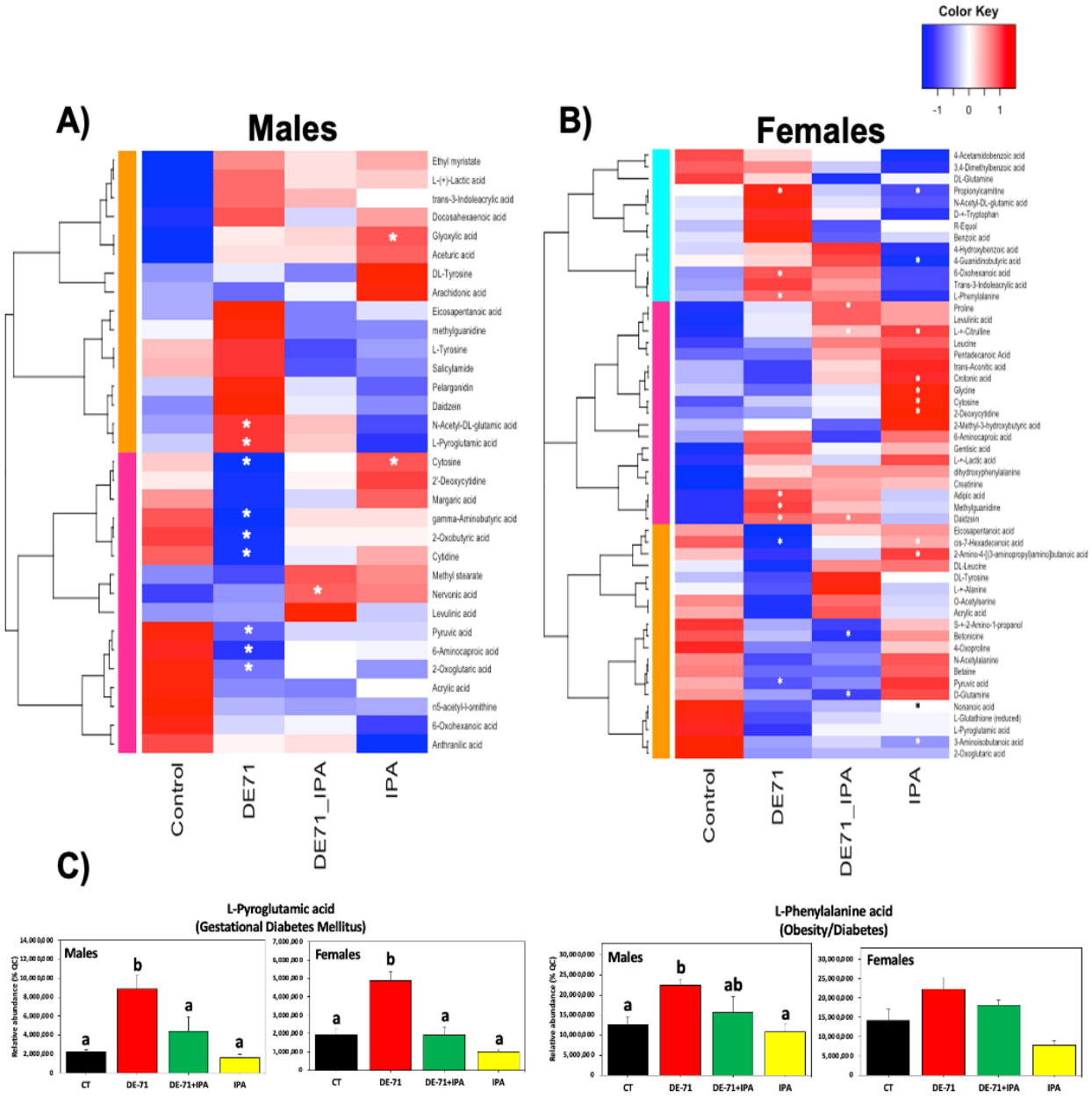
Color Key
-1
0
1
A)
Males
Ethyl myristate
L-(+)-Lactic acid
trans-3-Indoleacrylic acid
Docosahexaenoic acid
Glyoxylic acid
Aceturic acid
DL-Tyrosine
Arachidonic acid
Eicosapentanoic acid
methylguanidine
L-Tyrosine
Salicylamide
Pelargonidin
Daidzein
N-Acetyl-DL-glutamic acid
L-Pyroglutamic acid
Cytosine
2'-Deoxycytidine
Margaric acid
gamma-Aminobutyric acid
2-Oxobutyric acid
Cytidine
Methyl stearate
Nervonic acid
Levulinic acid
Pyruvic acid
6-Aminocaproic acid
2-Oxoglutaric acid
Acrylic acid
n5-acetyl-l-ornithine
6-Oxohexanoic acid
Anthranilic acid
Control
DE71
DE71_IPA
IPA
B)
Females
4-Acetamidobenzoic acid
3,4-Dimethylbenzoic acid
DL-Glutamine
Propionylcarnitine
N-Acetyl-DL-glutamic acid
D-+Tryptophan
R-Equol
Benzoic acid
4-Hydroxybenzoic acid
4-Guanidinobutyric acid
6-Oxohexanoic acid
Trans-3-Indoleacrylic acid
L-Phenylalanine
Proline
Levulinic acid
L-+-Citrulline
Leucine
Pentadecanoic Acid
trans-Aconitic acid
Cicitonic acid
Glycine
Cytosine
2-Deoxycytidine
2-Methyl-3-hydroxybutyric acid
6-Aminocaproic acid
Gentisic acid
L-+-Lactic acid
dihydroxyphenylalanine
Creatinine
Adipic acid
Methylguanidine
Daidzein
Eicosapentanoic acid
cis-7-Hexadecenoic acid
2-Amino-4-[(3-aminopropyl)amino]butanoic acid
DL-Leucine
DL-Tyrosine
L-+-Alanine
O-Acetylserine
Acrylic acid
S-+-2-Amino-1-propanol
Betonicine
4-Oxoproline
N-Acetylalanine
Betaine
Pyruvic acid
D-Glutamine
Nonanoic acid
L-Glutathione (reduced)
L-Pyroglutamic acid
3-Aminoisobutanoic acid
2-Oxoglutaric acid
Control
DE71
DE71_IPA
IPA
C)
L-Pyroglutamic acid
(Gestational Diabetes Mellitus)
Males
Females
Relative abundance (% QC)
a
b
a
a
CT
DE-71
DE-71+IPA
IPA
L-Phenylalanine acid
(Obesity/Diabetes)
Males
Females
a
b
ab
a
CT
DE-71
DE-71+IPA
IPA

# Figure 6

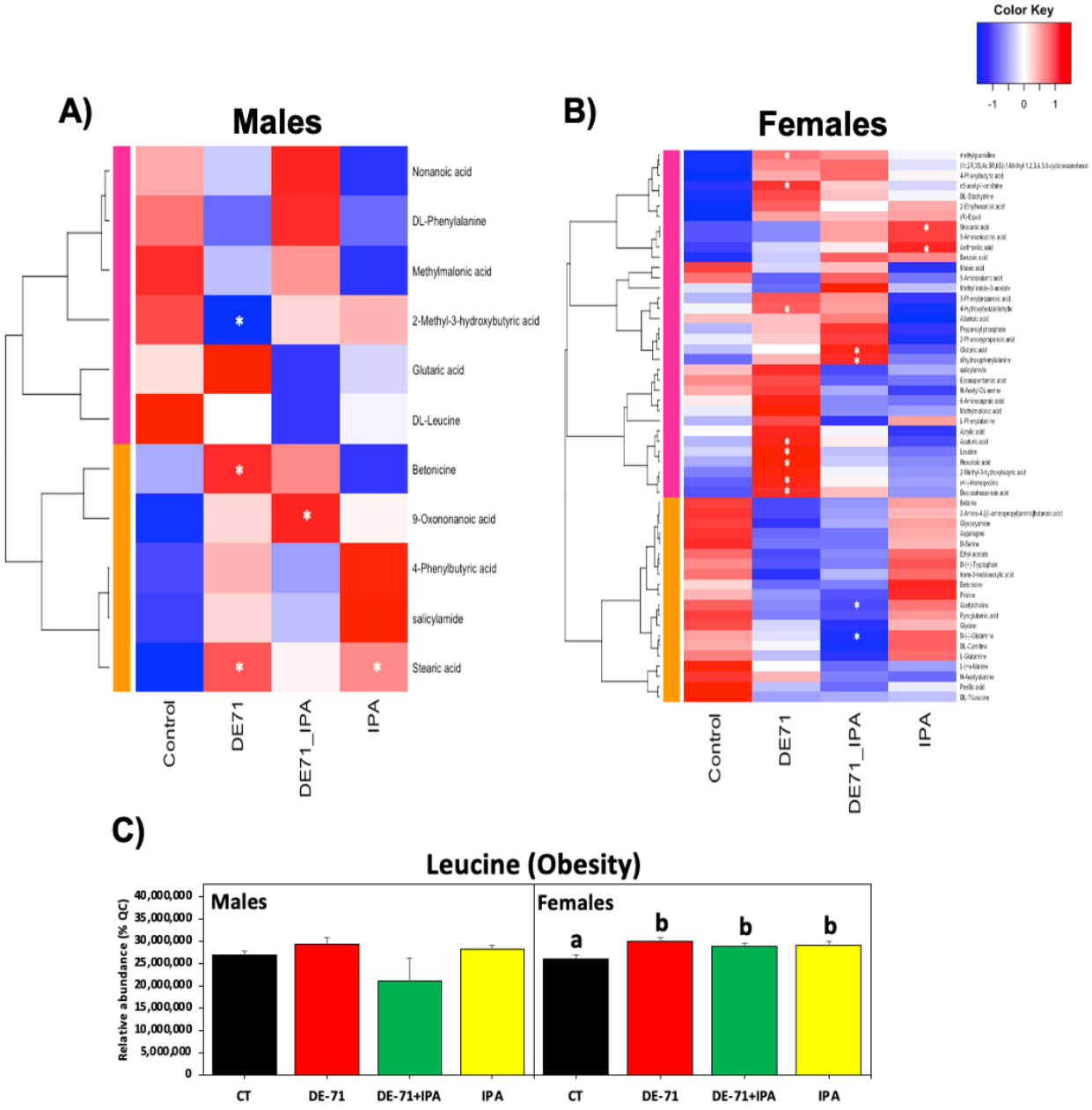
Color Key
-1
0
1
A)
Males
Nonanoic acid
DL-Phenylalanine
Methylmalonic acid
2-Methyl-3-hydroxybutyric acid
Glutaric acid
DL-Leucine
Betonicine
9-Oxononanoic acid
4-Phenylbutyric acid
salicylamide
Stearic acid
Control
DE71
DE71_IPA
IPA
B)
Females
Control
DE71
DE71_IPA
IPA
C)
Leucine (Obesity)
Males
Females
Relative abundance (% QC)
40,000,000
35,000,000
30,000,000
25,000,000
20,000,000
15,000,000
10,000,000
5,000,000
0
a
b
b
b
CT
DE-71
DE-71+IPA
IPA
CT
DE-71
DE-71+IPA
IPA

# Figure 7

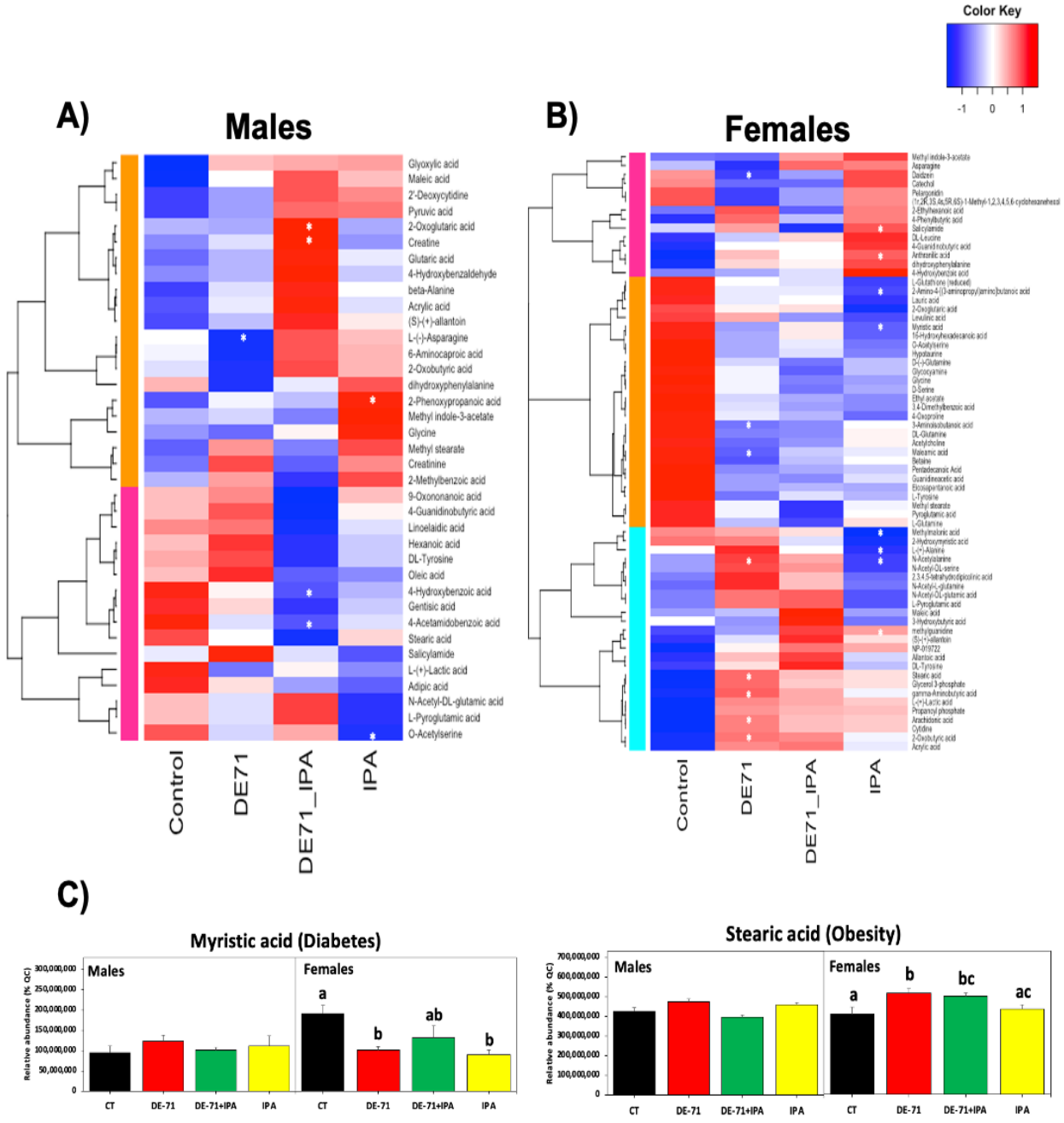
Color Key
-1
0
1
A)
Males
Glyoxylic acid
Maleic acid
2'-Deoxycytidine
Pyruvic acid
2-Oxoglutaric acid
Creatine
Glutaric acid
4-Hydroxybenzaldehyde
beta-Alanine
Acrylic acid
(S)-(+)-allantoin
L-(-)-Asparagine
6-Aminocaproic acid
2-Oxobutyric acid
dihydroxyphenylalanine
2-Phenoxypropanoic acid
Methyl indole-3-acetate
Glycine
Methyl stearate
Creatinine
2-Methylbenzoic acid
9-Oxononanoic acid
4-Guanidinobutyric acid
Linoelaidic acid
Hexanoic acid
DL-Tyrosine
Oleic acid
4-Hydroxybenzoic acid
Gentisic acid
4-Acetamidobenzoic acid
Stearic acid
Salicylamide
L-(+)-Lactic acid
Adipic acid
N-Acetyl-DL-glutamic acid
L-Pyroglutamic acid
O-Acetylserine
Control
DE71
DE71_IPA
IPA
B)
Females
Control
DE71
DE71_IPA
IPA
C)
Myristic acid (Diabetes)
Males
Females
Relative abundance (% QC)
CT
DE-71
DE-71+IPA
IPA
a
b
ab
b
Stearic acid (Obesity)
Males
Females
a
b
bc
ac

# Figure 8

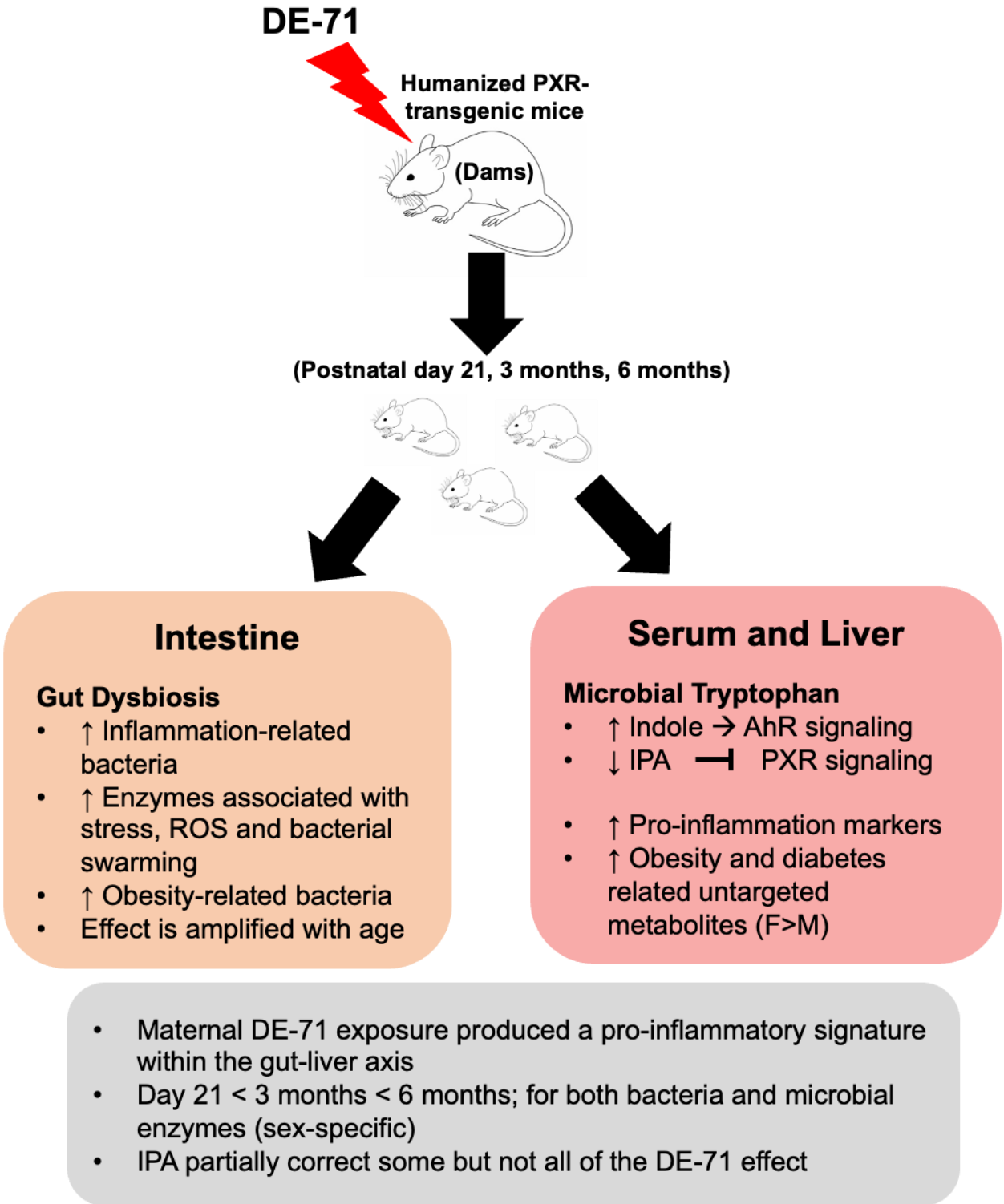
DE-71
Humanized PXR-transgenic mice
(Dams)
(Postnatal day 21, 3 months, 6 months)
Intestine
Gut Dysbiosis
• ↑ Inflammation-related bacteria
• ↑ Enzymes associated with stress, ROS and bacterial swarming
• ↑ Obesity-related bacteria
• Effect is amplified with age
Serum and Liver
Microbial Tryptophan
• ↑ Indole → AhR signaling
• ↓ IPA ⊣ PXR signaling
• ↑ Pro-inflammation markers
• ↑ Obesity and diabetes related untargeted metabolites (F>M)
• Maternal DE-71 exposure produced a pro-inflammatory signature within the gut-liver axis
• Day 21 < 3 months < 6 months; for both bacteria and microbial enzymes (sex-specific)
• IPA partially correct some but not all of the DE-71 effect

## SUPPLEMENTAL FIGURE LEGENDS

**Figure S1.** Differentially regulated bacteria at phylum level at PND 21 **(A)**, 3-months of age **(B)**, and 6-months of age **(C)**. Asterisks (*) represent statistically significant differences between the control group (two-way ANOVA; statistical significance was considered at $p < 0.05$).

**Figure S2.** Differentially regulated bacteria at class level at PND 21 **(A)**, 3-months of age **(B)**, and 6-months of age **(C)**. Asterisks (*) represent statistically significant differences between the control group (two-way ANOVA; statistical significance was considered at $p < 0.05$).

**Figure S3.** Differentially regulated DNA encoding bacterial enzymes in intestinal content (n = 5 per group) at PND 21 (A), 3-months of age **(B)**, and 6-months of age **(C)**. Statistical analysis was done by one-way ANOVA followed by Duncan's post hoc test, *p*-value < 0.05. Groups a, b, and ab represent different post hoc groups.

**Figure S4.** RT-qPCR quantification of mRNAs of the prototypical target genes of the major xenobiotic-sensing transcription factors in livers of male and female pups (n = 4-5 per group) at 21-days of age **(A)**, 3 months of age **(B)**, and 6-months of age **(C)**. Statistical analysis was done by one-way ANOVA followed by Duncan's post hoc test, *p*-value < 0.05. Groups a, b, ab, ac, and c represent different post hoc groups.

**Figure S5.** RT-qPCR quantification of mRNAs of the prototypical target genes of the major xenobiotic-sensing transcription factors in ileum of male and female pups (n = 4-5 per group) at 21-days of age **(A)** and 6-months of age **(B)**. Statistical analysis was done by one-way ANOVA followed by Duncan's post hoc test, p-value < 0.05. Groups a, b, ab, ac, and c represent different post hoc groups.

**Figure S6.** RT-qPCR quantification of inflammation-related mRNAs in the male and female livers of maternal DE-71 exposed hPXR pups (n = 4-5 per group). **A.** PND 21; **B.** 3-months of age; **C.**

6-months of age. Statistical analysis was done by one-way ANOVA followed by Duncan's post hoc test, p-value < 0.05. Groups a, b, ab, ac, and c represent different post hoc groups.

**Figure S7.** H&E staining of livers of mouse pups of the four exposure groups at PND 21, 3-months of age, and 6-months of age.

**Figure S8.** Quantification of PBDE concentrations in the liver samples using GC-MS. **A.** Concentration of BDE-47 in the livers of different groups. **B.** Concentration of BDE-99 in the livers of different groups. We found no or minimal levels of these chemicals in the samples.

# Figure S1

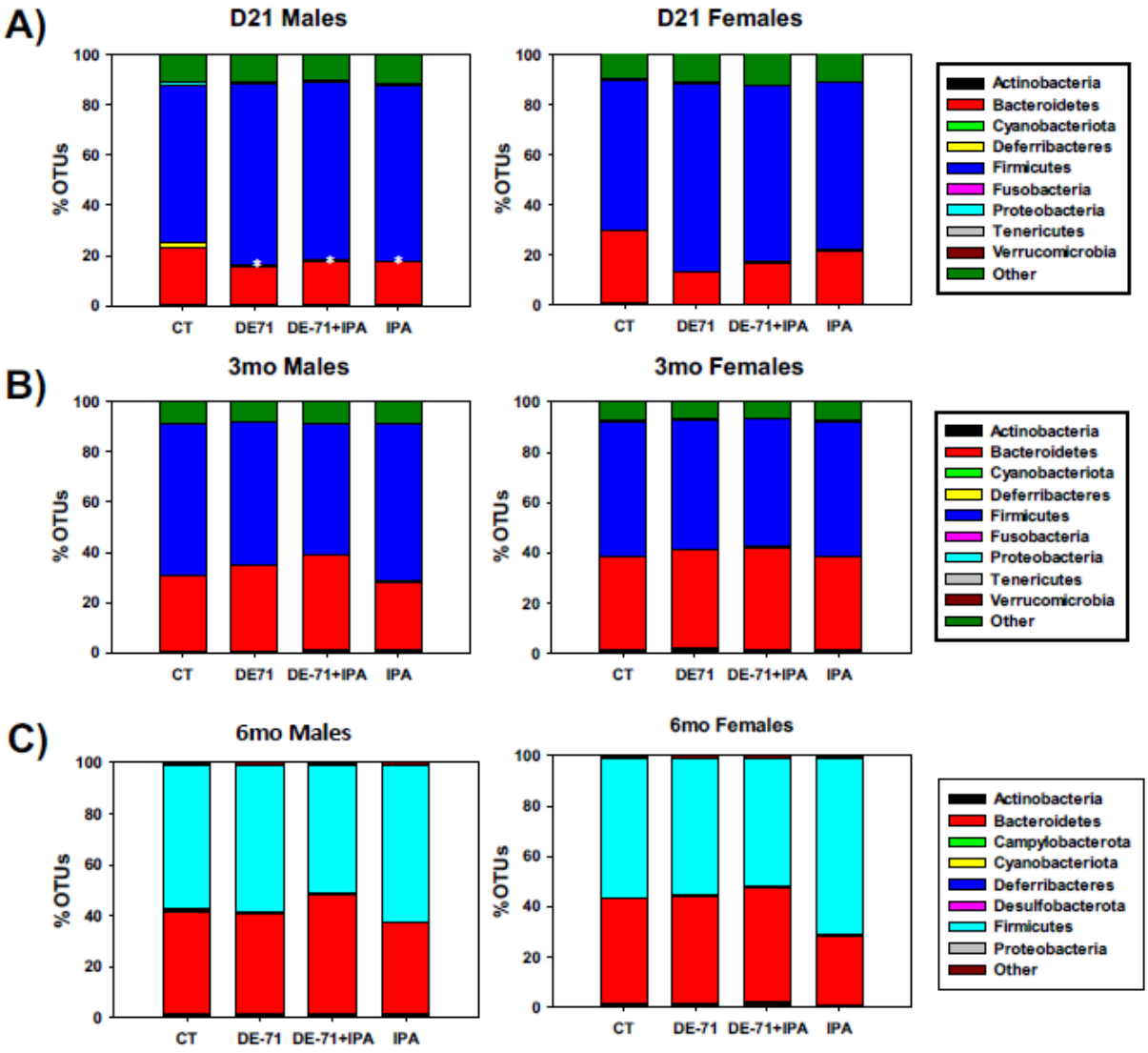
A)
D21 Males
D21 Females
B)
3mo Males
3mo Females
C)
6mo Males
6mo Females
% OTUs
CT
DE71
DE-71
DE-71+IPA
IPA
Actinobacteria
Bacteroidetes
Campylobacterota
Cyanobacteriota
Deferribacteres
Desulfobacterota
Firmicutes
Fusobacteria
Proteobacteria
Tenericutes
Verrucomicrobia
Other

# Figure S2

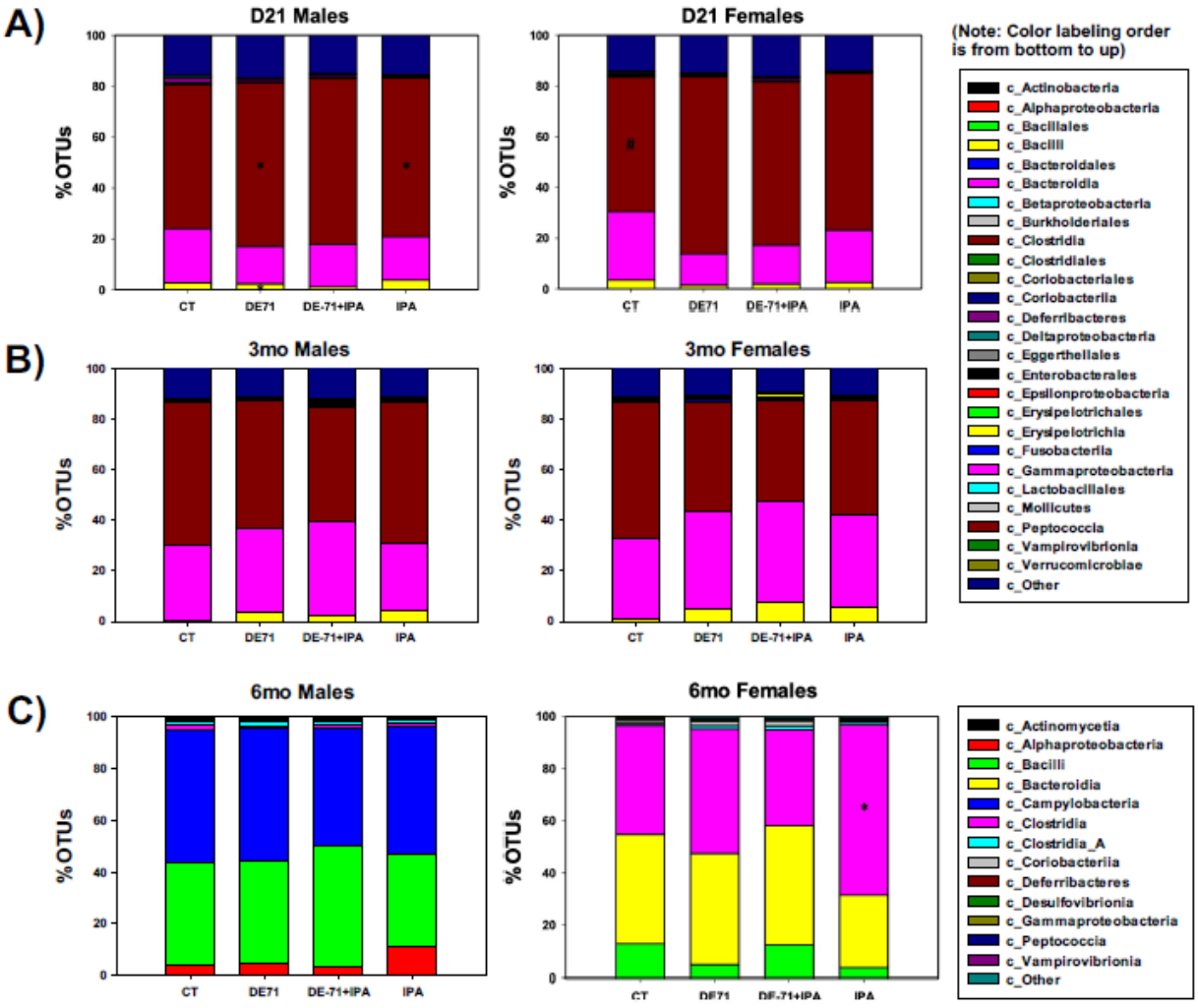
A)
D21 Males
D21 Females
B)
3mo Males
3mo Females
C)
6mo Males
6mo Females
% OTUs
CT
DE71
DE-71+IPA
IPA
(Note: Color labeling order is from bottom to up)
c_Actinobacteria
c_Alphaproteobacteria
c_Bacillales
c_Bacilli
c_Bacteroidales
c_Bacteroidia
c_Betaproteobacteria
c_Burkholderiales
c_Clostridia
c_Clostridiales
c_Coriobacteriales
c_Coriobacteriia
c_Deferribacteres
c_Deltaproteobacteria
c_Eggerthellales
c_Enterobacterales
c_Epsilonproteobacteria
c_Erysipelotrichales
c_Erysipelotrichia
c_Fusobacteriia
c_Gammaproteobacteria
c_Lactobacillales
c_Mollicutes
c_Peptococcia
c_Vampirovibrionia
c_Verrucomicrobiae
c_Other
c_Actinomycetia
c_Alphaproteobacteria
c_Bacilli
c_Bacteroidia
c_Campylobacteria
c_Clostridia
c_Clostridia_A
c_Coriobacteriia
c_Deferribacteres
c_Desulfovibrionia
c_Gammaproteobacteria
c_Peptococcia
c_Vampirovibrionia
c_Other

# Figure S3

## A) Day 21

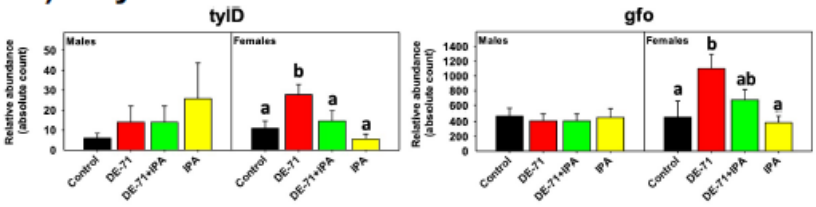


## B) 3 months

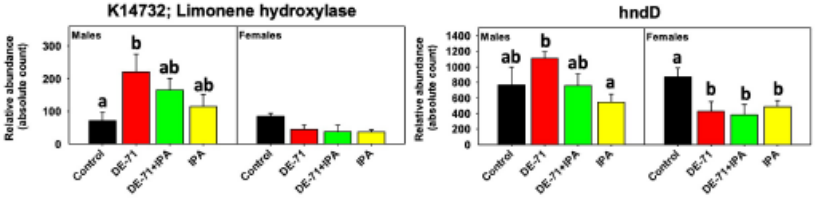


## C) 6 months

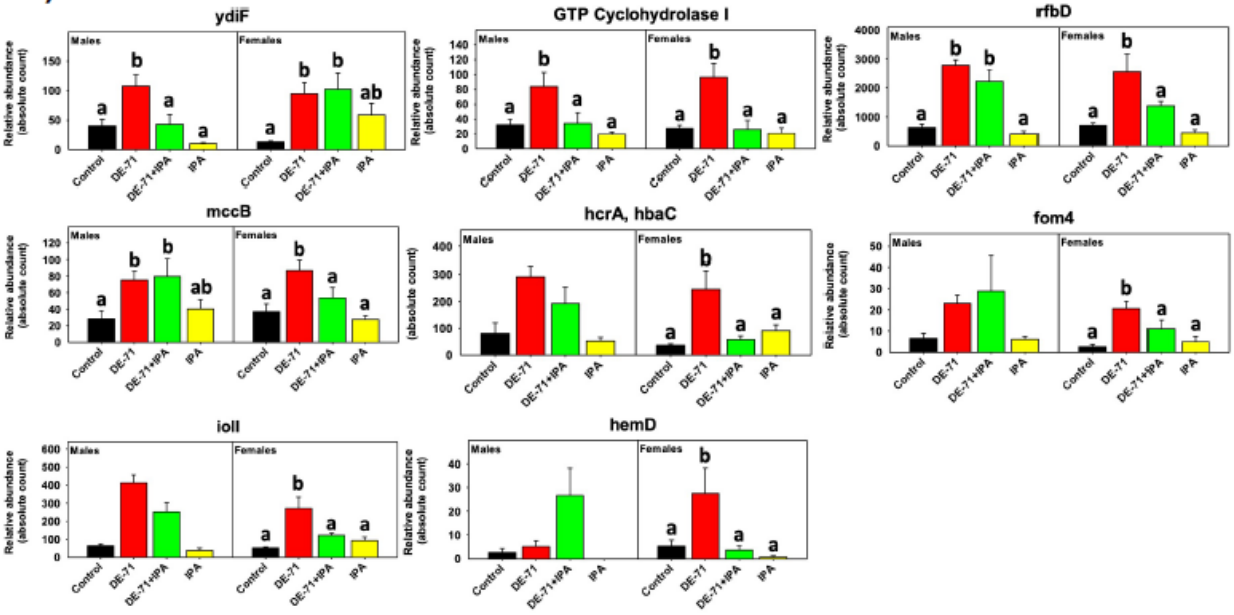

# Figure S4

## A) Day 21

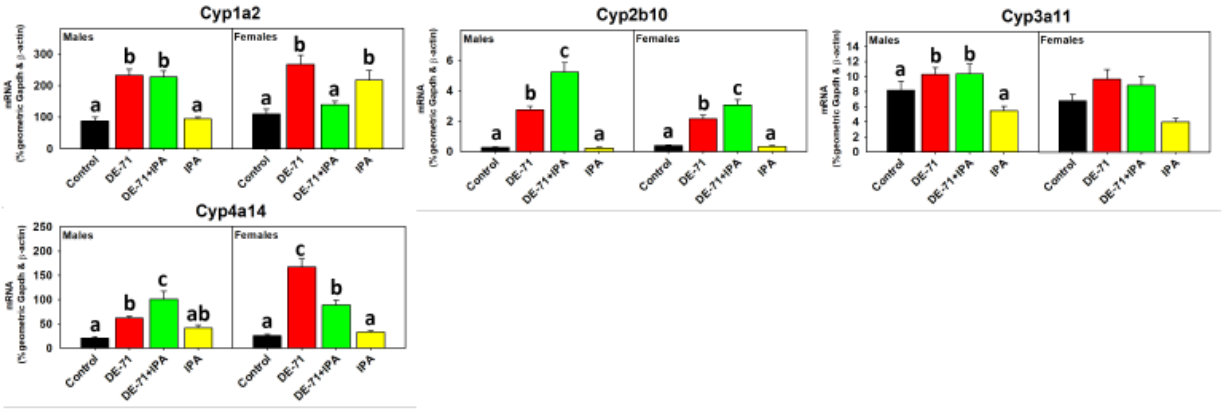


## B) 3 months

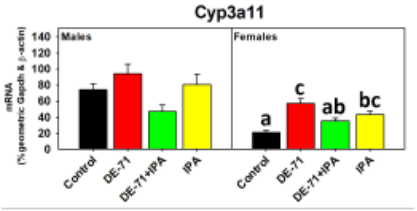


## C) 6 months

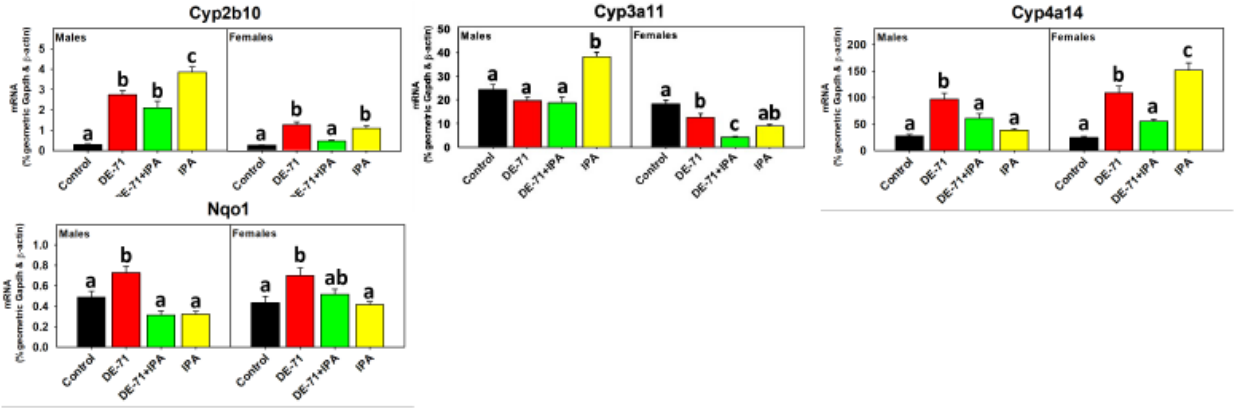

# Figure S5

## A) Day 21

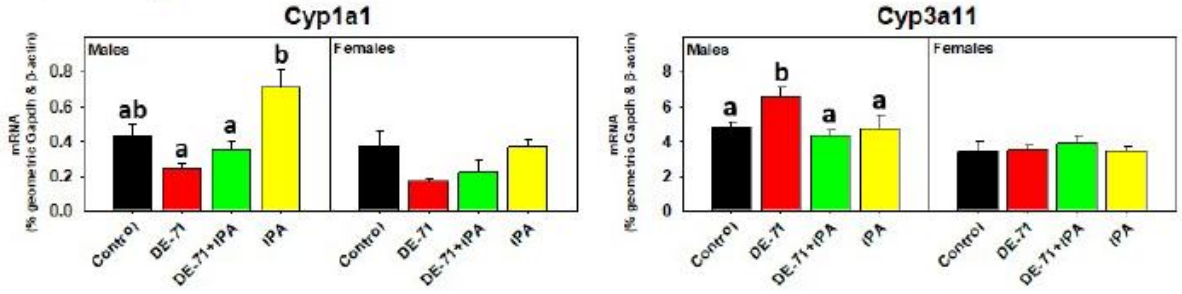


## B) 6 months

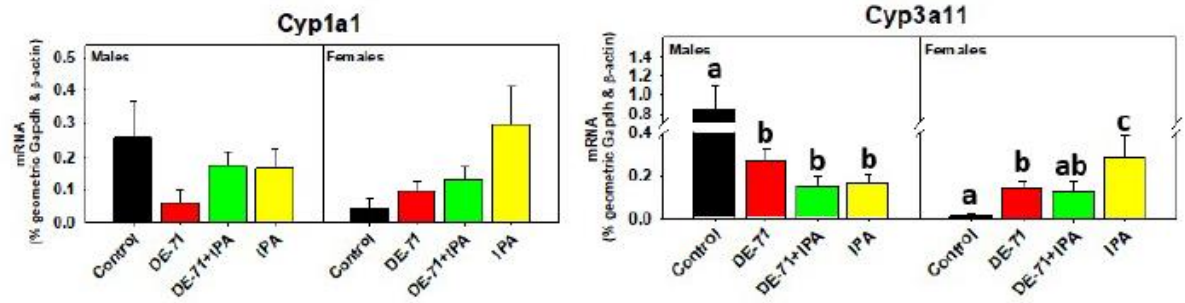

# Figure S6

## A) Day 21

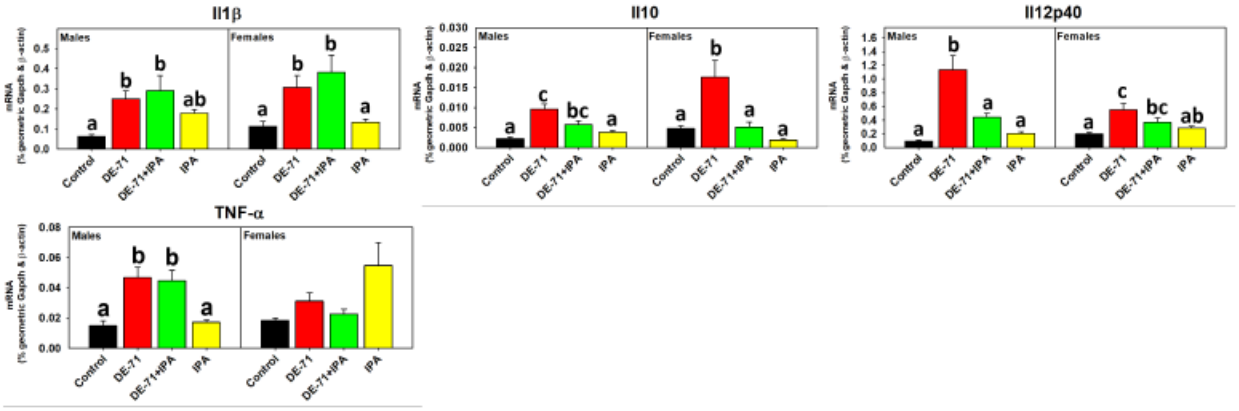


## B) 3 months

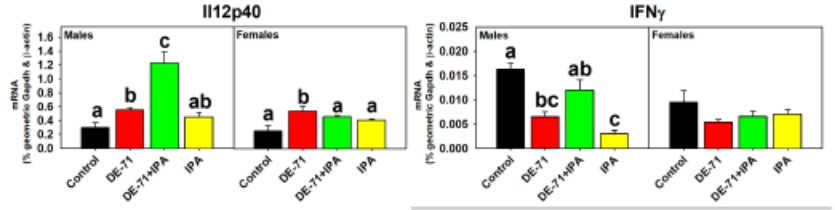


## C) 6 months

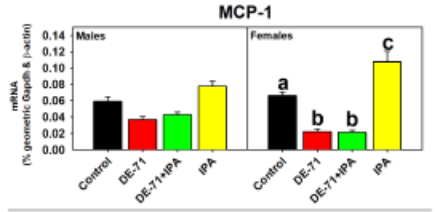

# Figure S7

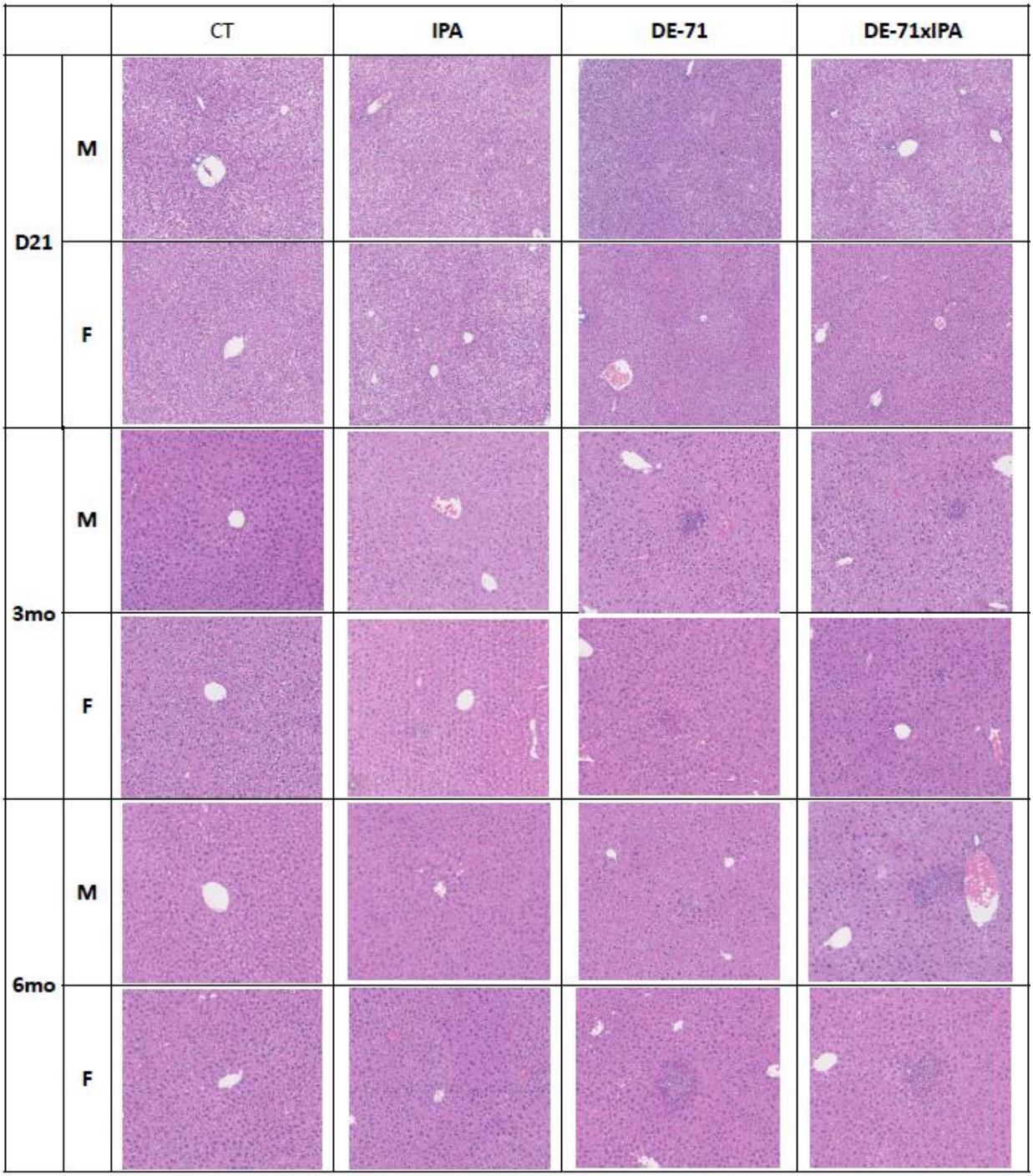

# Figure S8

A)

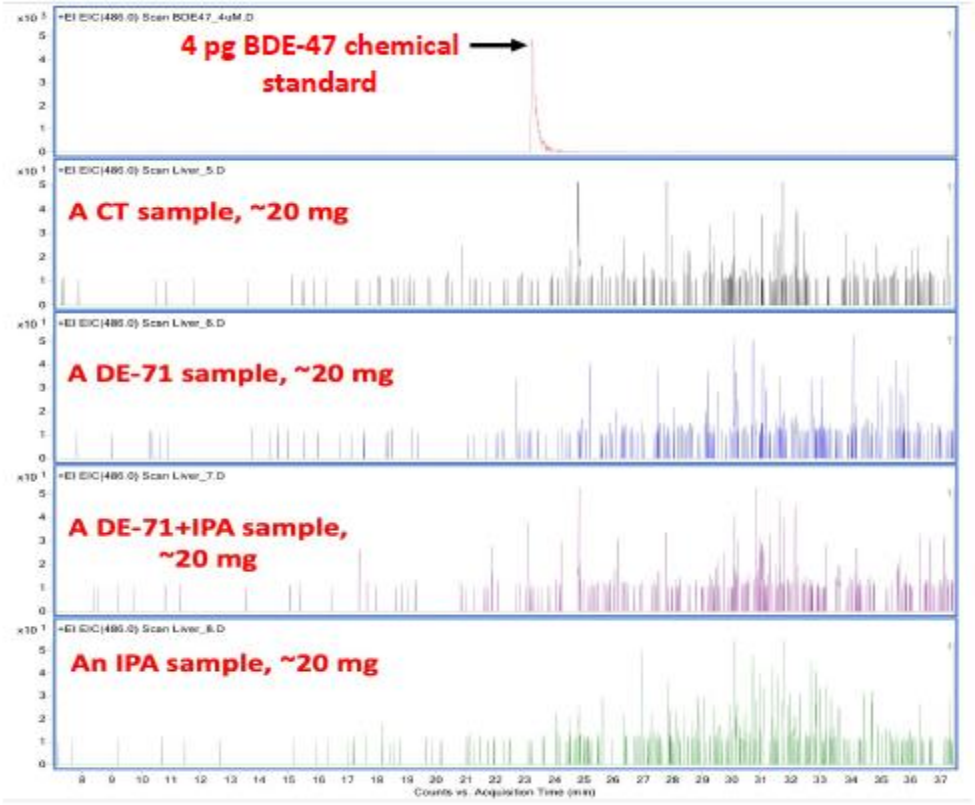
4 pg BDE-47 chemical standard
A CT sample, ~20 mg
A DE-71 sample, ~20 mg
A DE-71+IPA sample, ~20 mg
An IPA sample, ~20 mg
Counts vs. Acquisition Time (min)

B)

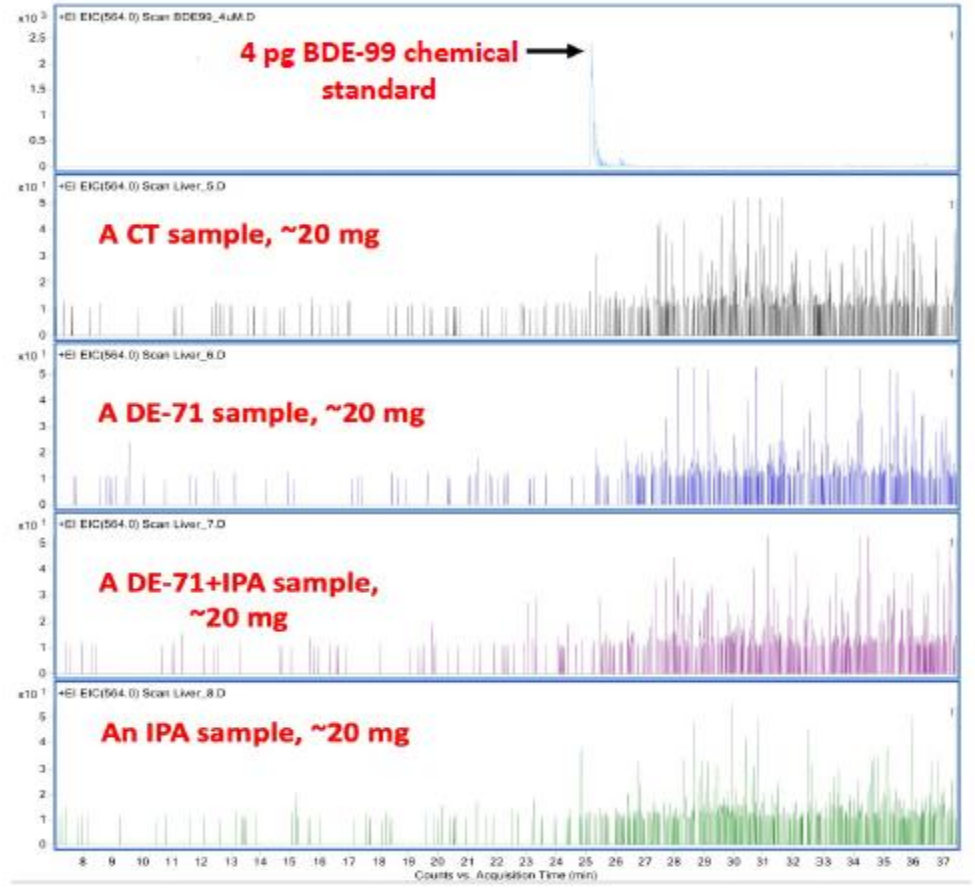
4 pg BDE-99 chemical standard
A CT sample, ~20 mg
A DE-71 sample, ~20 mg
A DE-71+IPA sample, ~20 mg
An IPA sample, ~20 mg
Counts vs. Acquisition Time (min)

## Chapter 4

**Exploring the chemical basis of the gut microbiome-driven tryptophan metabolism and tissue-specific responses via metabolic flux analysis in male humanized PXR-transgenic mice**

*I plan to submit this work to Drug Metabolism and Disposition.*

**ABSTRACT**

The host nuclear receptor pregnane X receptor (PXR) and the gut microbiome are both critical regulators of xenobiotic metabolism and metabolic diseases. These systems are intrinsically linked, as several microbial metabolites have been identified as endogenous activators of PXR. One such metabolite is indole-3-propionic acid (IPA), a tryptophan-derived compound known to have anti-inflammatory and anti-obesity properties. In this study, we utilized $^{13}C_{11}$-L-tryptophan isotope tracing-based metabolic flux analysis to examine gut microbiome-dependent tryptophan metabolism in vivo, using both conventional (CV) and germ-free (GF) humanized PXR-transgenic (hPXR-TG) mice. We hypothesized that the presence or absence of the gut microbiome would differentially influence the incorporation of tryptophan-derived carbons into host metabolic pathways in a tissue-specific manner. Three-month-old male CV and GF hPXR-TG mice (n = 3-4 per group) were orally administered $^{13}C_{11}$-L-tryptophan (20 mg/kg), and tissues including serum, liver, duodenum, jejunum, ileum, colon, and brain were harvested 30 min post-gavage. LC-MS-based metabolic flux analysis revealed distinct compartmentalized metabolic profiles between CV and GF mice, as shown by principal component analysis. The colon exhibited the greatest number of gut microbiome-dependent metabolites incorporating tryptophan-derived carbons, followed by the small intestine and liver, while the brain was minimally affected likely due to restricted metabolite transport across the blood-brain barrier. Interestingly, indoxyl sulfate, a known product of host sulfotransferase (Sult) from indole, was elevated in the liver and various intestinal regions of GF mice, consistent with previous findings of Sult upregulation in GF models. The absence of the gut microbiome redirected tryptophan-derived carbon flux into several amino acid metabolic pathways across the liver and intestine. These pathways include homocysteine and methionine (linked to cardiovascular function), glutathione and cysteine (antioxidant defense),

neurotransmitter-related pathways (glutamate, tyrosine, taurine), immune-related amino acids (lysine, histidine), and key metabolic regulators (serine, aspartate, glycine, and branched-chain amino acids). Additionally, pathways including bile acid biosynthesis, purine metabolism, and fatty acid and caffeine metabolism were impacted. In conclusion, these results demonstrate that the gut microbiome plays a fundamental role in directing the fate of dietary tryptophan, modulating its transformation and incorporation into host metabolic networks in a tissue-specific manner. These findings underscore the extensive impact of host-microbiome interactions on systemic metabolism and provide mechanistic insight into how microbiome alterations may influence disease susceptibility.

## INTRODUCTION

Metabolic flux analysis (MFA) is a powerful quantitative approach for determining the rates of metabolic reactions within cells. By combining isotopic labeling experiments with computational modeling, MFA enables the tracking of metabolite flow through cellular biochemical networks. This methodology provides critical insights into cellular metabolism, identifying key regulatory nodes and rate-limiting steps. MFA has proven particularly valuable in metabolic engineering, where it guides the optimization of microbial systems for enhanced production of biofuels, pharmaceuticals, and other high-value compounds by adjusting specific metabolic fluxes (Di Domenico et al. 2017; Shi et al. 2020). Moreover, isotope tracing-based MFA reveals how metabolic pathways are reprogrammed in response to environmental perturbations, offering deeper insights into cellular physiology and potential avenues for therapeutic targeting (Sauer 2006).

Metabolism underpins nearly all biological processes, and disruptions in metabolic function often signal underlying health problems or directly contribute to conditions such as metabolic syndrome, cardiovascular disease, neurological disorders, and cancer (DeBerardinis and Thompson 2012; Matsumoto and Kuhara 1996). Resources like the Kyoto Encyclopedia of Genes and Genomes (KEGG) provide comprehensive annotations of metabolites and pathways, offering critical insights into disease mechanisms. A well-known example is the Warburg effect, a metabolic hallmark of many cancers, in which cells preferentially utilize glycolysis over oxidative phosphorylation even in the presence of oxygen (J. Kim and Dang 2006). This metabolic reprogramming results in elevated lactate production, supporting rapid cell proliferation and tumor progression (Vander Heiden, Cantley, and Thompson 2009; Martinez-Outschoorn et al. 2017). Such shifts highlight the importance of integrating metabolite profiling with genomic and

proteomic data to uncover disease mechanisms and identify novel therapeutic targets, reinforcing metabolism as a pivotal and dynamic area of biomedical research.

Pregnane X receptor (PXR) is an essential nuclear receptor that bridges host metabolism and the gut microbiome. Predominantly expressed in the liver and intestines, PXR serves as a xenobiotic sensing nuclear receptor that regulates the transcription of genes involved in xenobiotic biotransformation, lipid metabolism, and immune modulation (Xie and Chiang 2013; Kliewer, Goodwin, and Willson 2002). Recent studies highlight the bidirectional interplay between PSR and the gut microbiome, showing that PXR activation can remodel microbial communities and alter the production of microbial metabolites with implications for host metabolic health and disease (Little et al. 2022; Dempsey et al. 2019; Mohandas and Vairappan 2017; Koppel, Maini Rekdal, and Balskus 2017; Drissi et al. 2014). Microbial-derived metabolites can modulate PXR activity thereby influencing the expression of genes governing inflammation and metabolic homeostasis (Venkatesh et al. 2014b). This dynamic crosstalk positions PXR as a central mediator in host-microbe interactions. Several microbial metabolites are known PXR ligands, where lithocholic acid (LCA), a secondary bile acid generated by gut microbiota, activates PXR to promote detoxification pathways and reduce bile acid toxicity (Staudinger et al. 2001). Another key microbial metabolite, indole-3-propionic acid (IPA), a tryptophan derivative produced by *Clostridium sporogenes*, also activates PXR and has been associated with antioxidant properties and enhance intestinal barrier integrity (Venkatesh et al. 2014a). Together, these findings highlight the essential role of microbial metabolites in regulating PXR activity and underscore the importance of PXR in maintaining metabolic and immune balance through its interactions with the gut microbiome.

Mouse and human PXR differ significantly in their ligand-binding specificity and transcriptional activity due to sequence variations within their ligand-binding domains. Human PXR (hPXR) exhibits broader ligand promiscuity, being activated by compounds such as rifampin and LCA, whereas mouse PXR (mPXR) is selectively responsive to ligands like pregnenolone 16α-carbonitrile (PCN) (Moore et al. 2003). These species-specific distinctions have led to the development of humanized PXR-transgenic (hPXR-TG) mouse models, which serve as a valuable platform for investigating human-relevant PXR activation. hPXR-TG mice replicate human-specific drug responses and pharmacokinetic interactions and enable mechanistic studies of microbial metabolites like LCA and IPA, which preferentially activate hPXR (Ma et al. 2007). Originally generated by Frank Gonzalez and colleagues, this transgenic model provides a critical translational tool for studying human PXR biology in vivo (Ma et al. 2007).

MFA is most commonly conducted in in vitro systems, such as cultured cells or isolated tissues, where experimental conditions can be tightly controlled to investigate specific metabolic pathways (H. He et al. 2020). These in vitro models provide valuable insights into cellular metabolism and are well-suited for mechanistic studies. However, a key limitation of in vitro MFA is the lack of physiological complexity, particularly the absence of multi-organ interactions that critically influence systemic metabolic flux. Furthermore, tissue-specific differences in metabolite bioavailability and the expression of metabolic enzymes can result in differential incorporation of labeled carbons across organs, limiting the extrapolation of in vitro findings to in vivo contexts.

Therefore, the objective of this study was to implement MFA in an in vivo system to enable comprehensive tracing of metabolite incorporation across multiple bio-compartments. Specifically, we employed $^{13}C_{11}$-L-tryptophan isotope tracing-based MFA in conventional (CV) and germ-free (GF) hPXR-TG mice to investigate gut microbiome-dependent tryptophan

metabolism and tissue-specific metabolic responses in vivo. We hypothesized that the presence or absence of the gut microbiome would distinctly influence the incorporation of tryptophan-derived carbons into host metabolic pathways in a tissue-specific manner.

## MATERIALS AND METHODS

### Chemical preparation

The overall experimental design is illustrated in Figure 1. The $^{13}C_{11}$-labeled L-tryptophan isotope was provided by Dr. Haiwei Gu at Arizona State University (No. 202114-65-5, Cambridge Isotope Laboratories, Inc.). Tryptophan isotope (20 mg/kg) was prepared in freshwater. The mixture was then aliquoted into 1.5 mL tubes and stored at -80°C until use.

### Animals and exposures

The hPXR-TG mice were generously provided by Dr. Frank Gonzalez (National Cancer Institute, Bethesda, MD), as previously described (Ma et al. 2007). Breeder pairs were acclimated to the animal facility at the University of Washington and bred for at least two generations prior to experimentation. All mice were housed in accordance with the guidelines of the Association for Assessment and Accreditation of Laboratory Animal Care International (AAALAC). Animals were maintained in individually ventilated cages with autoclaved Enrich-N'Pure bedding (Andersons, Maumee, OH) and had *ad libitum* access to non-acidified, autoclaved drinking water with LabDiet 5010 chow (St. Louis, MO). All procedures approved by the Institutional Animal Care and Use Committee (IACUC) at the University of Washington. At 3 months of age, males CV and GF hPXR-TG male mice (n = 3-4 per group) were orally gavaged with 20 mg/kg of $^{13}C_{11}$-labeled L-tryptophan. In addition, 6 months of age males CV and GF male mice received identical

treatment (n = 3-4 per group). Thirty min following oral gavage, animals were euthanized via $CO_2$ for tissue collection. Whole blood was obtained via cardiac puncture and transferred to MiniCollect serum separator tubes (Greiner Bio-One, Kremsmünster, Austria), held on ice for a minimum of 30 min to allow coagulation, and centrifuged at 4,000 rpm (1,503 × g) for 20 min at 4°C. Serum was collected and stored at −80°C. Large intestinal contents (LICs) were flushed with 10 mL of ice-cold phosphate-buffered saline (PBS), immediately snap-frozen on dry ice, and stored at −80°C. Liver and brain tissues were flash-frozen in liquid nitrogen and stored at −80°C until further use.

**Large-scale targeted LC-MS/MS metabolomics**

The large-scale targeted LC-MS/MS method employed in this study was adapted from established protocols used in previous research (Carroll et al. 2015a; Eghlimi et al. 2020; Jasbi et al. 2019; Shi et al. 2020; Gu et al. 2015a). All analyses were conducted using an Agilent 1290 UPLC coupled to a 6490 triple quadrupole mass spectrometer (QQQ-MS; Agilent Technologies, Santa Clara, CA). Approximately 20 mg of each tissue sample was homogenized in 200 µL of methanol:phosphate-buffered saline (MeOH:PBS, 4:1, v/v) containing 1810.5 µM $^{13}C_3$-lactate and $^{13}C_5$-glutamic acid, using a Bullet Blender homogenizer (Next Advance, Averill Park, NY). These isotopically labeled internal standards were included to monitor instrument stability rather than for the quantification of indoles. Following homogenization, an additional 800 µL of the MeOH:PBS extraction buffer was added, and the samples were vortexed for 10 s, incubated at −20°C for 30 min, and then sonicated in an ice bath for 30 min. Samples were centrifuged at 14,000 rpm for 10 min at 4°C, and 800 µL of the supernatant was transferred to new tubes and dried under vacuum using a CentriVap Concentrator (Labconco, For Scott, KS). Prior to LC-MS analysis, the dried

extracts were reconstituted in 150 µL of 60% acentonitrile (ACN)/40% PBS. Each sample was injected twice: 10 µL for negative ion mode and 4 µL for positive ion mode. Chromatographic separation was performed in hydrophilic interaction liquid chromatography (HILIC) mode using a Waters XBridge BEH Amide column (150 x 2.1 mm, 2.5 µm particle size; Waters Corporation, Milford, MA). The mobile phases consisted of Solvent A (10 mM ammonium acetate, 10 mM ammonium hydroxide in 95% $H_2O$/5% ACN) and Solvent B (10 mM ammonium acetate, 10 mM ammonium hydroxide in 95% ACN/5% $H_2O$). The gradient began with 90% B for 1 min, decreased to 40% B over 11 min, held for 4 min, and then returned to 90% B for column re-equilibration. The flow rate was 0.3 mL/min, with the autosampler maintained at 4°C and the column at 40°C. Mass spectrometric detection was performed using an ESI source in multiple-reaction monitoring (MRM) mode. Data acquisition and instrument control were conducted using Agilent MassHunter Workstation software, and peak integration was performed with Agilent MassHunter Quantitative Analysis software (Agilent Technologies, Santa Clara, CA).

**Statistical analysis**

One-way or two-way analysis of variance (ANOVA) followed by Duncan's post hoc test was performed within each sex and species group to assess the effects of tryptophan isotope incorporation. Statistical significance was determined at an adjusted $p$-value < 0.05 using SPSS software Version 29.0.1.0 (IBM, Armonk, NY). For principal component analysis (PCA) and volcano plots, prcomp function and limma R packages were used and controlled for errors of multiple testing (adjusted $p$-value < 0.05).

## RESULTS

### Metabolic flux analysis in male conventional (CV) and germ-free (GF) mice

To assess how the presence or absence of the gut microbiome influences the incorporation of tryptophan-derived carbons into host metabolic pathways, large-scale targeted LC-MS/MS metabolomics was performed on tissues collected 30 min after oral gavage with $^{13}C_{11}$-L-tryptophan in male CV and GF mice. Principal component analysis (PCA) and volcano plots revealed distinct metabolic flux profiles in serum, liver, and brain tissues between CV and GF groups, highlighting systemic differences in tryptophan metabolism (Figure 2).

In parallel, analysis of gastrointestinal compartments, including the duodenum, jejunum, ileum, and colon, demonstrated compartment-specific metabolic flux differences between CV and GF mice (Figure 3). Each intestinal region exhibited unique metabolic signatures, reflecting spatial heterogeneity and underscoring the gut microbiota's influence on localized tryptophan metabolism.

Collectively, the PCA plots in Figures 2 and 3 revealed clear separation between CV an GF groups across all examined tissues, indicating that the microbiome plays a pivotal role in shaping tissue-specific metabolic landscapes. Volcano plot analyses further identified key metabolic features altered by microbiome status, emphasizing the microbiota's role in regulating both systemic and intestinal metabolic homeostasis.

### Enriched metabolite pathway analysis in male CV and GF mice

Pathway enrichment analysis revealed distinct and tissue-specific alterations in metabolite regulation between CV and GF male mice across serum, liver, and intestinal compartments (Figure 4). In serum, the most significantly enriched pathways included glutathione metabolism, aspartate

metabolism, and tryptophan metabolism. Glutathione metabolism exhibited the highest enrichment ratio, indicating a robust systemic response to microbial absence, particularly in redox and amino acid pathways. In the liver, enrichment was observed in aspartate metabolism, tyrosine metabolism, and purine metabolism, highlighting the liver's central role in amino acid and nucleotide processing influenced by tryptophan-derived flux. Within the duodenum, purine metabolism, taurine and hypotaurine metabolism, and glutathione metabolism were significantly enriched, suggesting heightened nucleotide synthesis and sulfur amino acid processing at the proximal intestinal segment. In the ileum, homocysteine and methionine metabolism were notably enriched, with homocysteine metabolism showing the highest enrichment ratio across all tissues analyzed. This finding underscores the ileum's role in sulfur amino acid metabolism and one-carbon/methylation pathways. In the colon, diverse pathways including homocysteine degradation, taurine and hypotaurine metabolism, and tryptophan metabolism were enriched, suggesting enhanced sulfur compound detoxification and microbial-host co-metabolism in this compartment. Overall, these results demonstrate that the absence of the gut microbiota induces tissue-specific metabolic rewiring, especially impacting amino acid, nucleotide, and sulfur-containing compound pathways along the gut-liver axis.

**Differentially regulated metabolites between male CV and GF mice**

Two-way hierarchical clustering analysis revealed distinct patterns of metabolite regulation across serum, liver, and intestinal tissues in male CV and GF mice (Figure 5). The heatmaps illustrate compartment-specific metabolomic differences, while the accompanying Venn diagram highlights overlapping and unique metabolite alterations across tissues.

In the serum, 18 metabolites were significantly upregulated in GF mice. Notably, *p*-cresyl

sulfate, a uremic toxin associated with oxidative stress and chronic kidney disease, was elevated (Gryp et al. 2017). Similarly, 3β-hydroxy-5-cholenoic acid, a primary bile acid associated in hepatobiliary dysfunction, was increased likely due to impaired microbial conversion to secondary bile acids in the absence of a microbiome (Sugiyama et al. 1986; Heinken et al. 2019). Indoleacrylic acid, a microbial tryptophan metabolite known to enhance epithelial barrier integrity and suppress inflammation, was also elevated (Wlodarska et al. 2017). In contrast, seven serum metabolites were significantly downregulated in GF mice. These included N-acetylaspartic acid, a precursor of the neuropeptide acetyl aspartyl glutamate, with roles in brain energy homeostasis and axon-glial signaling (Moffett et al. 2007). Acetyl-β-methylcholine, a parasympathetic muscarinic agonist involved in gastrointestinal motility, was also reduced (Fisher et al. 2004; Lopes et al. 2006). In addition, n-benzylformamide, an alcohol dehydrogenase inhibitor involved in detoxification, was significantly decreased (Schindler, Berst, and Plapp 1998). These changes suggest that microbial absence disrupts systemic metabolic functions related to inflammation, detoxification, bile acid metabolism, and neuromodulation.

In the liver, 13 metabolites were significantly upregulated in GF mice. This included adenyl succinic acid, a compound shown to enhance insulin secretion and reverse β-cell dysfunction (Gooding et al. 2015), and indoxyl sulfate, a microbial metabolite linked to tight junction disruption and oxidative stress-induced liver and kidney injury (Y. Huang et al. 2020; W.-C. Liu, Tomino, and Lu 2018). Nine liver metabolites were significantly downregulated in GF mice. As observed in serum, n-benzylformamide was decreased, reinforcing the theme of disrupted detoxification. In addition, docosatetraenoylethanolamide, an anti-inflammatory ethanolamide that interacts with cannabinoid receptors, was downregulated (Hanus et al. 1993; Alhouayek et al. 2017). These findings indicate that the absence of gut microbiota leads to pronounced alterations

in host metabolite profiles, especially in pathways related to inflammatory regulation, bile acid metabolism, neuronal signaling, and detoxification. These shifts underscore the microbiome's central role in maintaining systemic metabolic homeostasis.

In the intestinal compartments, heatmaps revealed distinct clustering patterns across the duodenum, jejunum, ileum, and colon, indicating a high degree of tissue-specific metabolic regulation. In the duodenum, 51 metabolites were significantly upregulated in GF mice. Among these, adenylsuccinic acid and indoxyl sulfate were also elevated in the liver, suggesting consistent systemic alterations. Reduced glutathione, a key antioxidant involved in inflammation control and detoxification, was upregulated in GF mice; dysregulation of its metabolism has been implicated in cancer and neurodegenerative disease (Vickers, Fisher, and Sinclair 2010; Townsend, Tew, and Tapiero 2003). Conversely, 19 metabolites were significantly downregulated in the duodenum of GF mice. Val-Ser, a dipeptide involved in amino acid metabolism, was significantly reduced and has been associated with gastrointestinal disorders such as ulcerative colitis and irritable bowel syndrome (Schirmer et al. 2024; X.-Y. Zhao et al. 2019). These findings indicate the critical role of the gut microbiome in modulating duodenal metabolic functions, particularly those related to inflammation, antioxidant defense, and amino acid homeostasis.

In the jejunum, 33 metabolites were significantly upregulated in GF mice. Notably, N-acetylornithine, an intermediate in arginine biosynthesis and the urea cycle, was elevated where reduced levels of this metabolite have been associated with liver disease (Soga et al. 2011). Acetyl-β-methylcholine was also increased, in contrast to its downregulation in serum. Indoxyl sulfate, a uremic toxin, was elevated in the jejunum, consistent with its increase in the duodenum and liver. Meanwhile, 9 metabolites were involved in oxidative stress mitigation and anti-inflammatory responses (Pekala et al. 2011; Fortin 2011), and methyldopa, an L-tyrosine derivative with

immunomodulatory properties (Ostrov et al. 2018). These changes reflect the microbiome's role in regulating amino acid metabolism, detoxification, and inflammatory processes in the jejunum.

In the ileum, 39 metabolites were significantly upregulated in GF mice. Indoxyl sulfate and acetyl-β-methylcholine were again elevated, indicating persistent effects across intestinal regions. In contrast, 22 metabolites were significantly downregulated. These included genistein, an isoflavonoid with tumor-suppressive activity (Brown et al. 2016; Walsh et al. 2007), and furoic acid, known to inhibit fatty acid and cholesterol synthesis and associated with cancer risk (Guseva et al. 2011; Seow et al. 2019). These findings suggest the microbiome regulates pathways related to oxidative stress, intestinal signaling, and oncogenic suppression in the ileum.

The colon exhibited the most extensive metabolic alterations, with 88 metabolites significantly increased and 59 metabolites decreased in GF mice. Upregulated metabolites included adenylsuccinic acid, reduced glutathione, and p-cresylsulfate, all of which were elevated in other tissues as well. Notably, hypaphorine, an indole alkaloid with anti-obesity, insulin-sensitizing, and anti-inflammatory properties, was significantly downregulated (Sun et al. 2017; Luan et al. 2017). Other downregulated compounds included 1-(β-D-ribofuranosyl)thymine, involved in tRNA stability and linked to colorectal cancer (Altobelli, Angeletti, and Latella 2016), and daidzein-7-O-glucuronide, an antioxidant isoflavonoid (Islam et al. 2015). These alterations emphasize the critical role of the gut microbiome in modulating colon-specific detoxification and metabolic disease susceptibility.

Brain tissue exhibited the fewest differentially regulated metabolites, with three significantly upregulated and four downregulated in GF mice. Among the upregulated metabolites, tixocortol, a glucocorticoid receptor agonist, suggesting potential modulation of stress, metabolism, and inflammation (Frank, Ortlund, and Liu 2021). Pilocarpine, a muscarinic agonist

and therapeutic agent for glaucoma, was also elevated, indicating altered cholinergic signaling (Carlson and Kraus 2025). Conversely, cladribine, an immunosuppressive and antineoplastic agent (Liliemark 1997), was significantly downregulated, alongside 2,3,4,5-tetrahydrodipicolinic acid, a bacterial lysine synthesis intermediate (Angrish, Lalwani, and Khare 2023), suggesting microbial contributions to brain metabolic signaling. These findings highlight the influence of the gut microbiome on brain metabolic pathways, linked to neurotransmitter function and immune modulation, underscoring the importance of the gut-brain axis.

The Venn diagram (Figure 5, bottom right) illustrates the overlap of differentially regulated metabolites across serum, liver, and intestinal compartments. The colon exhibited the highest number of unique metabolites, reflecting its distinct metabolic responsiveness to the presence or absence of gut microbiota. Substantial overlap between serum and liver metabolites points to coordinated metabolic regulation, likely influenced by systemic microbial-derived metabolites.

In summary, these findings indicate the critical role of the gut microbiome in shaping tissue-specific metabolic responses. The pronounced alterations across intestinal, hepatic, and even neural compartments in GF mice reveal the microbiome's broad impact on metabolic homeostasis. These insights highlight the need for further *in vivo* mechanistic studies to better understand host-microbe metabolic interactions across organ systems.

## DISCUSSION

This study provides compelling evidence that the gut microbiome significantly modulates host metabolism, especially with respect to the incorporation of tryptophan-derived carbons into tissue-specific metabolic pathways (Figure 6). Using LC-MS/MS-based metabolic flux analysis, we observed distinct metabolomic profiles between CV and GF male mice, indicating that the

microbiome exerts broad and compartmentalized effects on host metabolic networks.

PCA and volcano plot analyses demonstrated clear separations in metabolic profiles between CV and GF mice across systemic (serum) and localized (liver, brain, and intestinal) tissues (Figures 2-3). These findings provide the microbiome's pivotal role in shaping host tryptophan metabolism, aligning with previous work linking microbial modulation of tryptophan pathways to immune regulation and neurotransmitter synthesis (Agus, Planchais, and Sokol 2018; G. Clarke et al. 2014).

The enriched metabolite pathway analysis further revealed tissue-specific metabolic rewiring in GF male mice (Figure 4). In serum, enriched pathways such as glutathione, aspartate, and tryptophan metabolism suggest a systemic compensatory response to the absence of microbiota, likely reflecting altered redox and amino acid homeostasis (K. Gao et al. 2020; Mardinoglu et al. 2015). In the liver, enhanced aspartate and tyrosine metabolism pathways confirm its central role in nutrient processing modulated by gut microbial signals (Schwabe and Jobin 2013). The colon showed the most enrichment in homocysteine degradation and taurine metabolism, highlighting its role in sulfur amino acid turnover and detoxification (Louis, Hold, and Flint 2014).

Consistent with our previous findings, indoxyl sulfate, a hepatic sulfotransferase (Sult)-derived metabolite from microbial indole, was significantly elevated in the liver, duodenum, jejunum, and ileum of GF male mice (Figure 5). This supports the concept that microbiome depletion diverts tryptophan-derived carbon into amino acid pathways including those for aspartate, glutamate, taurine, methionine, serine, and branched-chain amino acids (Fu et al. 2016; Selwyn, Cui, and Klaassen 2015).

Region-specific shifts in intestinal metabolism were particularly evident in the colon, which showed the greatest number of differentially regulated metabolites in GF mice. This supports the notion that microbial presence directly shapes metabolic activity in distal gut segments. In contrast, the brain showed limited metabolic changes; however, the upregulation of pilocarpine and tixocortol and downregulation of cladribine and tetrahydrodipicolinic acid in GF mice suggest disruption of gut-brain axis signaling, possibly due to altered blood-brain barrier permeability and lack of microbial-derived neuroactive metabolites (Braniste et al. 2014; Cryan and Dinan 2012).

Venn diagram analyses revealed overlapping and distinct tissue responses. The shared metabolite changes between serum and liver suggest systemic coordination, whereas the colon-specific changes emphasize localized microbiome-host metabolic interactions.

There are some limitations to this study. First is the use of single time point (30 min post gavage), which may not fully capture the temporal dynamics of microbial-tryptophan metabolism. Second is the sex differences, where this study only focused on male mice and inclusion of females in future work is necessary to assess sex-specific differences.

Despite these limitations, this study provides the first in vivo MFA showing that the presence or absence of the gut microbiome differentially alters tryptophan-derived carbon incorporation into host metabolic networks in a tissue-specific manner. These findings highlight the microbiome's regulatory influence on host metabolism and emphasize the need for further studies to identify specific microbial taxa and pathways involved. Such insights will be critical for developing microbiome-targeted interventions for metabolic diseases.

**Figure legends**

**Figure 1.** Experimental design of the study. Three-month-old male conventional (CV) and germ-free (GF) humanized PXR-transgenic (hPXR-TG) mice (n = 3-4 per group) were orally gavaged $^{13}C_{11}$-L-tryptophan (20 mg/kg) and collected various tissues after 30 min. LC-MS was used to perform untargeted metabolic flux analysis in serum, liver, duodenum, jejunum, ileum, colon, and brain with bioinformatics listed above.

**Figure 2.** Principal component analysis (PCA) and volcano plots of serum, liver, and brain metabolic flux between CV and GF male mice using the prcomp function and limma R package controlled for errors of multiple testing (adjusted *p*-value < 0.05).

**Figure 3.** PCA and volcano plots of intestinal compartments (duodenum, jejunum, ileum, and colon) metabolic flux between CV and GF male mice using the prcomp function and limma R package controlled for errors of multiple testing (adjusted *p*-value < 0.05).

**Figure 4.** Differentially regulated enriched metabolite pathway analysis of serum, liver, duodenum, jejunum, ileum, and colon using MetaboAnalyst (adjusted *p*-value < 0.05).

**Figure 5.** Two-way hierarchical clustering of differentially regulated metabolites in different tissues. Y-axis numbers indicate the total number of differentially regulated genes by $^{13}C_{11}$-L-tryptophan (adjusted *p*-value < 0.05). Red represents relatively high expression and blue represents relatively low expression. Venn diagram shows the common and uniquely regulated metabolites by $^{13}C_{11}$-L-tryptophan in serum, liver, and intestines (duodenum, jejunum, ileum, and colon).

**Figure 6.** Summary diagram of the major findings of this study. Overall, the in vivo tryptophan metabolic flux analysis demonstrated that the absence of the gut microbiome significantly altered tissue-specific metabolic pathways. In addition, it showed disrupted regulation of detoxification and inflammation pathways in multiple tissues, with colon exhibiting the most pronounced metabolic changes.

# Figure 1

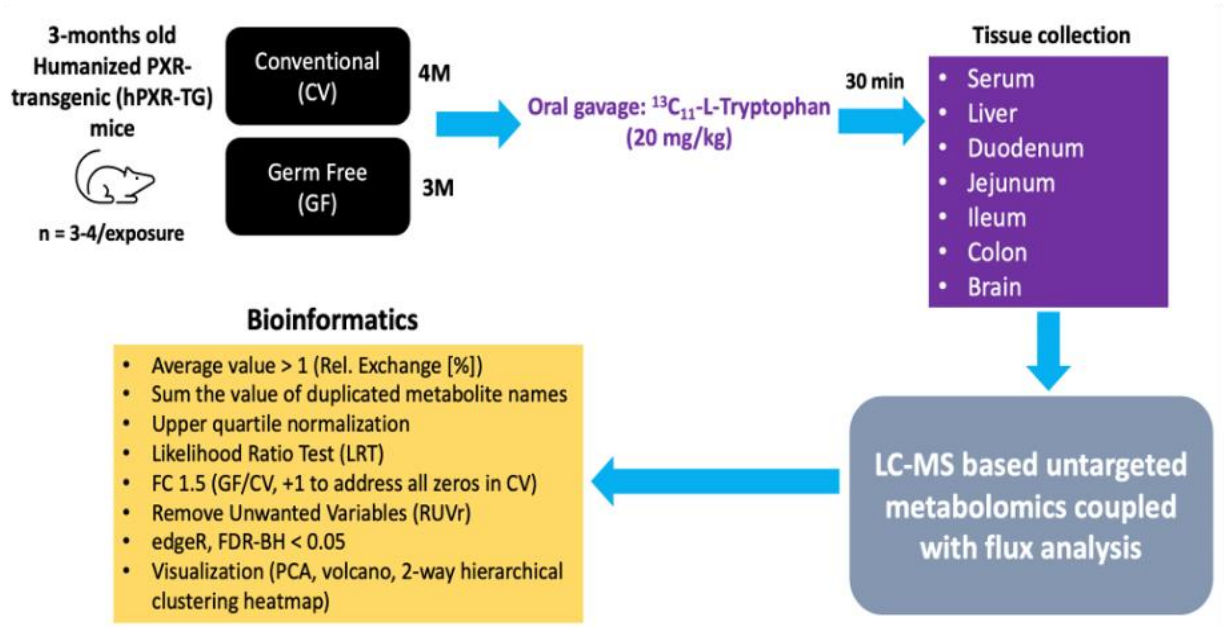
3-months old Humanized PXR-transgenic (hPXR-TG) mice
n = 3-4/exposure
Conventional (CV)
4M
Germ Free (GF)
3M
Oral gavage: $^{13}C_{11}$-L-Tryptophan (20 mg/kg)
30 min
Tissue collection
Serum
Liver
Duodenum
Jejunum
Ileum
Colon
Brain
LC-MS based untargeted metabolomics coupled with flux analysis
Bioinformatics
Average value > 1 (Rel. Exchange [%])
Sum the value of duplicated metabolite names
Upper quartile normalization
Likelihood Ratio Test (LRT)
FC 1.5 (GF/CV, +1 to address all zeros in CV)
Remove Unwanted Variables (RUVr)
edgeR, FDR-BH < 0.05
Visualization (PCA, volcano, 2-way hierarchical clustering heatmap)

# Figure 2

Serum

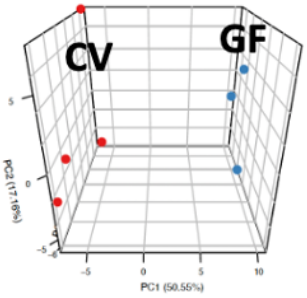


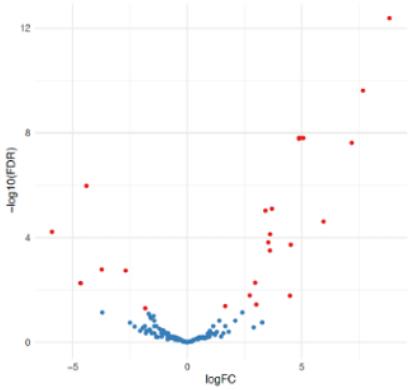


Liver

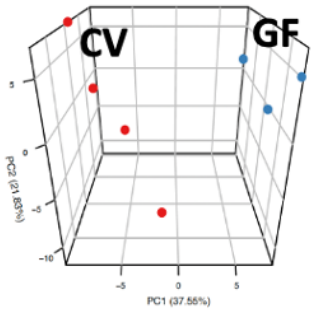


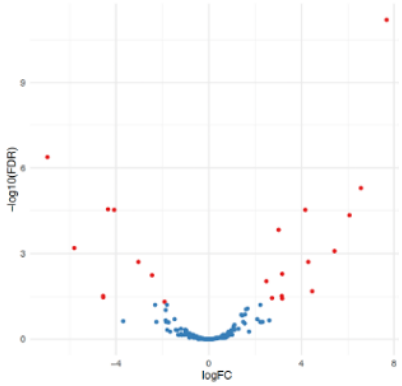


Brain

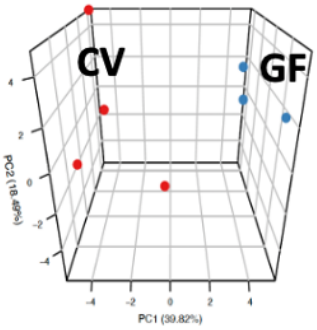


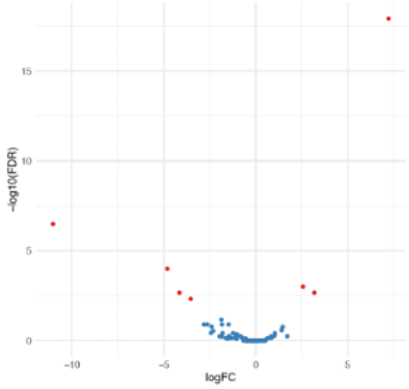

# Figure 3

Duodenum

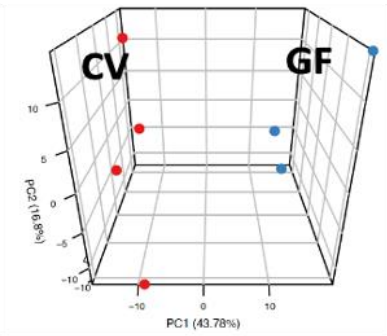


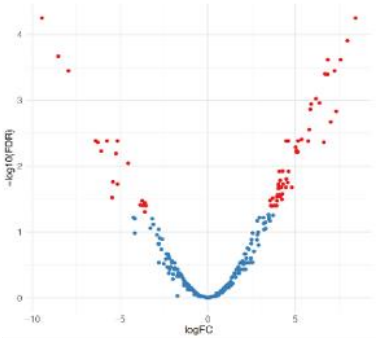


Jejunum

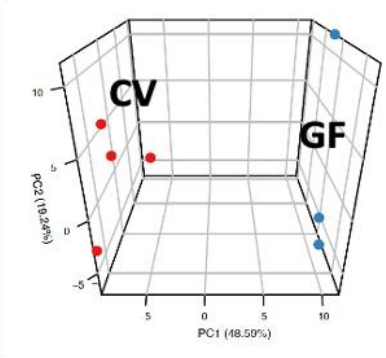


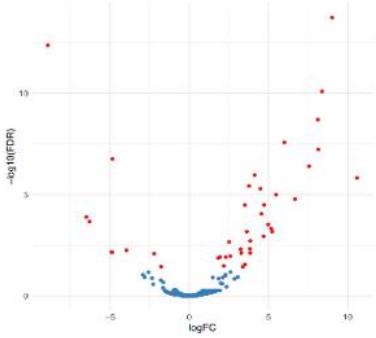


Ileum

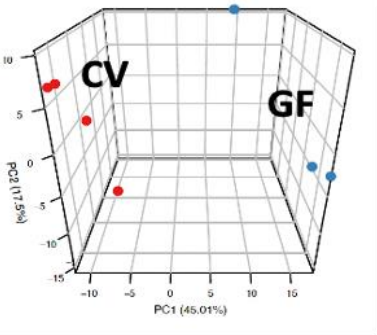


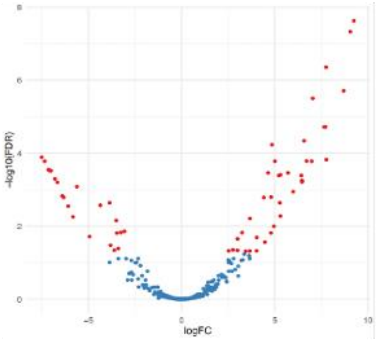


Colon

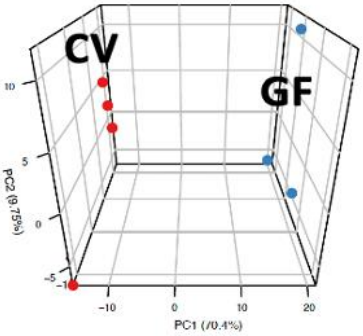


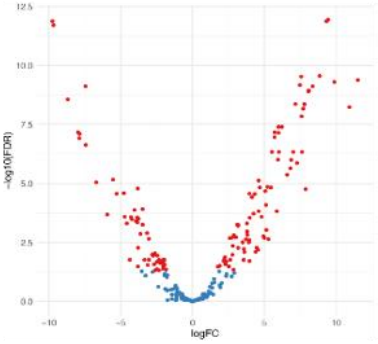

# Figure 4

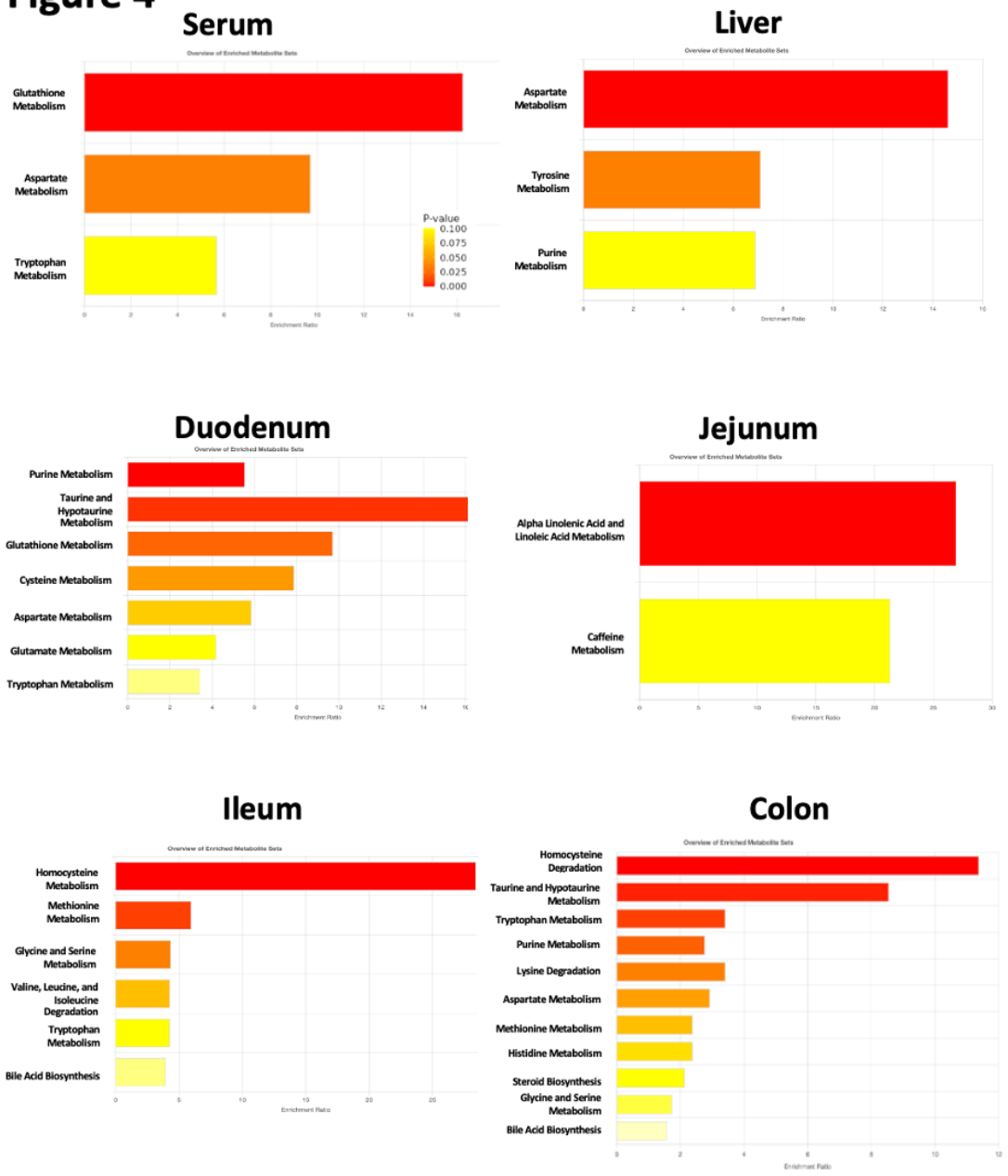
Serum
Glutathione Metabolism
Aspartate Metabolism
Tryptophan Metabolism
P-value
0.100
0.075
0.050
0.025
0.000
Liver
Aspartate Metabolism
Tyrosine Metabolism
Purine Metabolism
Duodenum
Purine Metabolism
Taurine and Hypotaurine Metabolism
Glutathione Metabolism
Cysteine Metabolism
Aspartate Metabolism
Glutamate Metabolism
Tryptophan Metabolism
Jejunum
Alpha Linolenic Acid and Linoleic Acid Metabolism
Caffeine Metabolism
Ileum
Homocysteine Metabolism
Methionine Metabolism
Glycine and Serine Metabolism
Valine, Leucine, and Isoleucine Degradation
Tryptophan Metabolism
Bile Acid Biosynthesis
Colon
Homocysteine Degradation
Taurine and Hypotaurine Metabolism
Tryptophan Metabolism
Purine Metabolism
Lysine Degradation
Aspartate Metabolism
Methionine Metabolism
Histidine Metabolism
Steroid Biosynthesis
Glycine and Serine Metabolism
Bile Acid Biosynthesis

# Figure 5

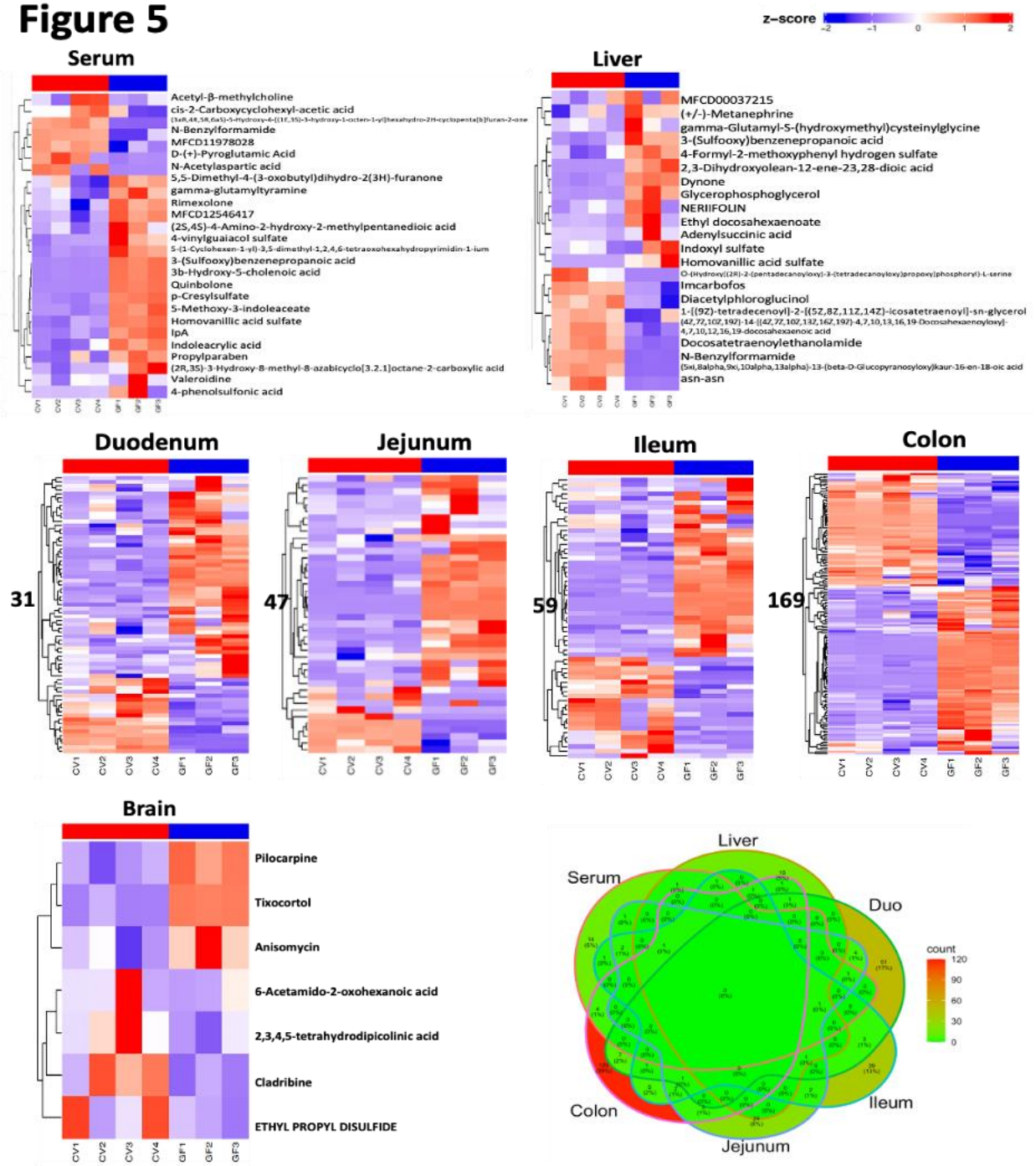
z–score
−2
−1
0
1
2
Serum
Acetyl-β-methylcholine
cis-2-Carboxycyclohexyl-acetic acid
N-Benzylformamide
MFCD11978028
D-(+)-Pyroglutamic Acid
N-Acetylaspartic acid
5,5-Dimethyl-4-(3-oxobutyl)dihydro-2(3H)-furanone
gamma-glutamyltyramine
Rimexolone
MFCD12546417
(2S,4S)-4-Amino-2-hydroxy-2-methylpentanedioic acid
4-vinylguaiacol sulfate
3-(Sulfooxy)benzenepropanoic acid
3b-Hydroxy-5-cholenoic acid
Quinbolone
p-Cresylsulfate
5-Methoxy-3-indoleaceate
Homovanillic acid sulfate
IpA
Indoleacrylic acid
Propylparaben
(2R,3S)-3-Hydroxy-8-methyl-8-azabicyclo[3.2.1]octane-2-carboxylic acid
Valeroidine
4-phenolsulfonic acid
Liver
MFCD00037215
(+/-)-Metanephrine
gamma-Glutamyl-S-(hydroxymethyl)cysteinylglycine
3-(Sulfooxy)benzenepropanoic acid
4-Formyl-2-methoxyphenyl hydrogen sulfate
2,3-Dihydroxyolean-12-ene-23,28-dioic acid
Dynone
Glycerophosphoglycerol
NERIIFOLIN
Ethyl docosahexaenoate
Adenylsuccinic acid
Indoxyl sulfate
Homovanillic acid sulfate
Imcarbofos
Diacetylphloroglucinol
Docosatetraenoylethanolamide
N-Benzylformamide
asn-asn
Duodenum
31
Jejunum
47
Ileum
59
Colon
169
CV1
CV2
CV3
CV4
GF1
GF2
GF3
Brain
Pilocarpine
Tixocortol
Anisomycin
6-Acetamido-2-oxohexanoic acid
2,3,4,5-tetrahydrodipicolinic acid
Cladribine
ETHYL PROPYL DISULFIDE
Liver
Serum
Duo
Colon
Ileum
Jejunum
count
120
90
60
30
0

# Figure 6

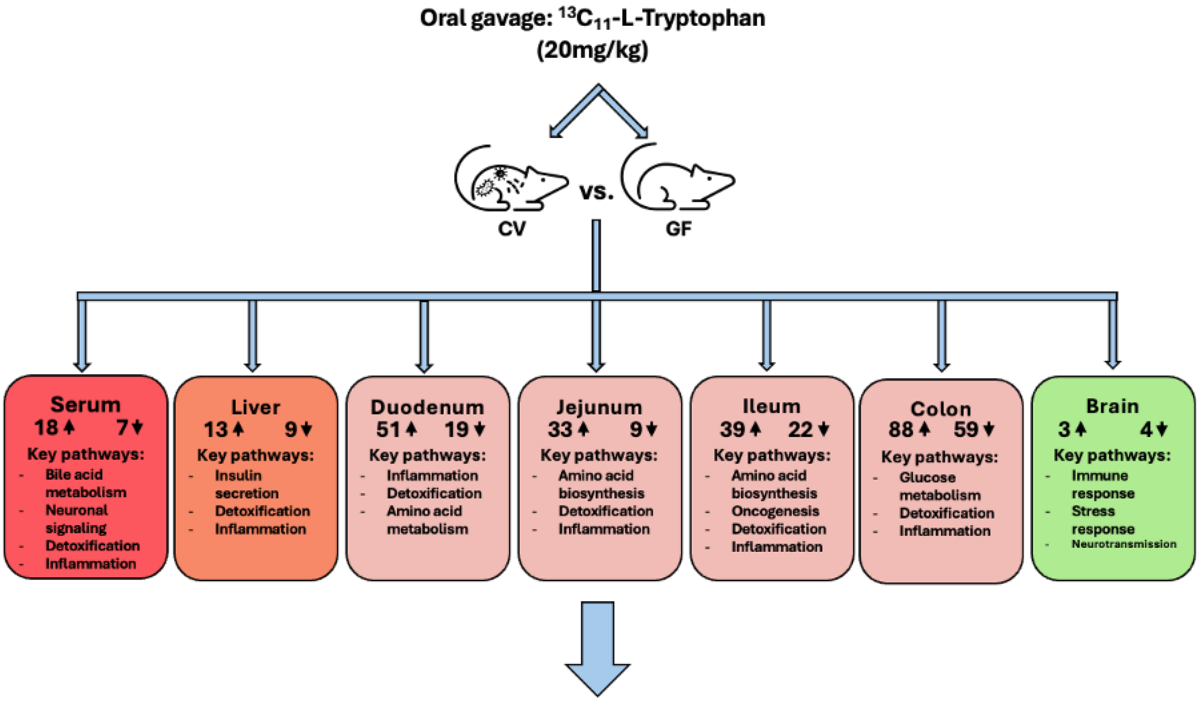


- ***In vivo*** **tryptophan metabolic flux analysis demonstrated that the absence of the gut microbiome significantly altered tissue-specific metabolic pathways.**
- **Disrupted regulation of detoxification and inflammation pathways were significantly shown in multiple tissues, with colon exhibiting the most pronounced metabolic changes.**

## Chapter 5

## Gut microbiome mechanistically contributes to PBDEs-mediated hepatic pro-inflammatory and immune signaling in humanized PXR-transgenic mice

*I plan to submit this work to Drug Metabolism and Disposition.*

**ABSTRACT**

Polybrominated diphenyl ethers (PBDEs) are legacy flame retardants that persist in human tissues, including maternal blood and breast milk. Prior studies have linked developmental PBDE exposure to an elevated risk of diabetes in both humans and animal models. PBDEs are recognized activators of the pregnane X receptor (PXR), a nuclear receptor central to xenobiotic metabolism and the regulation of metabolic disorders, often in concert with the gut microbiome. Our previous work demonstrated that maternal PBDE exposure induces a proinflammatory signature along the gut-liver axis, influenced by microbial tryptophan metabolism in a sex-specific manner. To elucidate the mechanistic role of the gut microbiome in mediating these effects–particularly its impact on PXR signaling, inflammation, and metabolic dysfunction–we conducted fecal microbiota transplant (FMT) studies in germ-free (GF) humanized PXR-transgenic (hPXR-TG) mice. At 3 and 6 months of age, GF hPXR-TG mice were orally gavaged with large intestinal contents from age-, sex-, and genotype-matched conventional (CV) donor mice that were exposed to control or developmentally exposed to DE-71, a human health-relevant industrial PBDE mixture. Tissues were collected one month post-transplantation (n = 3-5/group). Overall, microbiota from DE-71-exposed donors elicited more pronounced hepatic transcriptomic alterations in female recipients compared to males, with enriched pathways related to sterol and cholesterol metabolism and stress-activated protein kinase signaling. In contrast, GF male recipients showed enrichment in pathways involved in xenobiotic and fatty acid metabolism. In the large intestine, the tight junction gene transcripts *Tjp1* and *Tjp2* were consistently downregulated, indicative of compromised intestinal barrier integrity, or "leaky gut," likely driven by DE-71-induced microbial dysbiosis. In addition, hepatic inflammatory markers were more elevated in female recipients, suggesting a sex-specific response. In conclusion, these findings provide mechanistic evidence that gut microbiome

dysbiosis contributes to DE-71-induced proinflammatory hepatic transcriptomic changes, with more pronounced effects observed in females, highlighting the microbiome as a key mediator of sex-specific toxicant responses.

## INTRODUCTION

Polybrominated diphenyl ethers (PBDEs) have been extensively used in industrial applications and were once common as flame retardants. Because of their lipophilic nature, PBDEs persist in the environment and remain detectable in daily lives such as fatty foods and human breast milk. Exposure to PBDEs has been associated with elevated risk of metabolic disorders in both humans and animal models (Zhang et al. 2016). More recently, PBDEs have been frequently detected near electronic waste recycling sites, raising significant concerns about ongoing environmental contamination (Renzelli et al. 2023). DE-71, a human health-relevant PBDE mixture, contains BDE-47 and BDE-99 as its predominant congeners. Our previous research demonstrated that maternal exposure to DE-71 induces proinflammatory signatures along the gut-liver axis, which is linked to dysregulated microbial tryptophan metabolism in a sex-specific manner (S. Kim et al. 2023).

Pregnane X receptor (PXR) is a xenobiotic-sensing nuclear receptor that modulates the transcription of genes involved in the metabolism and clearance of both exogenous chemicals and endogenous compounds. PXR is predominantly expressed in the liver and intestines, it regulates a diverse set of genes encoding drug-metabolizing enzymes and transporters, including cytochrome P450 family (e.g. CYP3A4), ATP-binding cassette (ABC) transporters, and phase II conjugating enzymes (Brewer and Chen 2016). Through its ability to modulate a wide variety of xenobiotics and endogenous ligands, PXR plays a central role in maintaining chemical homeostasis and protecting against toxic insults. Beyond its main role in xenobiotic detoxification, PXR has also been implicated in lipid and glucose metabolism, bile acid homeostasis, inflammation, and immune modulation, linking to the pathogenesis of metabolic disorders and inflammatory disease (Lv et al. 2022; Shah et al. 2007). Its broad ligand promiscuity and functional crosstalk with other

nuclear receptors highlight its importance in toxicology, pharmacology, and disease pathogenesis.

The gut microbiome is increasingly recognized as a key regulator of host xenobiotic metabolism and metabolic disorders (Koppel, Maini Rekdal, and Balskus 2017; S. F. Clarke et al. 2012; Drissi et al. 2014). Early-life gut dysbiosis has been associated with inflammation and metabolic dysfunction later in life, including obesity, insulin resistance, and immune dysregulation (Bassols et al. 2016; Martinez and Guerra 2018; Scoville et al. 2019; Lim et al. 2021). PBDEs are known to bioaccumulate in human tissues and have been linked to development of metabolic syndrome in both human epidemiological studies and animal models. Our previous work demonstrated that maternal exposure to DE-71, a human-relevant industrial PBDE mixture, resulted in sustained gut dysbiosis and sex-specific alterations in microbial tryptophan metabolism in the offspring, highlighting the gut-liver axis as a key site of PBDE-induced metabolic toxicity (S. Kim et al. 2023). Germ-free (GF) mouse models have emerged as a powerful tool for elucidating the causal roles of the microbiome in disease pathogenesis. By allowing for controlled colonization with defined microbial communities, GF models can isolate microbiota-dependent effects of environmental toxicants, including PBDEs, and have revealed that gut microbiome changes may serve as mechanistic mediators and predictive biomarkers of metabolic disruptions (Aghighi and Salami 2024). Together, these findings highlight the importance of microbiome-toxicant interactions in shaping host metabolic outcomes and provide a foundation for future therapeutic strategies targeting microbial pathways.

However, the causal role of the gut-liver axis in mediating the effects of PBDE exposure on the development of metabolic disorders and inflammation later in life remains poorly understood. Therefore, the goal of this study is to elucidate the underlying mechanisms by investigating the contribution of gut microbiota to PBDE-induced toxicity. We hypothesize that

GF mice, which were not directly exposed to PBDEs but received fecal microbiota transplants from developmentally-exposed donors, would develop certain degree of inflammation- and obesity-related phenotypes in adulthood, thereby supporting a microbiome-mediated mechanism of PBDE-induced metabolic disruption.

## MATERIALS AND METHODS

### Animal experiments and fecal microbiota transplantation

Germ-free (GF) and conventional (CV) hPXR-TG mice, originally gifted from Dr. Frank Gonzalez (National Cancer Institute, Bethesda, Maryland) as described previously (Ma et al. 2007), were bred and maintained in the University of Washington gnotobiotic facility (Seattle, Washington) in sterile isolator under a 12-h light/dark cycle. All mice were housed according to the Association of Assessment and Accreditation of Laboratory Animal Care International guidelines and studies were approved by the Institutional Animal Care and Use Committee (IACUC) at the University of Washington. All mice were given ad libitum access to LabDiet No. 5010 (St. Louis, Missouri), which was autoclaved and sterility-tested prior to use. The inoculum for fecal microbiota transplantation (FMT) was prepared by sterile PBS dilution at 1:10 (w/v) of intestinal content collected from CV control-fed and DE-71-fed mice, which were described in detail in our previous study (S. Kim et al. 2023). Briefly, 3 months- and 6 months-old male and female GF mice were orally gavaged with 100 μL of the inoculum for one day (Figure 1). After a month of FMT, mice were sacrificed and the tissues including blood, liver, small and large intestines, small and large intestinal contents, and pancreas were collected, snap-frozen in liquid nitrogen, and kept at -80°C until processed for further analysis.

**Tissue collection**

Tissues were harvested after one month of FMT. Whole blood was collected via cardiac puncture and transferred to a MiniCollect serum separator (Greiner Bio-One, Kremsmünster, Austria), and was kept on ice for at least 30 min to allow sufficient time for blood coagulation. Serum was collected by centrifugation at 4000 rpm (1503 × g) at 4°C for 20 min and stored at −80°C until analysis. Large intestinal contents (LICs) were flushed with 10 mL of ice-cold phosphate-buffered saline (PBS), immediately frozen on dry ice, and stored at −80°C. Intestines were snap-frozen in liquid nitrogen. Liver histology samples were fixed in 10% neutral-buffered formalin. Rest of the liver samples were rapidly frozen in liquid nitrogen and stored at −80°C for subsequent analysis.

**Metagenomic shotgun sequencing and data analysis**

Bacterial DNA was isolated from large intestinal content (LIC) pellets using the OMEGA E.N.Z.A. Stool DNA Kit (OMEGA Biotech, Inc., Norcross, GA) following the manufacturer's protocol. DNA concentration was quantified using a Qubit fluorometer (Thermo Fisher Scientific, Waltham, MA). Metagenomic shotgun sequencing (Diversigen, New Brighton, MN) was conducted to assess gut microbiome composition and functional changes over time. DNA sequences were aligned to a curated database comprising all bacterial genomes from RefSeq, along with manually curated, high-quality metagenomically assembled and cell-cultured mouse-specific genomes. Alignments were performed at 97% identity against all reference genomes. Samples with >10,000 sequences were retained for downstream analysis, and operational taxonomic unit (OTU) counts were normalized to genome length. Functional microbiome changes were predicted by comparing aligned reads to the Kyoto Encyclopedia of Genes and Genomes (KEGG) Orthology

(KO) groups.

**Large-scale targeted LC-MS/MS metabolomics**

The large-scale targeted LC-MS/MS method utilized in this study was adapted from established protocols previously applied in numerous studies (Carroll et al. 2015b; Eghlimi et al. 2020; Gu et al. 2015b; 2016; Jasbi et al. 2019; 2021; Shi et al. 2019). All LC-MS/MS experiments were conducted using an Agilent 1290 UPLC-6490 QQQ-MS system (Santa Clara, CA). Tissue samples (~20 mg) were homogenized in 200 µL methanol (MeOH):PBS (4:1, v/v) containing 1810.5 µM $^{13}C_3$-lactate and 142 µM $^{13}C_5$-glutamic acid using a Bullet Blender homogenizer (Next Advance, Averill Park, NY). These internal standards were used to assess mass spectrometry signal stability but were not used for indole quantification, consistent with previous studies (Carroll et al. 2015b; Eghlimi et al. 2020; Gu et al. 2015b; 2016; Jasbi et al. 2019; 2021; Shi et al. 2019). An additional 800 µL MeOH:PBS (4:1, v/v, containing internal standards) was added, and samples were vortexed for 10 s, then stored at −20°C for 30 min. After 30 min of ice bath sonication, samples were centrifuged at 14,000 rpm for 10 min (4°C), and 800 µL of supernatant was transferred to a new tube. Samples were then vacuum-dried using a CentriVap Concentrator (Labconco, Fort Scott, KS). Before LC-MS/MS analysis, dried residues were reconstituted in 150 µL of 40% PBS/60% acetonitrile (ACN). A quality control (QC) sample was pooled from all study samples. Each sample was injected twice into the LC-MS/MS system, 10 µL for analysis using negative ionization mode and 4 µL for analysis using positive ionization mode. Both chromatographic separations were performed in hydrophilic interaction chromatography mode on a Waters XBridge BEH Amide column (150 × 2.1 mm, 2.5 µm particle size, Waters Corporation, Milford, Massachusetts). The flow rate was 0.3 mL/min, auto-sampler temperature was kept at

4°C, and the column compartment was set at 40°C. The mobile phase was composed of Solvents A (10 mM ammonium acetate, 10 mM ammonium hydroxide in 95% $H_2O$/5% ACN) and B (10 mM ammonium acetate, 10 mM ammonium hydroxide in 95% ACN/5% $H_2O$). After the initial 1 min isocratic elution of 90% B, the percentage of Solvent B decreased to 40% at t = 11 min. The composition of Solvent B was maintained at 40% for 4 min (t = 15 min), and then the percentage of B gradually went back to 90%, to prepare for the next injection.

The mass spectrometer utilized an electrospray ionization (ESI) source, and targeted data acquisition was performed in multiple-reaction-monitoring (MRM) mode. The entire LC-MS system was controlled using Agilent MassHunter Workstation software, with extracted MRM peaks integrated using Agilent MassHunter Quantitative Data Analysis (Santa Clara, CA).

**Untargeted LC-MS metabolomics**

The untargeted LC-MS metabolomics method used in this study was adapted from previously established protocols (Gu et al. 2015b; Qi et al. 2013; Y. Wei et al. 2021; Yao et al. 2014). LC-MS measurements were conducted using a Thermo Vanquish UPLC-Exploris 240 Orbitrap MS system (Waltham, MA). Leftover samples from targeted LC-MS/MS metabolomics were analyzed using this high-resolution mass spectrometer equipped with an ESI source. Untargeted data were collected over a mass range of 70–1050 m/z. Peak identification was performed using a combination of in-house chemical standards (~600 aqueous metabolites) and spectral searches against multiple metabolomics databases, including HMDB, LipidMaps, METLIN, mzCloud, Metabolika, and ChemSpider. For MS data extraction, the absolute intensity threshold was set at 1000, with a mass accuracy limit of 5 ppm. Metabolite identification and annotation were based on retention time (RT), exact mass, MS/MS fragmentation patterns, and

isotopic distributions. Thermo Compound Discoverer 3.3 was used for aqueous metabolomics data processing, including peak picking, alignment, and normalization. To ensure data quality and reproducibility, only signals/peaks with CV < 20% across QC pools, and the signals showing up in >80% of all the samples were included for further analysis.

**Gas Chromatography-Mass Spectrometry (GC-MS)**

GC-MS experiments were performed using an Agilent 7820A gas chromatography system coupled to an Agilent 5977B mass spectrometer (Agilent Technologies, Santa Clara, CA). Sample separation was achieved using an HP-5ms capillary column (30 m x 250 μm i.d., 0.25 μm film thickness) coated with 5% phenyl-95% methylpolysiloxane (Agilent Technologies). A 1 μL sample was injected, with a solvent delay time of 5 min. The oven temperature program was set as follows: initial hold at 60°C for 1 min, ramped to 325°C at a rate of 10°C/min, and held at 325°C for 10 min. Helium was used as the carrier gas at a constant flow rate of 0 mL/min. The inlet, transfer line, and electron impact (EI) ion source temperatures were set to 250°C, 290°C, and 230°C, respectively. The electron energy was maintained at −70 eV, and mass spectral data were collected in full scan mode (m/z 30–600).

Data processing was performed using Agilent MassHunter Workstation Software Quantitative Analysis (B.09.00). Peak identification, integration, and quantification were carried out with a signal-to-noise (S/N) ratio threshold of 3. The retention times (RT) and quantification masses for BDE-47 and BDE-99 were determined using chemical standards.

**RNA isolation**

Total RNA was extracted from frozen liver and large intestine tissues using RNA-Bee

reagent (Tel-Test Inc., Friendswood, TX) following the manufacturer's protocol. RNA concentration was determined by measuring absorbance at 260 nm using a NanoDrop 1000 Spectrophotometer (Thermo Scientific, Waltham, MA). RNA integrity was assessed by formaldehyde-agarose gel electrophoresis, with visualization of 18S and 28S rRNA bands under UV light. The quality of total RNA was further confirmed using an Agilent 2100 Bioanalyzer (Agilent Technologies Inc.).

**RT-qPCR quantification of liver and data analysis**

Total RNA was extracted from liver and intestinal tissues (n = 5 per group). RNA was reverse-transcribed into complementary DNA (cDNA) using the High-Capacity cDNA Reverse Transcription Kit (Life Technologies, CA). Quantitative PCR (qPCR) was performed using Sso Advanced Universal SYBR Green Supermix on a Bio-Rad CFX384 Real-Time PCR Detection System (Bio-Rad, Hercules, CA). Gene expression data were normalized to the geometric mean of the housekeeping genes *Gapdh* and *β-actin* using the ΔΔCq method and expressed as a percentage of housekeeping gene expression.

**H&E staining of liver sections**

Liver tissues were fixed in 10% neutral-buffered formalin, sectioned, and stained with hematoxylin and eosin (H&E) for blinded evaluation. Histopathological signs of necrosis included pyknosis, karyolysis, karyorrhexis, cytoplasmic hyper-eosinophilia, membrane disruption, and cell loss. Inflammatory markers were assessed based on edema and leukocyte accumulation. Fibrosis was identified by the replacement of damaged tissue with angiogenic connective tissue. Apoptosis features included chromatin condensation, cell shrinkage, and cytoplasmic bleb formation.

**Statistical analysis**

For each sex and age group, one-way ANOVA was used to evaluate chemical exposure effects, followed by Duncan's post-hoc test, with adjusted p-values $< 0.05$. Statistical analyses were conducted using SPSS software Version 29.0.1.0 (IBM, Armonk, NY).

## RESULTS

### Effects of FMT from DE-71-exposed donors on gut microbiome composition and functional pathways in GF mice

To evaluate the impact of FMT DE-71 exposure on GF gut microbiome composition and predicted functional pathways, metagenomic shotgun sequencing data were analyzed. Relative abundance at the phylum level showed that *Firmicutes* and *Bacteroidota* were the dominant phyla across all treatment groups and sexes (Figure 2A). Heatmap clustering analysis revealed distinct patterns of microbial functional enrichment related to metabolic pathways, demonstrating age- and sex-specific responses. Specifically, pathways involved in amino acid biosynthesis (valine, leucine, isoleucine, and lysine), one-carbon metabolism via folate, and fatty acid biosynthesis were prominently enriched in female pups at 6 months exposed to CV DE-71-expoxed donors when compared to those group of male pups and 3 months pups (Figure 2B). Conversely, metabolic functions such as nucleotide metabolism, mismatch repair, glycolysis/gluconeogenesis, and homologous recombination were variably impacted, showing distinctive patterns primarily on male pups at different developmental ages (3 months and 6 months).

The composition of the gut microbiome at the phylum level was analyzed in CV and GF mice following FMT from DE-71-exposed or control donors at 3 months and 6 months of age

(Supplemental Figure 1). At 3 months of age, GF control-recipient males exhibited increased *Bacteroidota* (42.1% to 57.6%), reduced *Firmicutes* (22.1% to 17.0%), markedly increased *Actinobacteria* (6.9% to 24.5%), and substantially decreased *Proteobacteria* (28.9% to 0.9%) compared to CV control-recipient males. Similarly, GF DE-71-exposed males showed increased *Bacteroidota* (48.1% to 62.4%), decreased *Firmicutes* (21.2% to 12.0%), increased *Actinobacteria* (8.6% to 14.5%), and decreased *Proteobacteria* (22.1% to 11.1%) compared to CV DE-71-exposed males. Female mice followed similar trends: GF control-recipient females showed notable increase in *Bacteroidota* (42.3% to 67.2%), decrease in *Firmicutes* (19.2% to 9.1%), increase in *Actinobacteria* (9.1% to 22.6%), and great decrease in *Proteobacteria* (29.4% to 0%). GF DE-71-exposed females demonstrated increased *Bacteroidota* (43.5% to 58.7%), decreased *Firmicutes* (15.0% to 12.1%), slightly increased *Actinobacteria* (17.4% to 18.0%), and decreased *Proteobacteria* (24.1% to 11.2%) when compared to CV DE-71-exposed females.

At 6 months of age, GF control-recipient males showed increase in *Bacteroidota* (44.1% to 71.5%), decrease in *Firmicutes* (24.1% to 11.7%), increase in *Actinobacteria* (12.2% to 14.5%), and decrease in *Proteobacteria* (19.6% to 2.2%) when compared to CV control-recipient males. GF DE-71-exposed males also displayed increase in *Bacteroidota* (40.0% to 64.3%), decrease in *Firmicutes* (21.6% to 6.2%), increase in *Actinobacteria* (13.4% to 27.7%), and decrease in *Proteobacteria* (25.0% to 1.7%) compared to CV DE-71-exposed males. Similarly, GF control-recipient females showed prominent increase in *Bacteroidota* (37.4% to 75.1%), decrease in *Firmicutes* (16.0% to 9.7%), increase in *Actinobacteria* (7.3% to 15.2%), and great decrease in *Proteobacteria* (39.3% to 0%). GF DE-71-exposed females showed great increase in *Bacteroidota* (43.1% to 81.6%), decrease in *Firmicutes* (20.3% to 7.6%), slight decrease in *Actinobacteria* (13.1% to 10.8%), and decrease in *Proteobacteria* (23.5% to 0%) when compared to CV DE-71-

exposed females.

Collectively, these results suggest that developmental exposure to DE-71 leads to sex-specific persistent alterations in the gut microbiota composition, with prominent shifts in the relative abundance of major bacterial phyla, potentially contributing to altered gut microbiome functionality and metabolic phenotype later in life.

**FMT DE-71-mediated functional changes predicted from the transcriptomic response in livers of GF groups**

As shown in Figure 3, Gene Ontology (GO) enrichment was performed to determine transcriptional changes in livers from GF hPXR-TG mice that received FMT from DE-71-exposed donors compared to control donors at different time points and sexes. At 3 months of age, male recipients exhibited significant enrichment in biological processes including fatty acid metabolism, xenobiotic metabolism, and cellular response to xenobiotics. In contrast, pathways related to the regulation of cellular response to growth factors and renal system vasculature development were notably down-regulated (Figure 3A). Female recipients at the same age displayed prominent enrichment pathways associated with sterol and cholesterol biosynthesis and metabolism, whereas antigen processing, immune responses, and peptide presentation pathways were down-regulated (Figure 3B).

At 6 months of age, male recipients showed significant enrichment in rhythmic processes and circadian regulation pathways, with pronounced down-regulation in xenobiotic metabolism, steroid metabolism, thyroid hormone metabolism, and oxidative detoxification pathways (Figure 3C). In female recipients at this age demonstrated significant up-regulation of pathways related to proteasomal degradation, ubiquitin-dependent protein catabolism, stress-activated kinase

signaling, and cellular carbohydrate metabolism. Conversely, pathways involved in protein folding, translation, fatty acid metabolism, and responses to misfolded proteins were down-regulated (Figure 3D).

Overall, these results indicate that gut microbiota from DE-71-exposed donors induce persistent, sex- and age-specific hepatic transcriptomic signatures, by disruptions in metabolic, inflammatory, oxidative stress, and detoxification pathways potentially contributing to long-term hepatic metabolic dysfunction.

**Effects of FMT DE-71 exposure on hepatic and ileal expression of inflammatory cytokines in GF mice**

The hepatic and ileal mRNA expression of inflammatory cytokines was assessed by RT-qPCR at 3 months and 6 months of age in control and DE-71-exposed mice, revealing tissue- and sex-dependent effects of developmental DE-71 exposure (Figures 4 and 5). In the liver of 3 months of age, DE-71 exposure significantly decreased the mRNA expression of interleukin-10 (*Il10*) and interleukin-12 subunit p40 (*Il12p40*) in males, with no significant effects observed in females (Figure 4A). Other cytokines, including interleukin-4 (*Il4*) and monocyte chemoattractant protein-1 (*Mcp-1*), were unaffected at this age. At 6 months of age, DE-71 exposure significantly increased hepatic Il4 mRNA expression in males but significantly decreased *Il10* and *Mcp-1* expression. However, *Il10* and *Mcp-1* expression was increased in female mice exposed to DE-71 (though statistically not significant). *Il12p40* and tumor necrosis factor-alpha (*Tnfα*) were not significantly altered in either sex, though a slight increase in *Tnfα* was noted in female mice exposed to DE-71 (Figure 4B).

In contrast, in the ileum of 3 months of age, DE-71 exposure significantly increased mRNA

expression of interferon-gamma (*Ifnγ*), increased *Il10* (not statistically significant), and decreased *Il12p35* in males. In female mice exposed to DE-71, interleukin-6 (*Il6*) was increased (not statistically significant) and the mRNA expressions of *Il10*, *Il12p35*, *Ifnγ* were decreased (Figure 5A). At 6 months of age, DE-71 exposure significantly increased *Il6*, *Il10*, and *Il12p35* mRNA expressions in females and decreased *Il6* mRNA expression in males (not statistically significant), suggesting sex-specific patterns of inflammation (Figure 5B).

We also measured the tight junction gene transcripts *Tjp1* and *Tjp2*, indicative of compromised intestinal barrier integrity or "leaky gut" (Clayburgh, Shen, and Turner 2004; Alaish et al. 2013) in the ileum of GF mice. In the ileum of 3 months of age, *Tjp1* was significantly down-regulated in DE-71-exposed males (Figure 5A). Moreover, in the ileum of 6 months of age, *Tjp1* and *Tjp2* genes were significantly down-regulated in DE-71-exposed males and females (Figure 5B). These findings suggest that DE-71-induced microbial dysbiosis contributes to compromised intestinal barrier integrity or "leaky gut" over time. In addition, the results highlight sex-, age-, and tissue-specific regulation of inflammatory cytokine expression following developmental DE-71 exposure.

**Effect of DE-71 exposure on the hepatic expression of xenobiotic-sensing transcription factor target genes in GF mice**

The mRNA expression of prototypical target genes of aryl hydrocarbon receptor (AhR), constitutive androstane receptor (CAR), pregnane X receptor (PXR), and nuclear factor erythroid 2-related factor 2 (Nrf2) was measured in the livers of recipient mice at 3 and 6 months of age (Figure 6). The mRNA transcript of *Cyp1a2*, which is a prototypical target gene of AhR (Flaveny, Murray, and Perdew 2010; Lo and Matthews 2012), was down-regulated in 3 months and 6 months

of DE-71-exposed females and was more up-regulated in 6 months of DE-71-exposed males when compared to control (Figure 6A and 6B). The mRNAs transcripts of *Cyp2b9* and *Cyp2b10*, which are the prototypical target genes of CAR (Cui and Klaassen 2016; Kiyosawa et al. 2008; Maglich et al. 2003), showed significant down-regulation of *Cyp2b9* in 3 months old DE-71-exposed males and *Cyp2b10* in 6 months old DE-71-exposed males when compared to control males. The mRNA transcript of *Cyp3a11*, which is a prototypical target gene of PXR (Cui and Klaassen 2016; Kiyosawa et al. 2008; Maglich et al. 2003), showed significant down-regulation in 6 months old DE-71-exposed males when compared to control males (Figure 6B). The mRNA transcript of *Nqo1* oxidative stress pathway, which is a prototypical target gene of *Nrf2* (F. He, Ru, and Wen 2020), showed significant down-regulation in 6 months old DE-71-exposed females when compared to control females (Figure 6B), suggesting potential suppression of antioxidant defense mechanisms. Taken together, these findings suggest that FMT from DE-71-exposed donors suppresses hepatic xenobiotic-sensing nuclear receptor pathways in a sex-specific manner over time, with more pronounced effects observed in male mice at 6 months of age.

**Effect of DE-71 exposure on the hepatic expression of Phase II conjugation enzyme genes in GF mice**

To determine whether microbiota from DE-71-exposed donors influence hepatic Phase II detoxification pathways, the mRNA expression levels of UDP-glucuronosyltransferase (Ugt) family genes (Meech et al. 2019; Peer et al. 2016) were measured in GF recipient mice at 3 and 6 months of age following FMT (Supplemental Figure 2). At 3 months of age, DE-71 exposure significantly down-regulated *Ugt2b36* in males and significantly down-regulated *Ugt1a1* in females (Supplemental Figure 2A). At 6 months of age, a divergent regulatory pattern emerged.

In males, DE-71 exposure significantly increased the expression of *Ugt1a1*, *Ugt1a9*, *Ugt2b34*, and *Ugt2b35*, indicating an up-regulation of hepatic glucuronidation capacity (Supplemental Figure 2B). In contrast, female recipients did not exhibit significant changes in any of the Ugt isoforms (although statistically not significant but showed slight up-regulation of *Ugt1a1*, *Ugt1a9*, and *Ugt2b34*). These findings demonstrate that DE-71-exposed mice alters hepatic Phase II detoxification gene expression in a sex- and age-dependent manner.

**Histopathological examination of livers following FMT DE-71 exposure to GF mice**

Representative H&E staining slides are shown in Supplemental Figure 3. At both 3 and 6 months of age, DE-71 exposure appeared to promote inflammation and apoptosis in livers of both male and female pups as evidenced by a diffusive pattern of nuclear shrinkage at the morphological level across the liver lobes when compared to the control donor recipients (male < female; 3 months < 6 months). In summary, FMT of DE-71 exposed donors modulated the hepatic proinflammatory cytokine and liver inflammation in an age- and sex-dependent manner.

**Effects of DE-71 exposure on tryptophan microbial metabolites in GF mice**

Since our previous study with CV mice showed that maternal DE-71 exposure persistently modified tryptophan microbial metabolism over time in an age- and sex-dependent manner (Kim et al. 2023), we performed targeted metabolomics in GF hPXR-TG mice following FMT from developmentally DE-71-exposed donors in various tissues (Figures 7, Supplemental Figure 4-5).

In targeted liver metabolomics, 3 months old male recipients exposed to DE-71 exhibited significant increases in nicotinamide mononucleotide, 5-hydroxyindoleacetic acid (HIAA),

nicotinic acid mononucleotide, kynurenine, and quinolinic acid (Figure 7A). In 3-months-old DE-71-exposed females, kynurenine, NAD, and nicotinic acid adenine dinucleotide were significantly increased, whereas nicotinamide and ADP ribose were significantly decreased (Figure 7A). At 6 months old, male recipients exposed to DE-71 displayed significant decrease in melatonin, anthranilic acid, NAD, and nicotinic acid adenine dinucleotide, while showed increase in indole levels (Figure 7B). In 6-months-old DE-71-exposed females, nicotinamide-adenine dinucleotide (NAD), nicotinic acid adenine dinucleotide, and anthranilic acid were significantly down-regulated.

In targeted serum metabolomics, 3 months old male recipients exposed to DE-71 exhibited significant increases in several tryptophan microbial metabolites, including tryptamine and indole-3-acetic acid. In contrast, serum levels of nicotinamide, HIAA, and L-kynurenine were significantly decreased (Supplemental Figure 4A). In 3-months-old DE-71-exposed females, only indole-3-pyruvic acid was significantly elevated, highlighting a sex-specific metabolic response to DE-71 exposure. At 6 months old, male recipients exposed to DE-71 showed a broader and more pronounced dysregulation of serum tryptophan metabolites. Metabolites significantly increased included 3-indolepropionic acid, ADP-ribose, nicotinic acid mononucleotide, NADH, and serotonin. Conversely, kynurenic acid, L-kynurenine, and HIAA were significantly decreased (Supplemental Figure 4B). Notably, no significant changes in serum tryptophan metabolites were detected in 6 months old female mice.

In targeted large intestinal contents (LIC) metabolomics, 3 months old male recipients exposed to DE-71 significantly increased N-formylkynurenine and significantly decreased indole-3-lactic acid, tryptophan, and indole (Supplemental Figure 5A). In 3-months-old DE-71-exposed

females, indole-3-lactic acid was significantly increased, whereas indole and melatonin were significantly decreased. At 6 months old, male recipients exposed to DE-71 showed significant decrease in NAD, indole, anthranilic acid, 3-hydroxykynurenine, nicotinic acid adenine dinucleotide, 3-indolepropionic acid, and ADP ribose, whereas 3-hydroxytryptophan, tryptophan, and indole-3-lactic acid were significantly increased (Supplemental Figure 5B). In 6 months old DE-71-exposed females, indole-3-lactic acid and tryptophan were significantly increased, whereas indole-3-pyruvic acid, nicotinic acid, xanthurenic acid, 3-indolepropionic acid, and kynurenic acid were significantly decreased (Supplemental Figure 5B).

In summary, tryptophan microbial metabolites in DE-71-exposed GF mice modulated tryptophan metabolism in a tissue- and sex-dependent manner.

**Effects of DE-71 exposure on other metabolites determined by untargeted metabolomics in GF mice**

To further investigate the systemic metabolic consequences of developmental DE-71 exposure in an unbiased manner, untargeted metabolomics analysis was conducted (Supplemental Figure 6-10). In the untargeted serum metabolomics, 3 months old DE-71-exposed female mice exhibited enrichment in multiple amino acid-related pathways, including arginine and proline metabolism, glycine, serine and threonine metabolism, lysine degradation, glutamate metabolism, taurine and hypotaurine metabolism, and cysteine and methionine metabolism (Supplemental Figure 6A). Additional enriched pathways included purine metabolism, biotin metabolism, and pantothenate and CoA biosynthesis, suggesting widespread disruption of amino acid and cofactor metabolism in females. At 6 months old, DE-71-exposed male mice showed enrichment pathways

included purine metabolism, taurine and hypotaurine metabolism, glycine, serine, and threonine metabolism, phenylalanine and tyrosine biosynthesis, and tryptophan biosynthesis, along with lipid-related pathways such as butanoate metabolism, lipoic acid metabolism, and ether lipid metabolism (Supplemental Figure 6B), suggesting persistent dysregulation of both nitrogen and lipid metabolic processes in males. In contrast, 6 months old DE-71-exposed female mice displayed distinct metabolic signature characterized by strong enrichment in butanoate metabolism, alanine, aspartate, and glutamate metabolism, valine, leucine, and isoleucine biosynthesis, and TCA cycle activity, indicating disruptions in branched-chain amino acid and energy metabolism. Other enrichment pathways included fructose and mannose metabolism, galactose metabolism, and lipoic acid metabolism, pointing to broad changes in carbohydrate and mitochondrial function (Supplemental Figure 6C).

In the untargeted liver metabolomics, 3 months old DE-71-exposed male mice displayed significant enrichment of multiple amino acid and energy metabolism pathways, such as glycine, serine, and threonine metabolism, arginine and proline metabolism, alanine, aspartate, and glutamate metabolism, purine metabolism, and butanoate metabolism (Supplemental Figure 7A). Notably, neomycin, kanamycin, and gentamicin biosynthesis were highly enriched. At 3 months old DE-71-exposed female mice, there were significant enrichment pathways related to nucleotide and amino acid metabolism, such as nicotinate and nicotinamide metabolism, purine metabolism, valine, leucine, and isoleucine biosynthesis, and taurine and hypotaurine metabolism (Supplemental Figure 7B). At 6 months old DE-71-exposed male mice, metabolic disruptions persisted with enrichment observed in the citrate cycle (TCA cycle), alanine, aspartate and glutamate metabolism, glyoxylate and dicarboxylate metabolism, and pentose phosphate pathway

(Supplemental Figure 8A). Additional pathways such as vitamin B6 metabolism, biotin metabolism, and butanoate metabolism were altered. In contrast, no significantly enriched metabolite sets were detected in 6 months old female livers (Supplemental Figure 8B).

In the untargeted LIC metabolomics, 3 months old DE-71-exposed male mice showed enrichment in various metabolic pathways, including arginine and proline metabolism, butanoate metabolism, alanine/aspartate/glutamate metabolism, glycolysis/gluconeogenesis, and nitrogen metabolism. Other enrichment pathways included tryptophan metabolism, sulfur metabolism, and purine metabolism (Supplemental Figure 9A). At 3 months old DE-71-exposed female mice, D-amino acid metabolism was the most enriched pathway, followed by pentose phosphate pathway and several amino acid and nucleotide metabolism pathways, including purine and pyrimidine metabolism, nitrogen metabolism, and arginine biosynthesis (Supplemental Figure 9B). At 6 months old DE-71-exposed male mice, several amino acid metabolisms were observed, such as arginine and proline metabolism, arginine biosynthesis, and tryptophan metabolism. In addition, enrichment of nicotinate and nicotinamide metabolism and phenylalanine/tyrosine/tryptophan biosynthesis were observed (Supplemental Figure 10A). At 6 months old DE-71-exposed female mice, it shows fewer enrichment pathways, such as tryptophan metabolism and arginine biosynthesis being the most prominent (Supplemental Figure 10B).

In summary, untargeted metabolomics analyses across multiple tissues revealed tissue-specific metabolic reprogramming following DE-71 exposure, characterized by distinct age- and sex-dependent enrichment patterns. Interestingly, tryptophan metabolism and related amino acid pathways were consistently altered across compartments over time, suggesting that developmental PBDE exposure disrupts microbial metabolite-host interactions in a sex-specific manner.

## DISCUSSION

The present study demonstrated that FMT exposure to DE-71 induces persistent, sex- and age-specific alterations in gut microbiome composition, hepatic gene expression, and host metabolic phenotypes, highlighting the microbiome's critical role in mediating xenobiotic-induced toxicity. Through FMT from DE-71-exposed CV donors into GF hPXR-TG mice, we observed significant shifts in gut microbial communities at the phylum level, characterized by increased *Bacteroidota* and decreased *Firmicutes* and *Proteobacteria*. These compositional changes were more pronounced in females and at 6 months of age, suggesting persistent gut dysbiosis shaped by developmental exposure and sex-specific factors (Figure 1 and Supplemental Figure 1). Functional pathway analysis revealed that DE-71 exposure significantly perturbed microbial metabolic functions, including amino acid biosynthesis, one-carbon metabolism, and lipid metabolism, which are tightly linked to host energy homeostasis and immune function (Figure 2). These results align with previous findings showing that environmental toxicants such as PBDEs modulate the gut microbiome and its metabolic output in a sex-dependent manner (Lim et al. 2021; Scoville et al. 2019; Kim et al. 2023).

In addition, GO enrichment analysis of hepatic transcriptomes revealed that microbiota from DE-71-exposed CV donors reprogrammed hepatic gene expression in a sex-dependent manner. In males, there were down-regulation of xenobiotic metabolism and oxidative stress pathways over time, accompanied by disrupted circadian rhythm and metabolic signaling (Figure 3). In contrast, females exhibited up-regulation of proteasomal degradation and stress-activated kinase signaling pathways, indicative of persistent hepatic stress and inflammation (Figure 3). Together, these transcriptomic signatures suggest a gut-liver axis disruption that may lead to hepatic dysfunction and metabolic disease later in life.

Developmental DE-71 exposure altered the expression of inflammatory cytokine gene in both the liver and ileum. In the liver, *Il10* and *Mcp-1* were down-regulated in DE-71-exposed males, whereas these markers were slightly elevated in females, indicating sex-specific immune responses (Figure 4). In the ileum, the tight junction genes (*Tjp1* and *Tjp2*) were down-regulated especially in males, suggesting compromised intestinal barrier integrity or "leaky gut" (Figure 5) (Clayburgh, Shen, and Turner 2004; Alaish et al. 2013). These findings suggest that PBDE-induced microbial dysbiosis contributes to immune dysregulation and epithelial barrier disruption, potentially facilitating translocation of bacterial products and exacerbating hepatic inflammation.

For nuclear receptor target genes (AhR, CAR, PXR, and Nrf2), it supports the hypothesis that developmental PBDE exposure impairs hepatic xenobiotic sensing and detoxification. Notably, male mice at 6 months exhibited significant down-regulation of *Cyp2b10*, *Cyp3a11*, and *Nqo1*, indicating reduced clearance of xenobiotic and mitigating oxidative stress (Figure 6). As for Phase II conjugation, hepatic expression of Ugt isoforms, which are responsible for glucuronidation, was significantly altered in DE-71-exposed males, with increased expression at 6 months of age (Supplemental Figure 2). This up-regulation may represent a delayed compensatory response to earlier suppression of detoxification pathways. In contrast, female DE-71-exposed recipients showed minimal or opposite changes, suggesting sex-specific regulation of Phase II detoxification (Supplemental Figure 2).

Targeted and untargeted metabolomics revealed various disruptions in tryptophan metabolism, which is a key microbial-host axis. For targeted metabolomics, DE-71 exposure decreased anti-inflammatory metabolites such as indole and kynurenic acid (Alexeev et al. 2018) in male large intestinal contents and serum, while increasing intermediates such as tryptamine and serotonin, which may contribute to hepatic inflammation (Osawa et al. 2011) (Supplemental

Figure 4-5). These effects were sex- and tissue-specific, with broader metabolic disruptions in males and minimal changes in female serum at 6 months (Supplemental Figure 4-5). The observed changes underscore the importance of microbial tryptophan metabolism in host-microbiome communication and suggest its dysregulation as a potential mechanism linking early-life PBDE exposure to metabolic disease later in life. In addition, untargeted metabolomics across serum, liver, and intestinal tissues, revealed age- and tissue-dependent enrichment of amino acid, lipid, and nucleotide metabolism pathways. DE-71-exposed male mice showed enrichment in TCA cycle, vitamin B6, and purine metabolism in the liver, while females showed changes in branched-chain amino acid metabolism and tryptophan metabolism in the intestine (Figure 7). These results suggest that microbial metabolites not only modulate hepatic gene expression but also reshape systemic metabolism in a sex-specific manner.

There are some limitations to this study. GF mice did not directly receive DE-71 exposure but instead were exposed via FMT from DE-71-exposed donors, which may not account for possible direct toxicant-host interactions. However, our main focus was to investigate the microbiome's role comparing with the CV mice. Since we only focused on the microbiome's role, future studies with metabolite supplementation, such as IPA, would be a great study to further explain some direct causal links.

Despite the limitations, these findings demonstrate that developmental PBDE exposure induces persistent alterations in gut microbiota, hepatic gene expression, and metabolic homeostasis in sex- and tissue-specific manners. The microbiome plays a crucial role in mediating these effects, potentially through microbial metabolites that regulate xenobiotic sensing, inflammatory signaling, and energy metabolism. These results emphasize the need to consider microbiome-host interactions in toxicological risk assessment and support the DOHaD hypothesis

that early-life exposures can have consequences on health later in life. Further work is needed to explore microbiome-targeted interventions that may mitigate these toxicant-induced effects.

**FUNDING STATEMENT**

Supported by National Institutes of Health (grants R01 ES030197, ES025708, and ES031098); the University of Washington (UW) Center for Exposures, Diseases, Genomics, and Environment (NIH P30 ES007033); UW DEOHS Environmental Health and Microbiome Research Center (EHMBRACE); the UW Sheldon D. Murphy Endowment (J.Y.C.); as well as the graduate student fellowship from the UW Provost funds (S.K.).

**ACKNOWLEDGEMENT**

The authors would like to thank the members of Dr. Cui's laboratory for their help in tissue collection and Dr. Gu laboratory for helping with manuscript revision.

**Figure legends**

**Figure 1.** Experimental design of the study. Germ-free (GF) humanized PXR-transgenic (hPXR-TG) breeders were exposed to standard rodent chow and standard water without PBDE exposure. The pups were weaned at postnatal day (PND) 28. At 3 months and 6 months of age, control and DE-71-exposed fecal microbiome transplant from CV mice were orally gavaged. After 1 month of FMT, tissues were collected. Intestinal contents were subjected to metagenomic shotgun sequencing. Serum, liver, and ileum tryptophan metabolites were quantified using LC-MS. Untargeted metabolomics was also performed in serum, liver, and ileum. RT-qPCR was performed to quantify the mRNA expression of distinct liver genes in these pups. Liver histology analysis was performed along with RNA sequencing. Because the primary focus of the study is the effect of chemicals, at each sex and age, one-way ANOVA was then performed followed by Duncan's post hoc test. Statistically significant differences were considered at $p < 0.05$.

**Figure 2.** Intestinal microbiome bacteria at phylum level in 2 ages of the pups (3 months and 6 months old age; n = 5 per group). **A.** Relative abundance of bacteria at phylum level in each group. **B.** Heatmap clustering analysis of microbial functional enrichment related to metabolic pathways.

**Figure 3.** Gene Ontology (GO) enrichment analysis in the livers of GF hPXR-TG mice that received FMT from DE-71-exposed donors compared to control donors of; **(A)** males 3 months of age, **(B)** females 3 months of age, **(C)** males 6 months of age, and **(D)** females 6 months of age.

**Figure 4.** Hepatic mRNA expression of inflammatory cytokines assessed by RT-qPCR at **(A)** 3 months and **(B)** 6 months of age in control and DE-71-exposed mice.

**Figure 5.** Ileal mRNA expression of inflammatory cytokines assessed by RT-qPCR at **(A)** 3 months and **(B)** 6 months of age in control and DE-71-exposed mice.

**Figure 6.** Hepatic mRNA expression of prototypical target genes at **(A)** 3 months and **(B)** 6 months of age in control and DE-71-exposed mice.

**Figure 7.** Tryptophan targeted metabolomics in the livers of GF hPXR-TG mice following FMT from developmentally DE-71-exposed donors in males and females of **(A)** 3 months of age and **(B)** 6 months of age.

# Figure 1

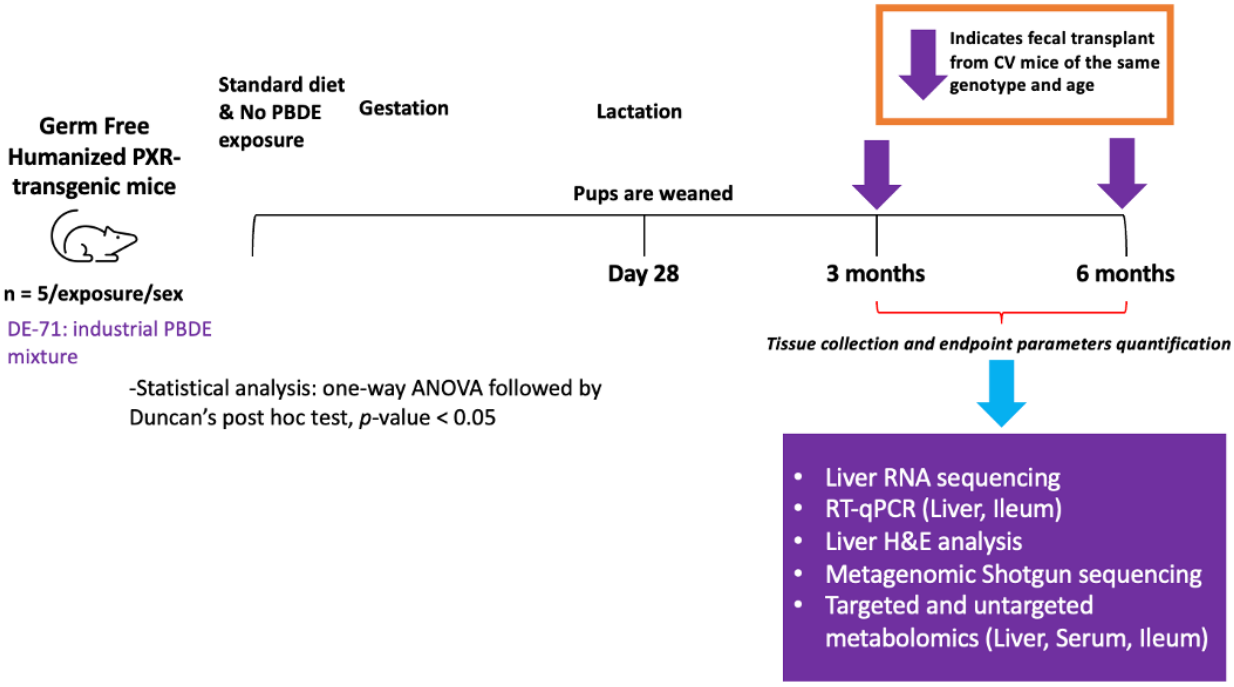
Indicates fecal transplant from CV mice of the same genotype and age
Germ Free Humanized PXR-transgenic mice
Standard diet & No PBDE exposure
Gestation
Lactation
Pups are weaned
Day 28
3 months
6 months
n = 5/exposure/sex
DE-71: industrial PBDE mixture
-Statistical analysis: one-way ANOVA followed by Duncan's post hoc test, p-value < 0.05
Tissue collection and endpoint parameters quantification
Liver RNA sequencing
RT-qPCR (Liver, Ileum)
Liver H&E analysis
Metagenomic Shotgun sequencing
Targeted and untargeted metabolomics (Liver, Serum, Ileum)

# Figure 2

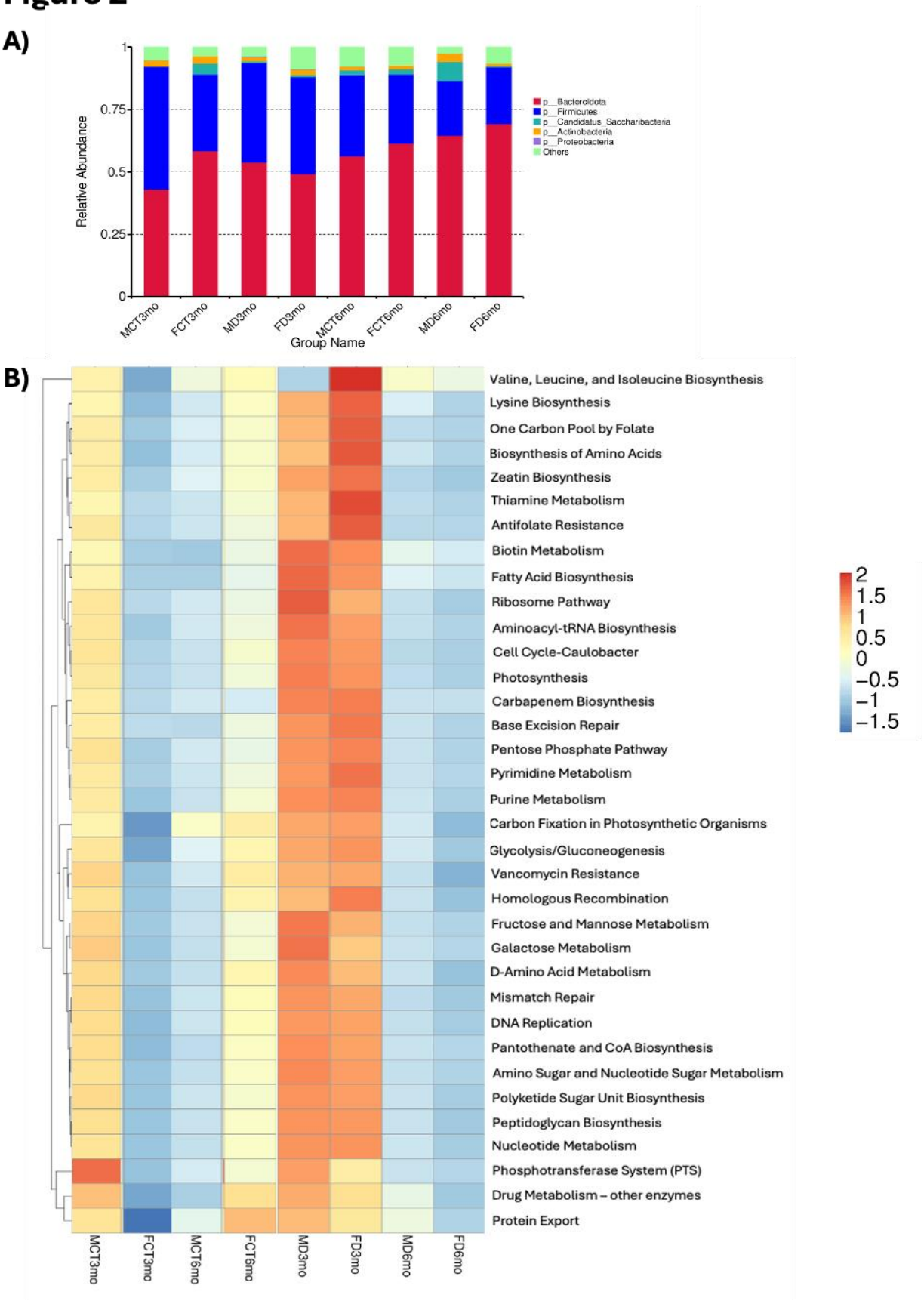
A)
Relative Abundance
1
0.75
0.5
0.25
0
p__Bacteroidota
p__Firmicutes
p__Candidatus_Saccharibacteria
p__Actinobacteria
p__Proteobacteria
Others
MCT3mo
FCT3mo
MD3mo
FD3mo
MCT6mo
FCT6mo
MD6mo
FD6mo
Group Name
B)
Valine, Leucine, and Isoleucine Biosynthesis
Lysine Biosynthesis
One Carbon Pool by Folate
Biosynthesis of Amino Acids
Zeatin Biosynthesis
Thiamine Metabolism
Antifolate Resistance
Biotin Metabolism
Fatty Acid Biosynthesis
Ribosome Pathway
Aminoacyl-tRNA Biosynthesis
Cell Cycle-Caulobacter
Photosynthesis
Carbapenem Biosynthesis
Base Excision Repair
Pentose Phosphate Pathway
Pyrimidine Metabolism
Purine Metabolism
Carbon Fixation in Photosynthetic Organisms
Glycolysis/Gluconeogenesis
Vancomycin Resistance
Homologous Recombination
Fructose and Mannose Metabolism
Galactose Metabolism
D-Amino Acid Metabolism
Mismatch Repair
DNA Replication
Pantothenate and CoA Biosynthesis
Amino Sugar and Nucleotide Sugar Metabolism
Polyketide Sugar Unit Biosynthesis
Peptidoglycan Biosynthesis
Nucleotide Metabolism
Phosphotransferase System (PTS)
Drug Metabolism – other enzymes
Protein Export
MCT3mo
FCT3mo
MCT6mo
FCT6mo
MD3mo
FD3mo
MD6mo
FD6mo
2
1.5
1
0.5
0
−0.5
−1
−1.5

# Figure 3

## A) Males 3 months

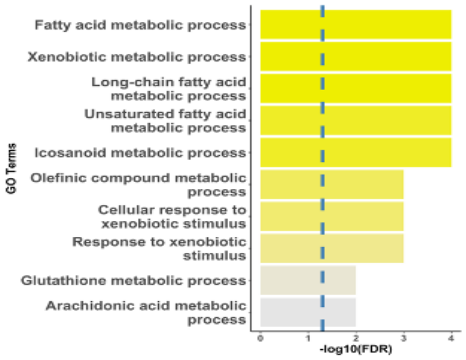


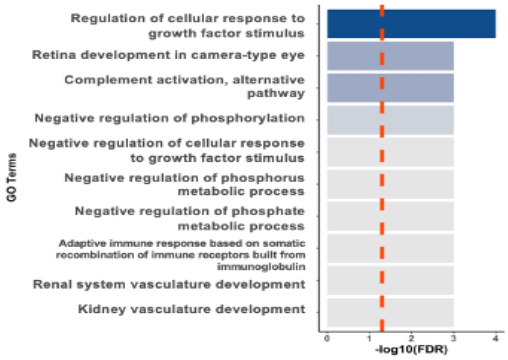


## B) Females 3 months

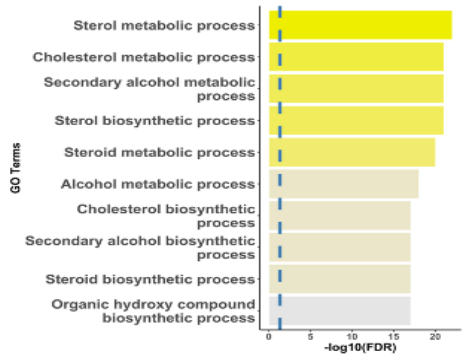


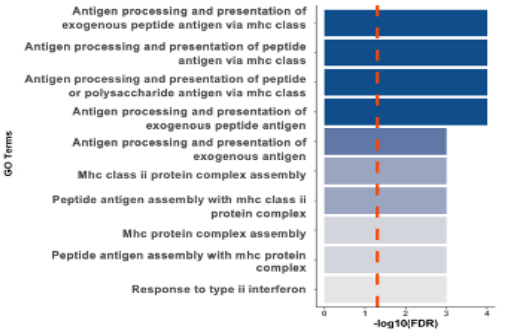


## C) Males 6 months

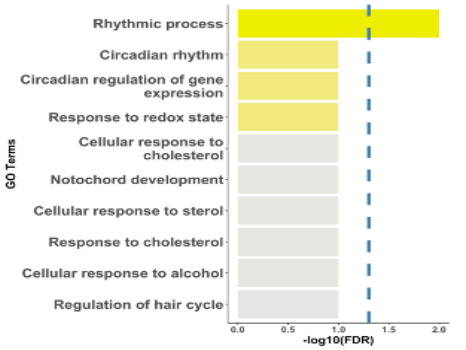


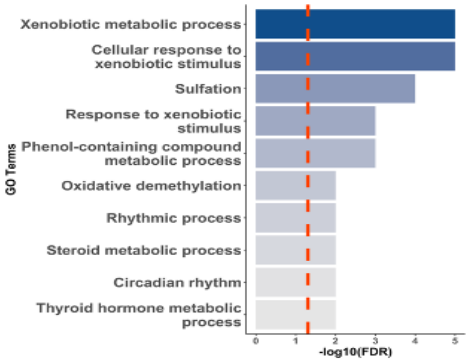


## D) Females 6 months

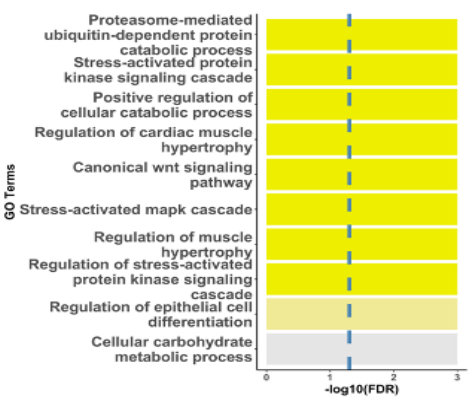


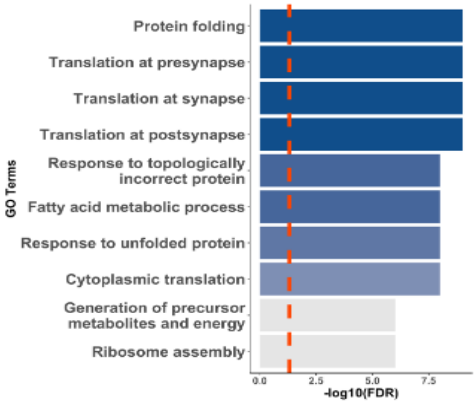

# Figure 4

## A) 3 months

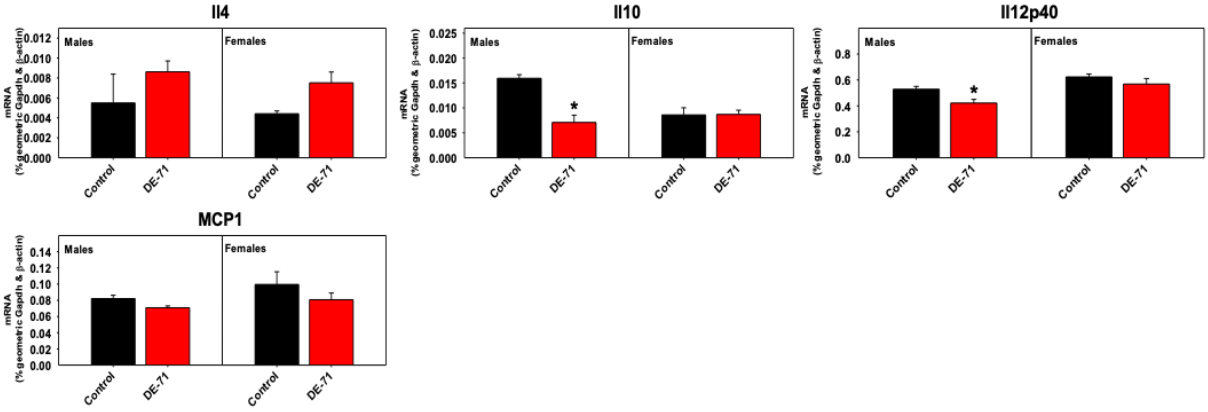


## B) 6 months

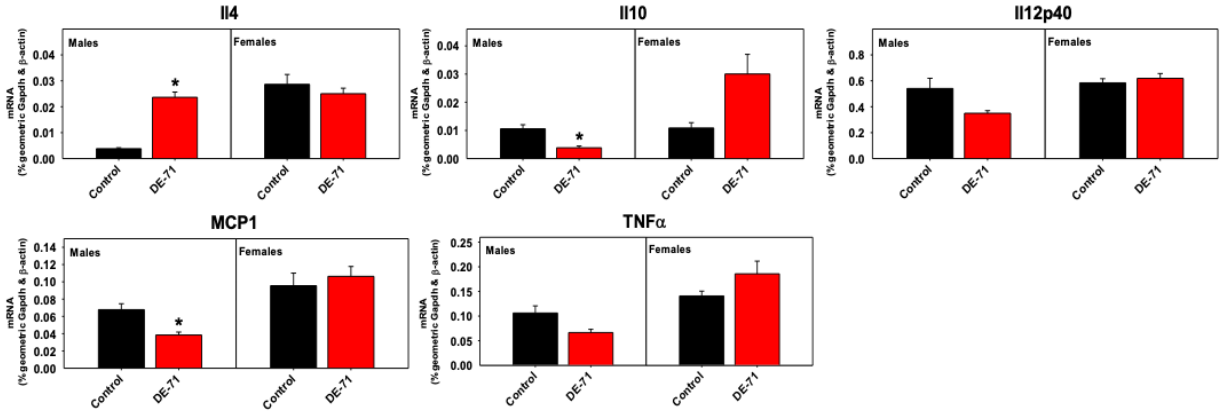

# Figure 5

## A) 3 months

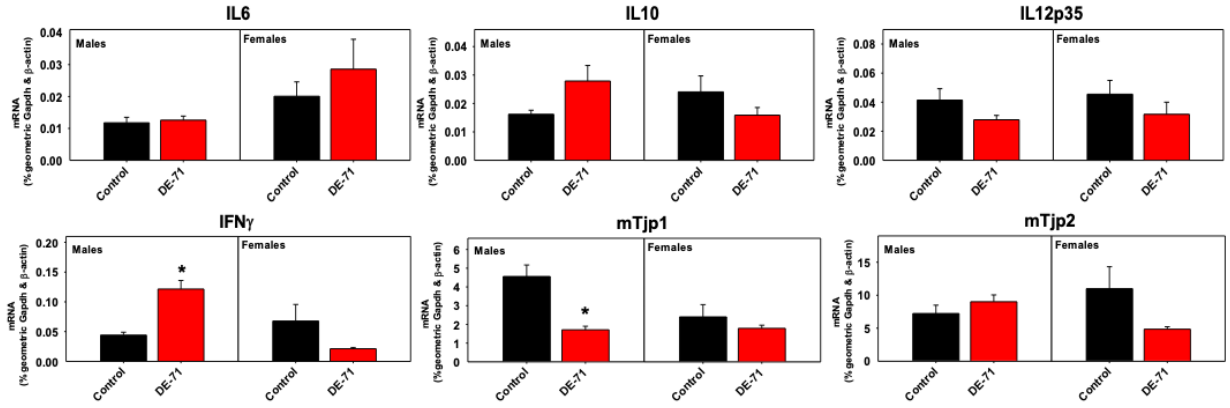


## B) 6 months

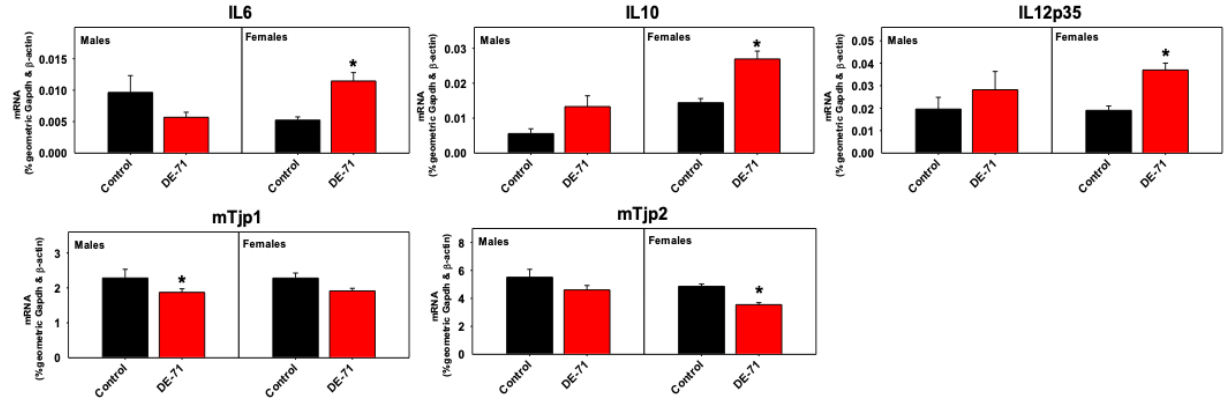

# Figure 6

## A) 3 months

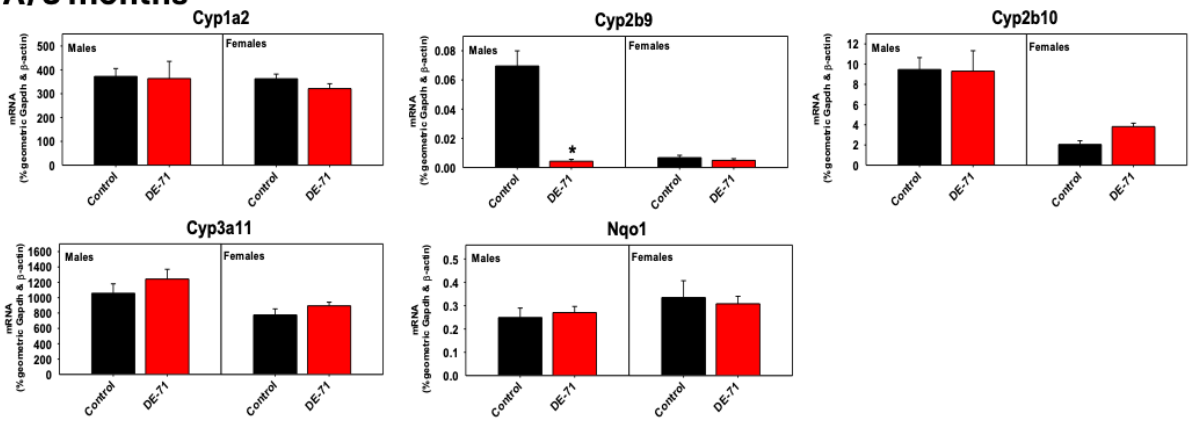


## B) 6 months

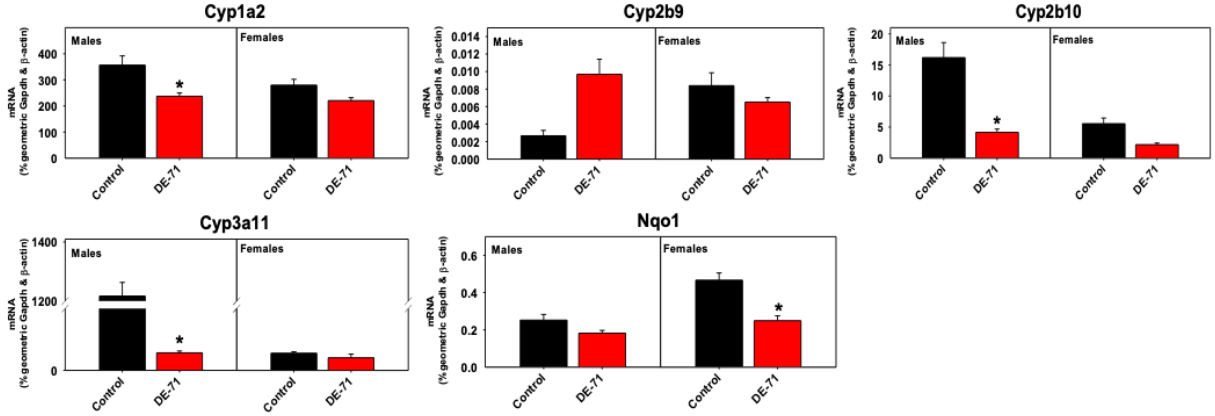

# Figure 7

## A) 3 months

### Males

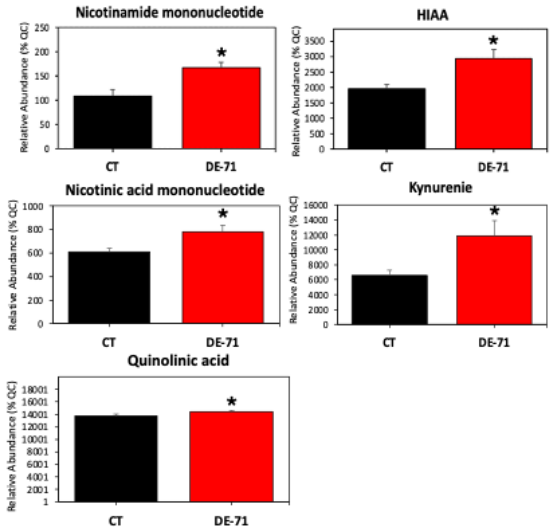


### Females

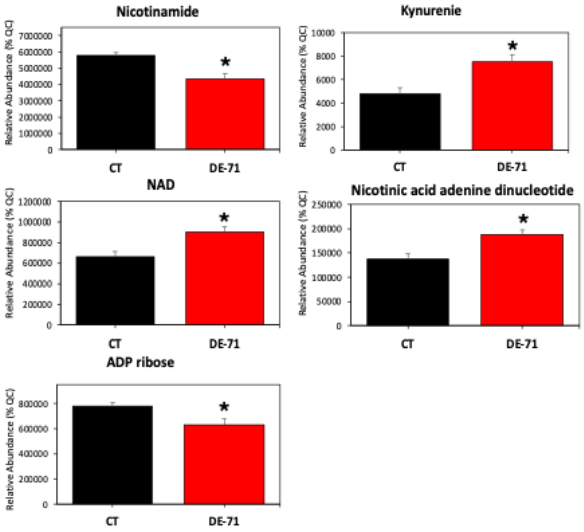


## B) 6 months

### Males

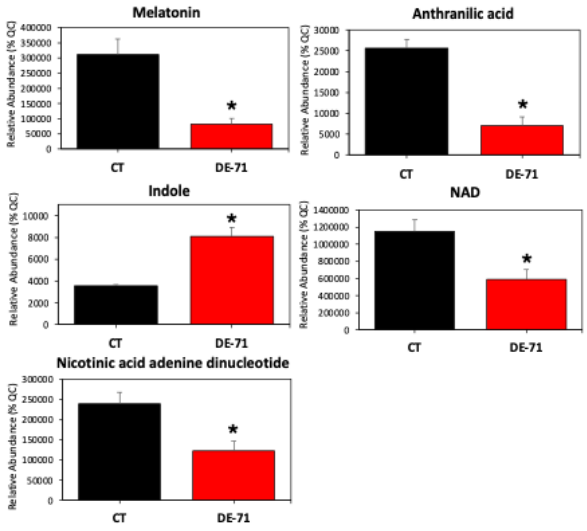


### Females

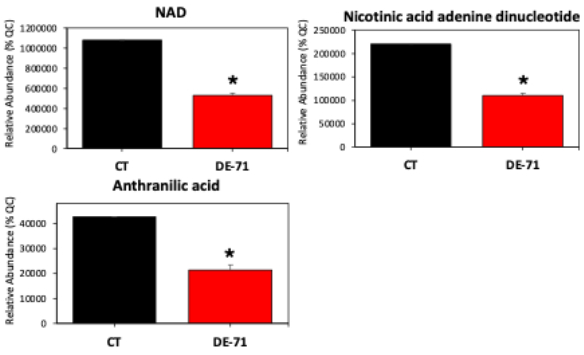

**SUPPLEMENTAL FIGURE LEGENDS**

**Figure S1.** Relative abundance of bacteria at phylum level at 3-months of age **(A)**, and 6-months of age **(B)**.

**Figure S2.** mRNA expression levels of UDP-glucuronosyltransferase (Ugt) family genes measured at 3 months **(A)** and 6 months **(B)** of age following FMT.

**Figure S3.** H&E staining of FMT livers of mouse pups at 3-months of age and 6-months of age.

**Figure S4.** Tryptophan targeted metabolomics in the serum of GF hPXR-TG mice following FMT from developmentally DE-71-exposed donors in males and females of **(A)** 3 months of age and **(B)** 6 months of age.

**Figure S5**. Tryptophan targeted metabolomics in the large intestinal content (LIC) of GF hPXR-TG mice following FMT from developmentally DE-71-exposed donors in males and females of **(A)** 3 months of age and **(B)** 6 months of age.

**Figure S6.** Untargeted metabolomics in the serum of GF hPXR-TG mice following FMT from developmentally DE-71-exposed donors in **(A)** females 3 months of age, **(B)** males 6 months of age, and **(C)** females 6 months of age.

**Figure S7.** Untargeted metabolomics in the livers of GF hPXR-TG mice following FMT from developmentally DE-71-exposed donors in **(A)** males 3 months of age and **(B)** females 3 months of age.

**Figure S8.** Untargeted metabolomics in the livers of GF hPXR-TG mice following FMT from developmentally DE-71-exposed donors in **(A)** males 6 months of age and **(B)** females 6 months of age.

**Figure S9.** Untargeted metabolomics in the LIC of GF hPXR-TG mice following FMT from developmentally DE-71-exposed donors in **(A)** males 3 months of age and **(B)** females 3 months

of age.

**Figure S10.** Untargeted metabolomics in the LIC of GF hPXR-TG mice following FMT from developmentally DE-71-exposed donors in **(A)** males 6 months of age and **(B)** females 6 months of age.

# Figure S1

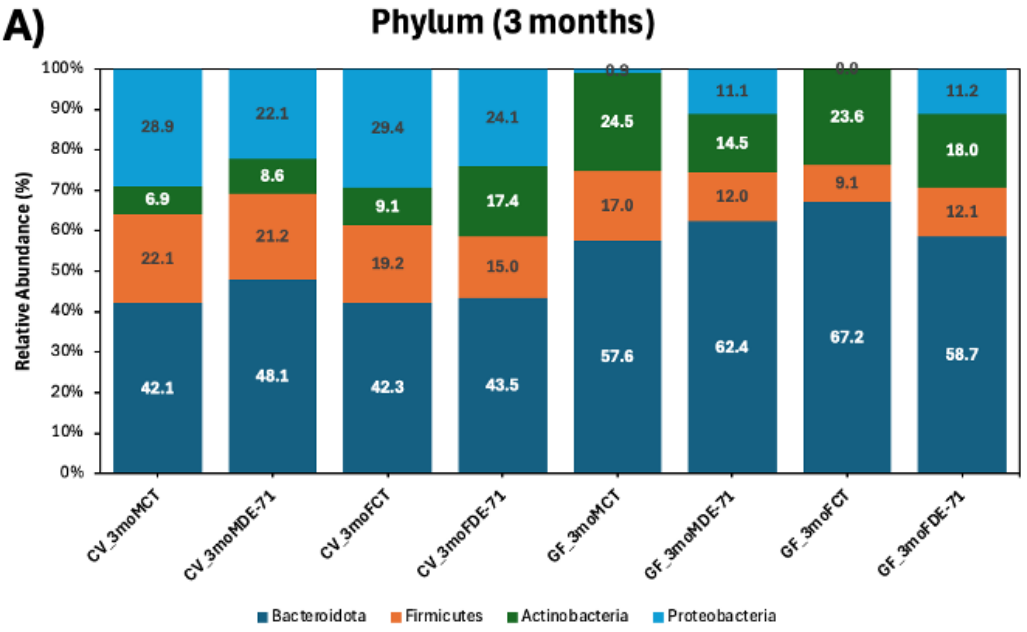
A)
Phylum (3 months)
Relative Abundance (%)
100%
90%
80%
70%
60%
50%
40%
30%
20%
10%
0%
28.9
6.9
22.1
42.1
22.1
8.6
21.2
48.1
29.4
9.1
19.2
42.3
24.1
17.4
15.0
43.5
24.5
17.0
57.6
11.1
14.5
12.0
62.4
23.6
9.1
67.2
11.2
18.0
12.1
58.7
CV_3moMCT
CV_3moMDE-71
CV_3moFCT
CV_3moFDE-71
GF_3moMCT
GF_3moMDE-71
GF_3moFCT
GF_3moFDE-71
Bacteroidota
Firmicutes
Actinobacteria
Proteobacteria

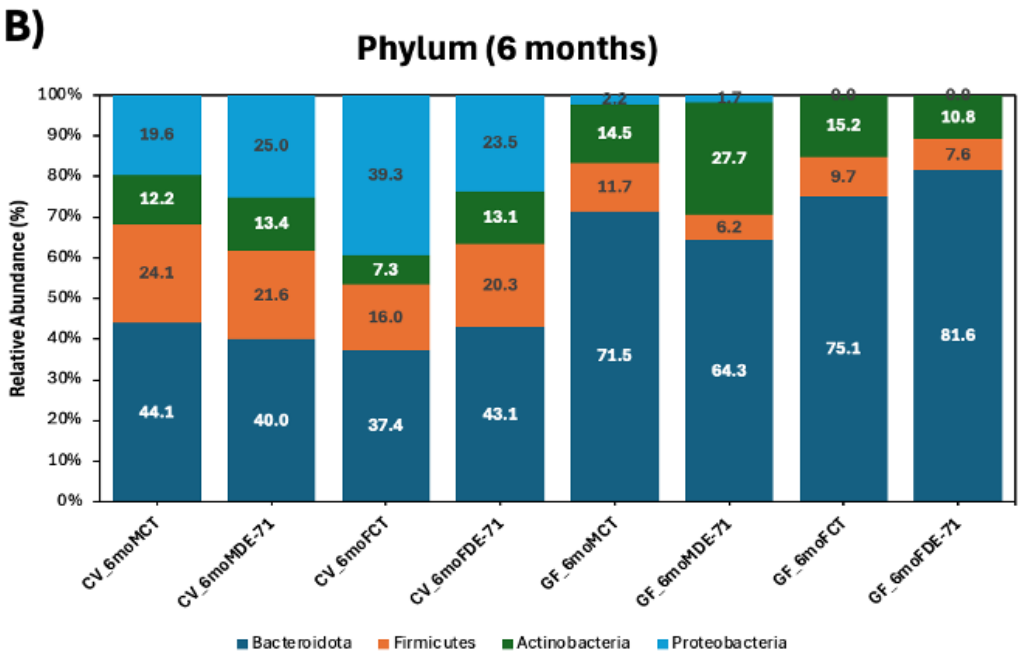
B)
Phylum (6 months)
Relative Abundance (%)
100%
90%
80%
70%
60%
50%
40%
30%
20%
10%
0%
19.6
12.2
24.1
44.1
25.0
13.4
21.6
40.0
39.3
7.3
16.0
37.4
23.5
13.1
20.3
43.1
14.5
11.7
71.5
27.7
6.2
64.3
15.2
9.7
75.1
10.8
7.6
81.6
CV_6moMCT
CV_6moMDE-71
CV_6moFCT
CV_6moFDE-71
GF_6moMCT
GF_6moMDE-71
GF_6moFCT
GF_6moFDE-71
Bacteroidota
Firmicutes
Actinobacteria
Proteobacteria

# Figure S2

## A) 3 months

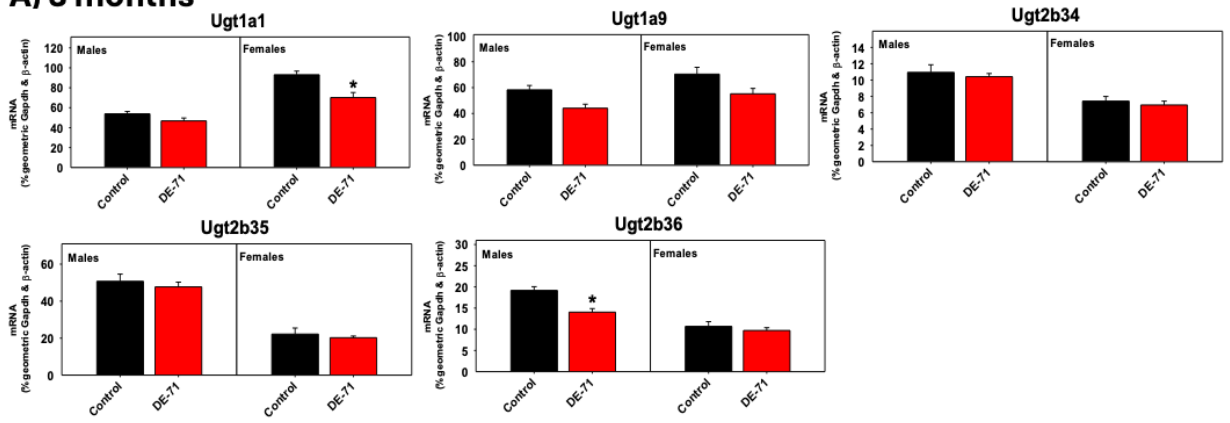


## B) 6 months

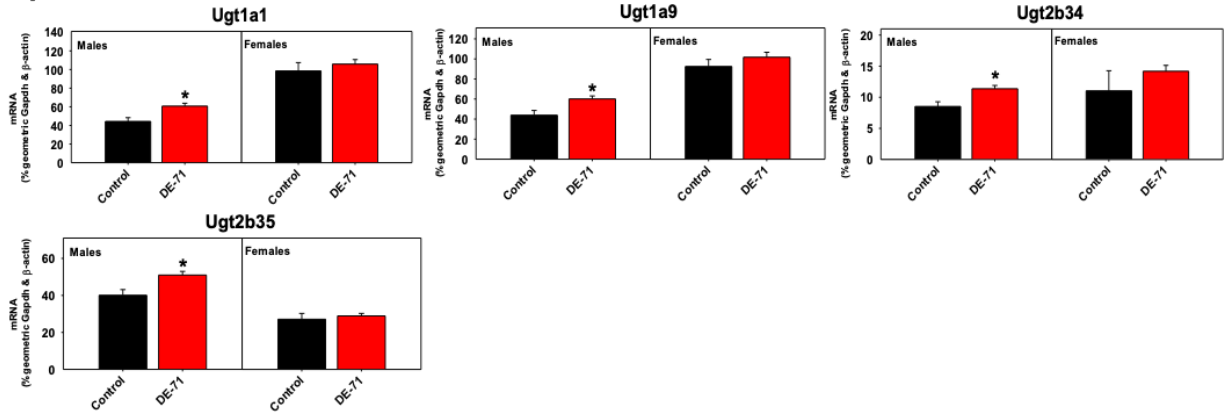

# Figure S3

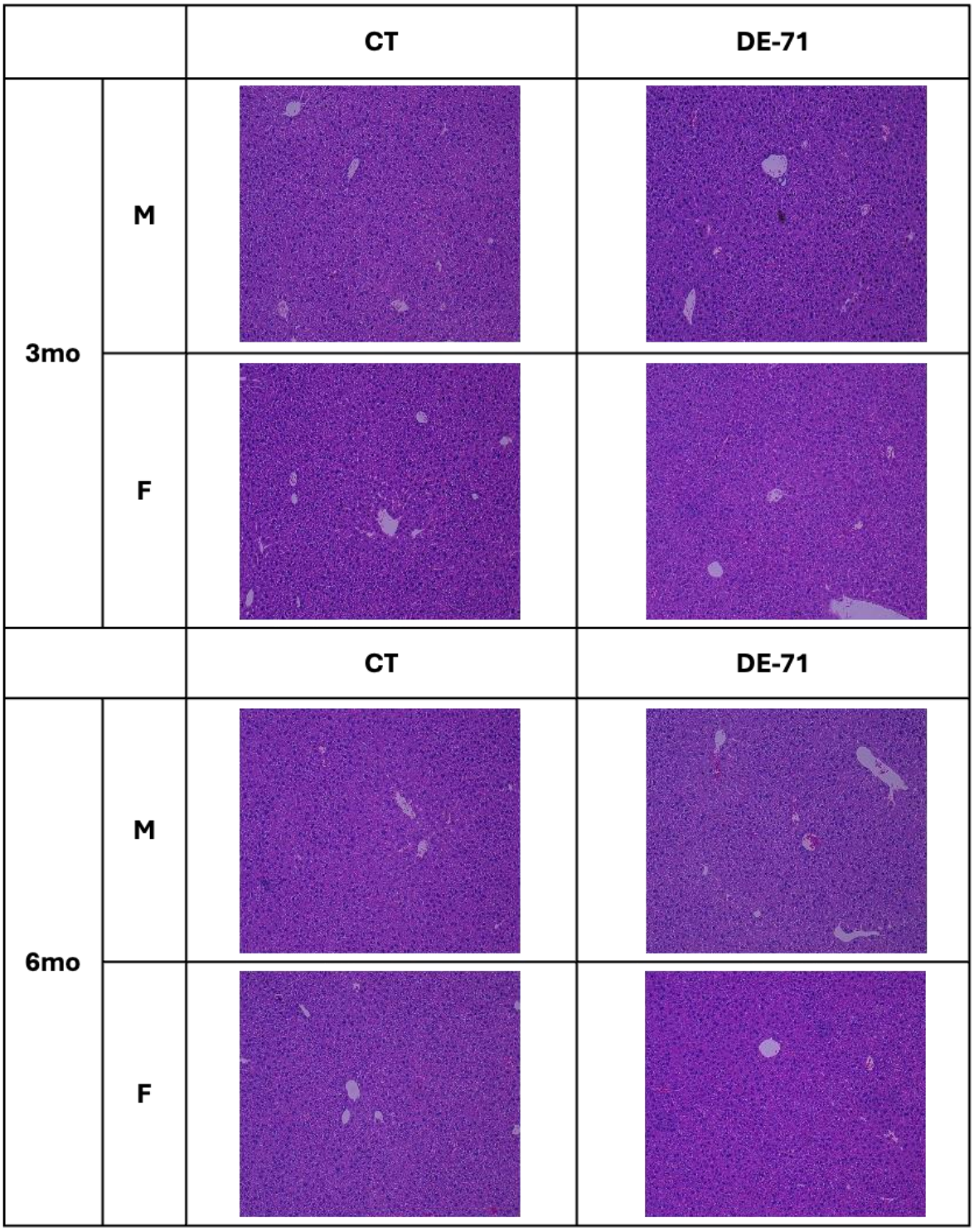

# Figure S4

## A) 3 months

### Males

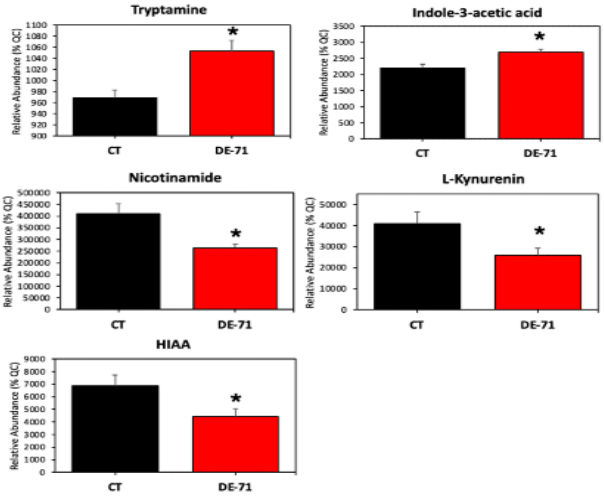


### Females

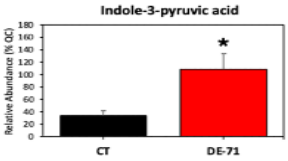


## B) 6 months

### Males

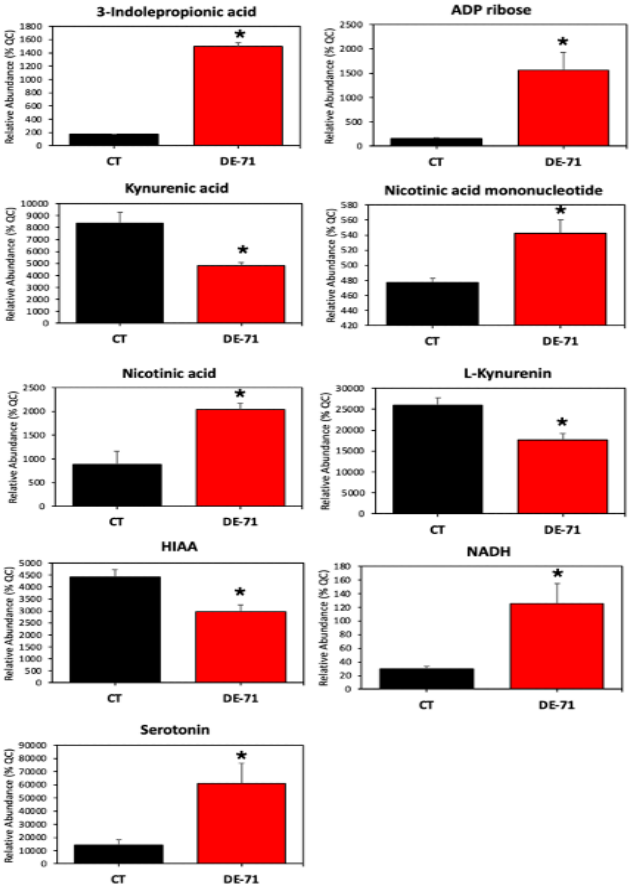


### Females

None

# Figure S5

## A) 3 months

### Males

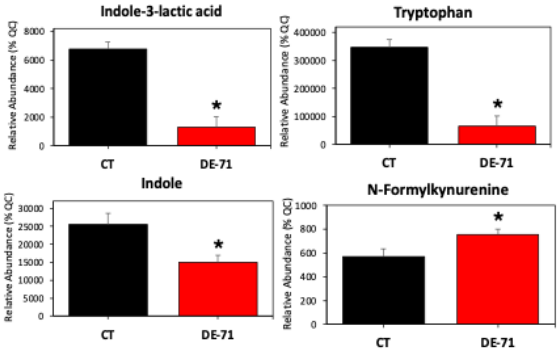


### Females

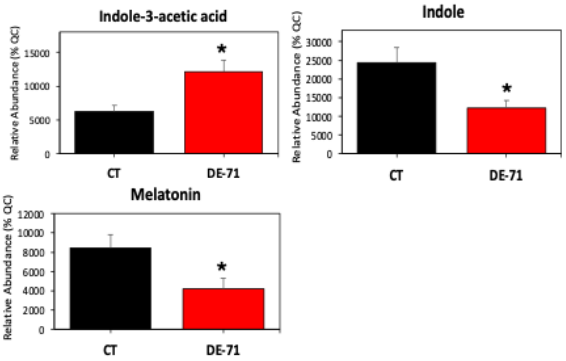


## B) 6 months

### Males

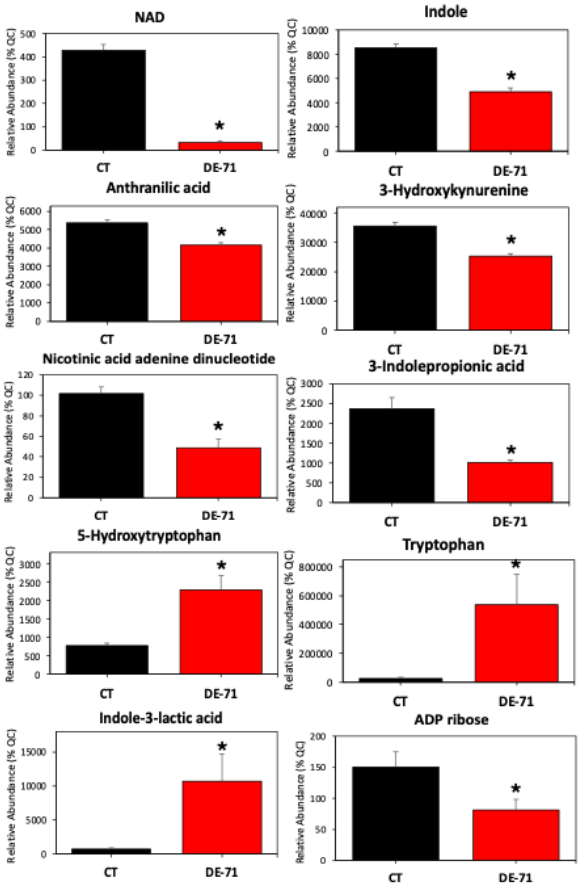


### Females

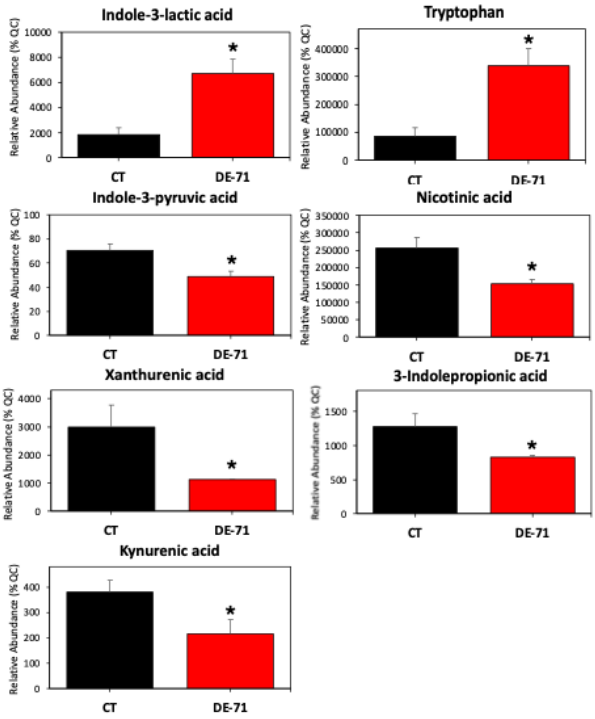

# Figure S6

## A) 3 months Female

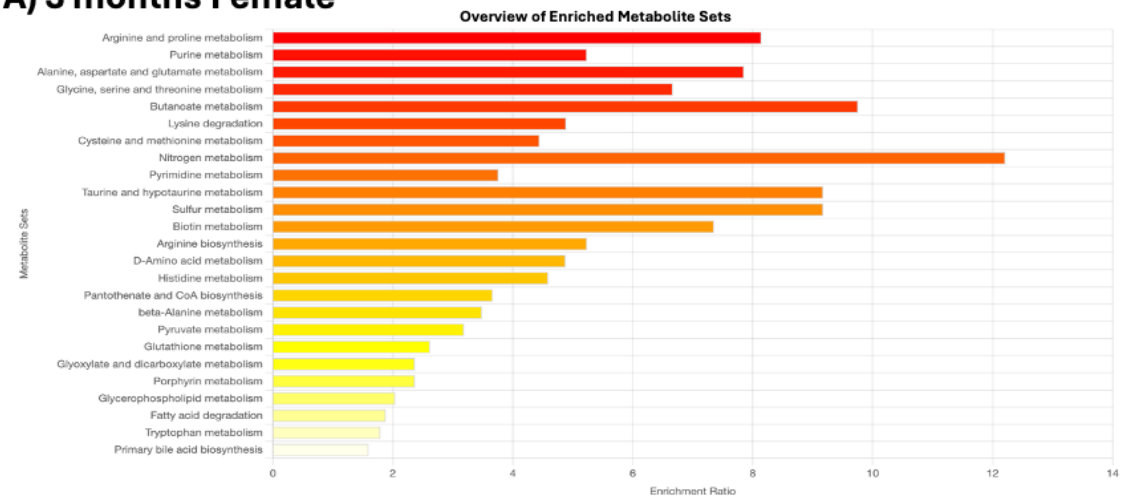


## B) 6 months Male

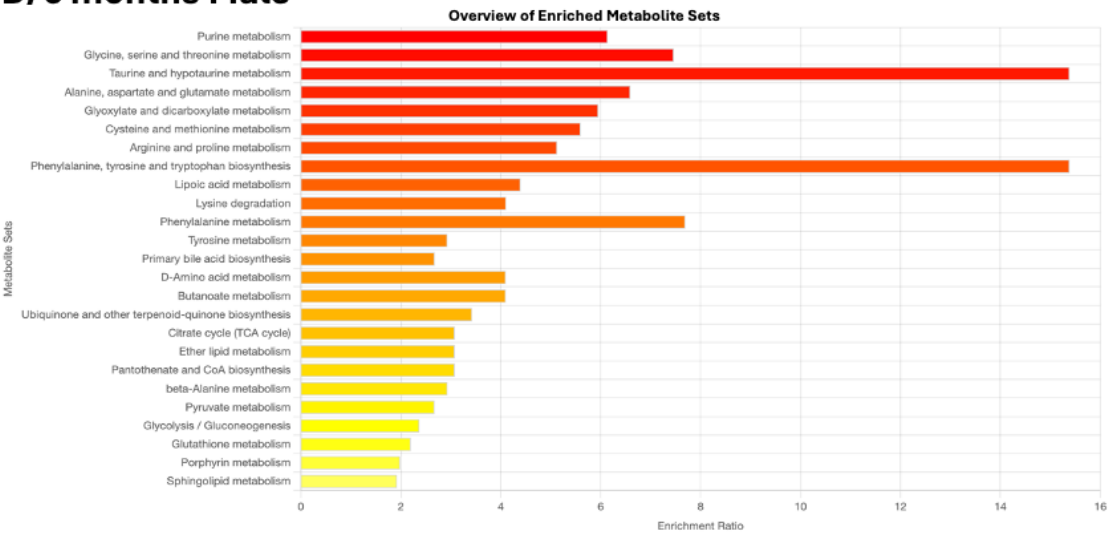


## C) 6 months Female

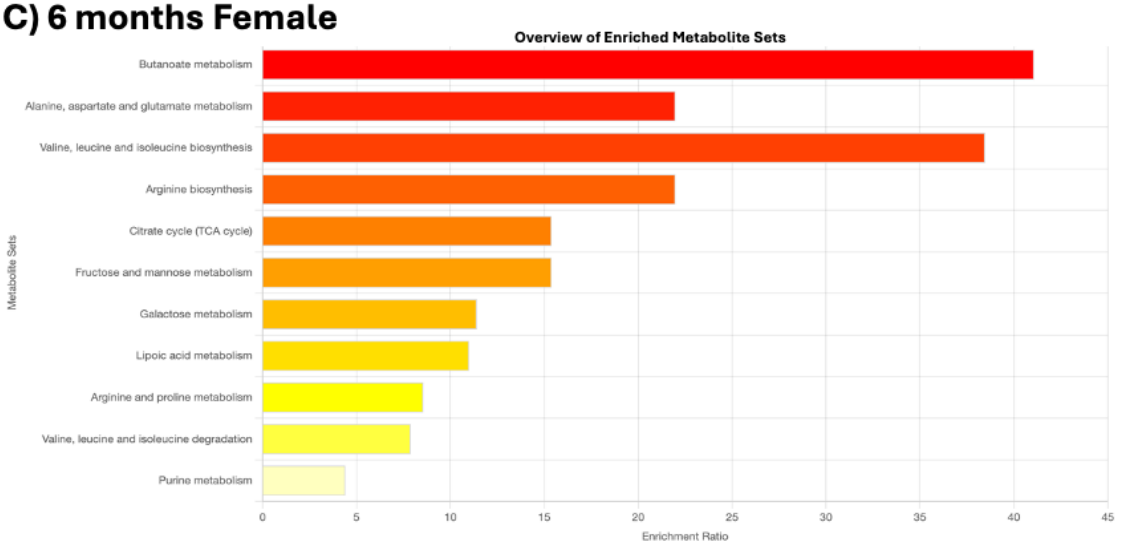

# Figure S7

## A) 3 months Male

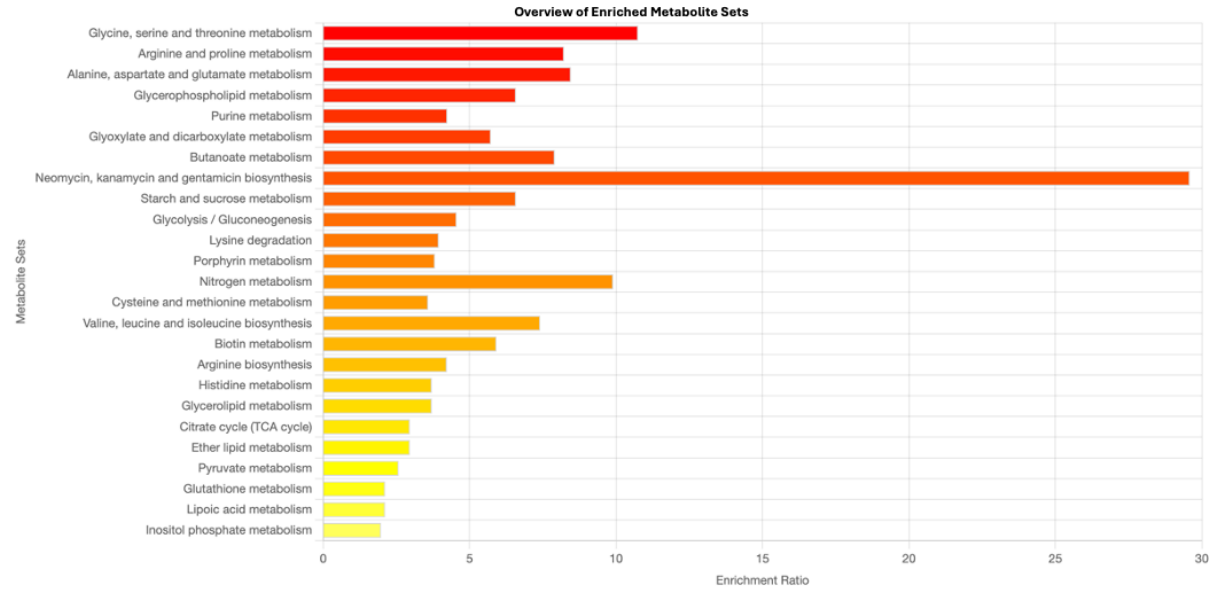


## B) 3 months Female

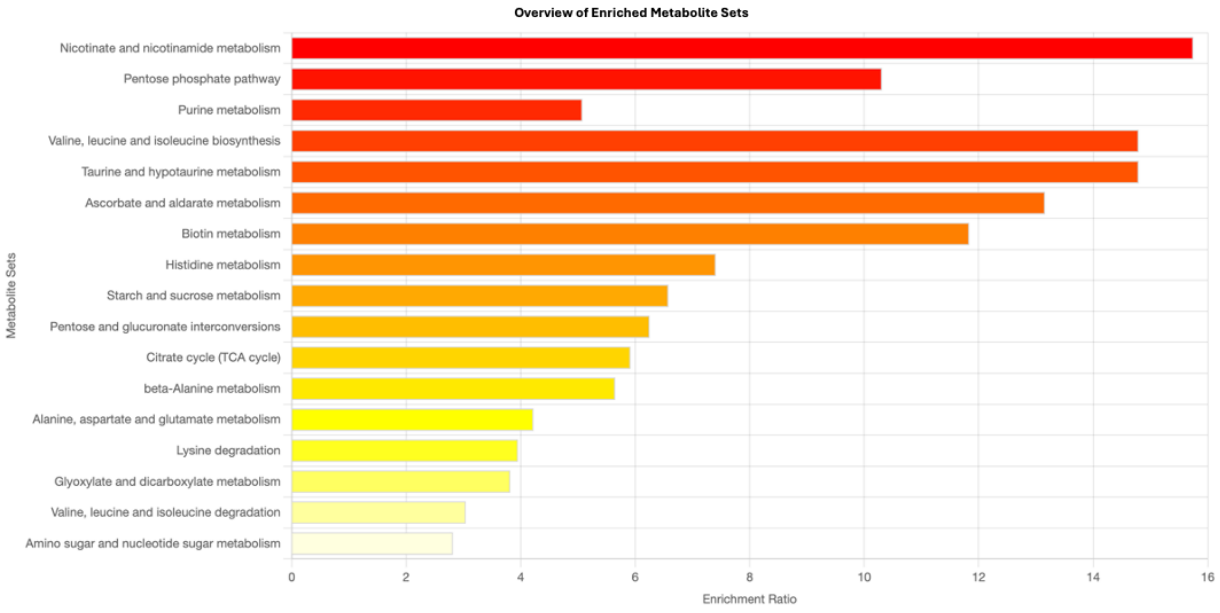

# Figure S8

## A) 6 months Male

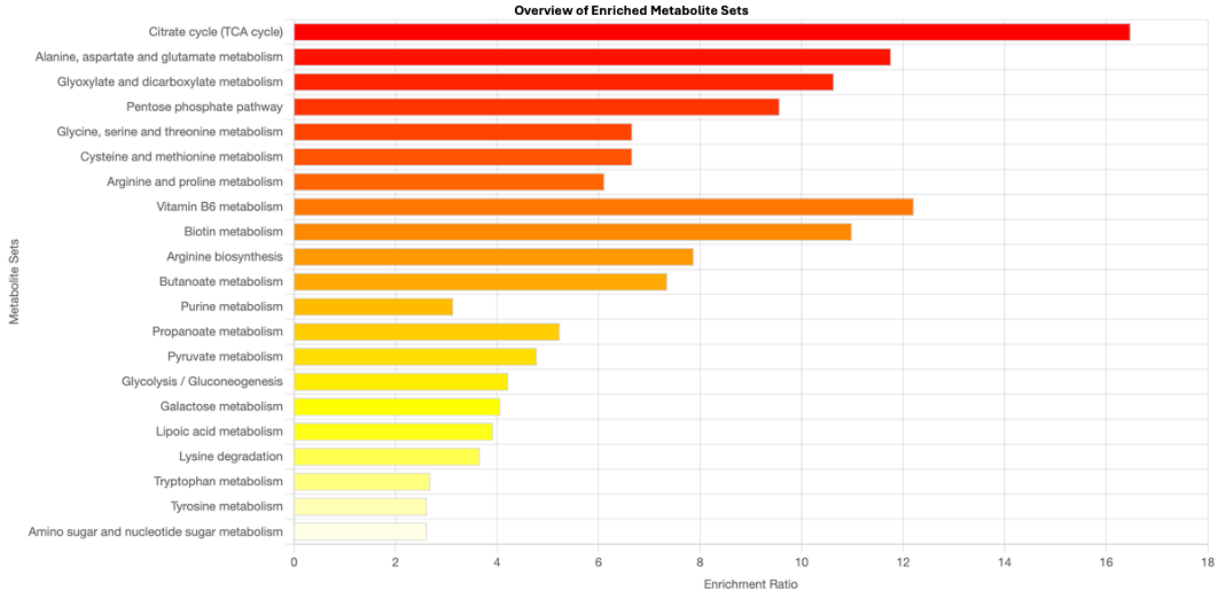


## B) 6 months Female

None

# Figure S9

## A) 3 months Male

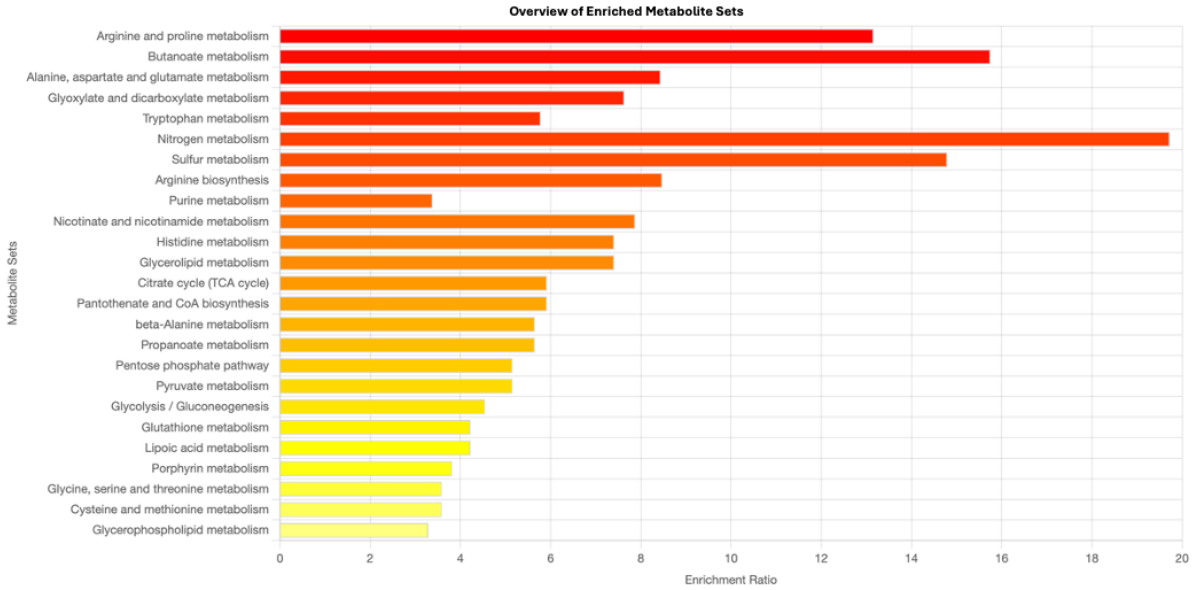


## B) 3 months Female

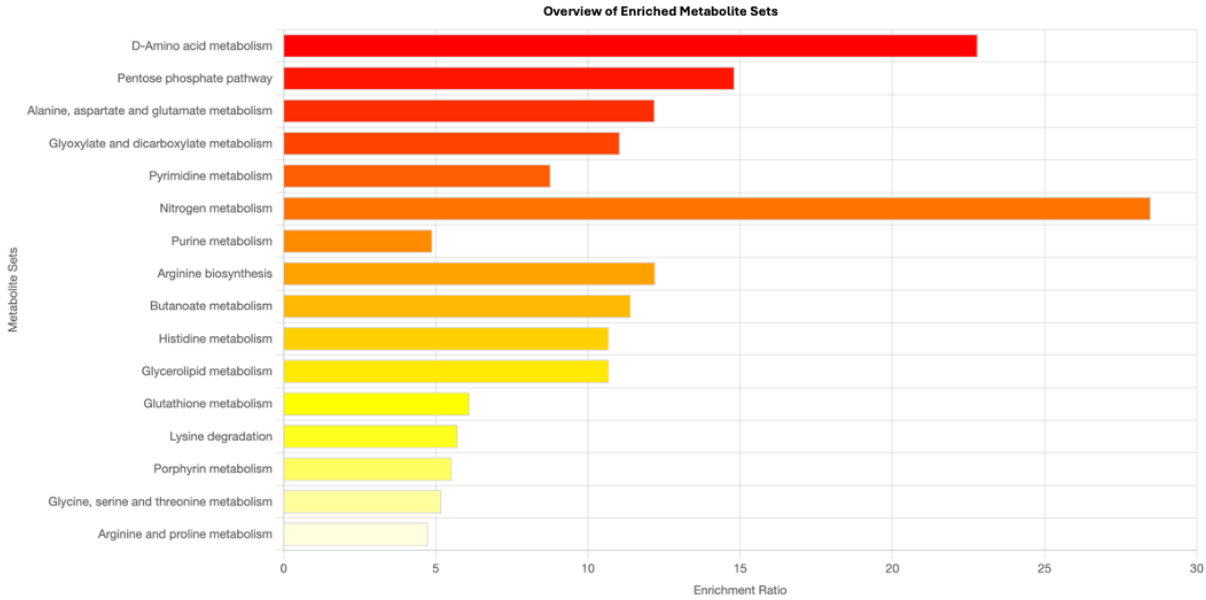

# Figure S10

## A) 6 months Male

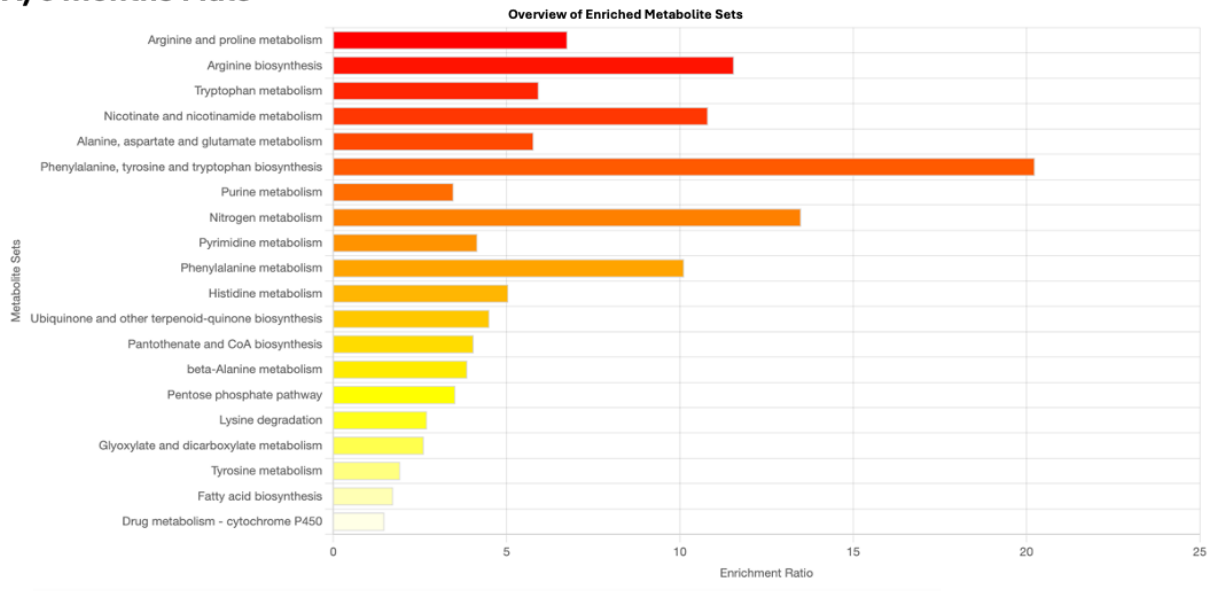


## B) 6 months Female

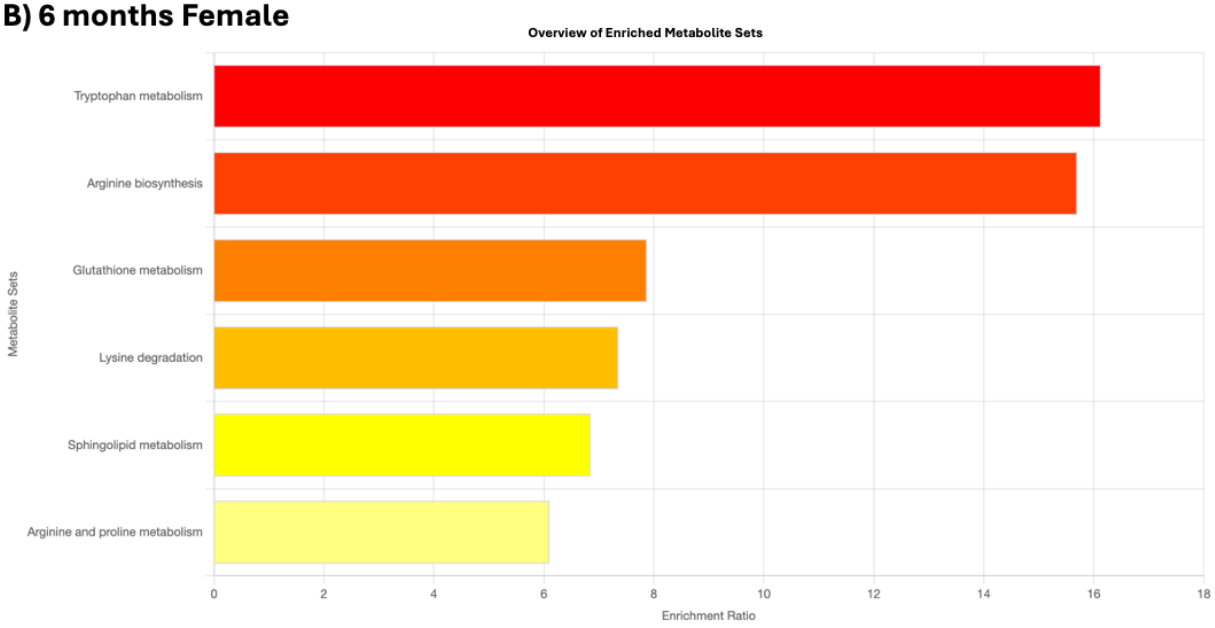

## Chapter 6

## Conclusion and Future work

Persistent organic pollutants (POPs), such as polybrominated diphenyl ethers (PBDEs), were widely used in industrial and consumer products for their flame-retardant properties and chemical stability. However, due to their lipophilicity and bioaccumulative nature, PBDEs have become a significant environmental concern and are considered legacy contaminants that persist in the environment despite being phased out in the early 2000s. These pollutants continue to contribute to long-term human exposure through sources such as aging household products, breast milk, meat, fish, and other consumable products. Although the acute and chronic hepatotoxic effects of PBDEs have been well established in prior research, the impact of maternal PBDE exposure on the gut microbiome and associated metabolic signatures linked to inflammation and metabolic disorders later in life remains poorly understood. My dissertation research was designed to address these critical gaps in toxicology and public health.

The developmental origins of health and disease (DOHaD) hypothesis states that exposure to environmental chemicals during critical early-life stages can increase the risk of developing diseases later in adulthood. Newborns are particularly vulnerable to chemical-induced toxicities, which may cause acute or persistent alterations in physiological systems and disease susceptibility later in life. Our previous work demonstrated that neonatal oral exposure to BDE-99, a PBDE congener, resulted in persistent gut dysbiosis in young adult male offspring. PBDEs remain environmentally persistent and are still ubiquitously detected in humans.

The gut microbiome is essential for regulating host metabolic processes, including xenobiotic and intermediary metabolism. It contributes to host health by producing short-chain fatty acids (SCFAs), modulating immune responses, and converting primary bile acids (BAs) into

secondary BAs. Additionally, microbial metabolites that are produced in the gut can influence pharmacological responses and facilitate the detoxification of toxic chemicals, such as heavy metals and environmental toxicants. One such metabolite is indole 3-propionic acid (IPA), an intestinal microbial metabolite of tryptophan that serves as a known ligand for pregnane X receptor (PXR). IPA has been shown to maintain mucosal barrier integrity and attenuate inflammation in a PXR-dependent manner. Furthermore, IPA is recognized as a protective biomarker associated with reduced risk of obesity, type 2 diabetes (T2D), and inflammation.

Alterations in the gut microbiome due to their diet or environmental pollutants can disrupt metabolic and physiological homeostasis, promoting the development of metabolic disorders. In this study, dietary and oral exposure will be the primary routes of PBDEs, making the gut the first site of interaction and metabolism that consists majority of the microbiome. Therefore, using conventional (CV) mice with an intact microbiome and germ-free (GF) mice lacking microbiota, and in the context of the DOHaD hypothesis, I hypothesized that maternal PBDE exposure leads to persistent gut dysbiosis, driving hepatic proinflammatory responses and contributing to the onset of metabolic disorders. To test this, CV humanized PXR-transgenic (hPXR) dams were assigned to one of four exposure groups beginning 4 weeks preconception until lactation: 1) standard rodent chow, 2) DE-71 (an industrial PBDE mixture, 0.1 mg/kg/day via diet, 3) IPA supplementation (20 mg/kg/day) via drinking water, and 4) DE-71 via diet + IPA supplementation via drinking water. The pups were weaned at postnatal day (PND) 21, at which point DE-71 exposure ceased, while IPA supplementation continued in the relevant groups (3 and 4). Tissues were collected at PND 21, 3 months, and 6 months of age. Metagenomic shogun sequencing was performed on large intestinal contents (LIC) for metabolic function prediction, along with untargeted and targeted metabolomics to compare the maternal PBDE exposure effects in CV and GF mice. I found that

differentially regulated microbial species changed by DE-71 exposure in CV mice were increased over time, indicating DE-71 effect was persistent and amplified over time in an age-dependent manner, where most of the differentially regulated species were linked to obesity and diabetes. IPA supplementation was able to partially prevent DE-71-derived changes in microbial species. In metabolic function predictions, maternal DE-71 exposure at PND 21 altered microbial genes involved in glucose metabolism and obesity-related pathways in the offspring at PND 21, including increased DNA abundance of oxidoreductases and cysteine peptidase family C16 in male pups, with these effects normalized by IPA supplementation. In female 3 months old, DE-71 increased serine peptidase family S51 primarily related to inflammation and was attenuated by IPA. In addition, DE-71 upregulated twitching motility protein genes in male 3 months of age, which are associated with gastrointestinal injury and biofilm formation that were reversed by IPA. At 6 months of age, maternal DE-71 exposure led to increased expression of microbial genes involved in glucose metabolism (oxidoreductases and isomerases) in female but not male offspring, and this was partially prevented by IPA supplementation. Overall, functional predictions of the microbiome revealed age- and sex-specific effects of DE-71 on pathways which were partially prevented by IPA.

Fecal microbiota transplantation (FMT) from DE–71-exposed donors into GF mice revealed persistent gut dysbiosis in a sex- and age-dependent manner. Specifically, DE-71 exposure increased the relative abundance of *Bacteroidota* while reducing *Firmicutes* and *Proteobacteria*, with more pronounced changes in females at 6 months of age. Functional pathway analysis indicated significant disruption of microbial metabolic functions in females, including amino acid biosynthesis and lipid metabolism, which is linked to host energy homeostasis. Gene ontology (GO) enrichment of hepatic transcriptomes showed that DE-71-associated microbiota

reprogrammed liver gene expression in a sex-specific manner. In males, FMT from DE-71-exposed mice led to downregulation of xenobiotic metabolism and oxidative stress pathways, as well as disrupted circadian rhythm and metabolic signaling. In contrast, females exhibited upregulation of proteasomal degradation and stress-activated kinase pathways, indicating sustained hepatic stress and inflammation. Analysis of inflammatory gene expression revealed greater elevations in hepatic and ileal cytokines in female recipients over time. In addition, tight junction genes (*Tjp1* and *Tjp2*) were persistently downregulated in both sexes, indicating compromised intestinal barrier integrity or "leaky gut" following DE-71-induced microbial dysbiosis. DE-71 exposure also impaired hepatic xenobiotic sensing and detoxification. Male recipients at 6 months of age showed downregulation of nuclear receptor target genes, *Cyp2b10*, *Cyp3a11*, and *Nqo1* and upregulation of phase II conjugation enzymes, Ugt isoforms, suggesting delayed compensatory responses. Targeted metabolomics identified reduced levels of anti-inflammatory microbial metabolites, such as indole and kynurenic acid and increased pro-inflammatory intermediates, such as tryptamine and serotonin in males, with broader sex- and tissue-specific disruptions. Untargeted metabolomics further supported these findings, revealing pathway enrichment in the liver of FMT from DE-71-exposed male mice related to the TCA cycle, vitamin B6, and purine metabolism. In contrast, females exhibited alterations in intestinal metabolism, including branched-chain amino acid and tryptophan pathways. These findings demonstrate that early-life DE-71 exposure induces persistent microbial dysbiosis and reprograms host metabolic and inflammatory responses in a sex- and tissue-dependent manner, potentially contributing to the development of metabolic disorders later in life. Future studies should further explore the role of the microbiome using GF mouse models, incorporating direct DE-71 exposure and supplementing with IPA to assess whether persistent signatures can be attenuated, and apply

computational modeling approaches, such as proteomics, to elucidate the gene-protein mechanism relationship.

By employing a multi-omics approach (metagenomics, metabolomics, and transcriptomics), this study provides critical insights into the role of the gut microbiome in mediating maternal PBDE-induced responses across the liver, serum, and intestine. Maternal DE-71 exposure led to persistent gut dysbiosis and proinflammatory signatures along the gut-liver axis in offspring, linked to dysregulated microbial tryptophan metabolism in a sex-dependent manner. These effects were validated in GF mice, and notably, supplementation with IPA partially mitigated several molecular and toxic outcomes of maternal DE-71 exposure. Our findings also point forward PXR as a candidate mechanistic driver, given its known activation by both PBDEs and tryptophan-derived microbial metabolites, such as IPA. Although hPXR-TG mice were used to enhance translational relevance, further studies using PXR-null mice and PXR antagonists (e.g., ketoconazole) are needed to directly test the necessity and sufficiency of PXR in mediating the observed outcomes (Kliewer 2003; Timsit and Negishi 2007). The observed sex-specific responses likely arise from multiple layers of biological regulation. One important factor is sex hormone signaling, particularly the influence of estrogen, which has been shown to modulate PXR expression and transcriptional activity in the liver and intestine (Masuyama et al. 2005; Barretto et al. 2021). Estrogen may enhance or suppress xenobiotic metabolism depending on the cellular context and receptor crosstalk and can also influence gut permeability and immune tone. Moreover, intrinsic differences in baseline microbiota composition between males and females contribute to distinct microbial metabolic outputs, including those involving tryptophan pathways (Kim et al. 2023; Barretto et al. 2021). For instance, female mice often harbor greater abundance of bacteria involved in short-chain fatty acid and indole production, which could interact with

nuclear receptors and modulate host responses differently than in males. These sex-driven microbiome-host interactions may amplify or lower responses to environmental toxicants, leading to divergent outcomes in inflammation, metabolism, and receptor activation. Furthermore, while the IPA dose (20 mg/kg/day in drinking water) used here exceeds average endogenous levels, it approximates the upper physiological range observed in humans with high microbial IPA production and has been shown to exert barrier-protective and anti-inflammatory effects in murine models (Venkatesh et al. 2014; Geddo et al. 2024). Future investigations leveraging these multi-omics platforms could support a causal modeling framework to dissect host-microbe-chemical interactions, guiding toxico-pharmaco-metagenomic strategies for preventing or treating metabolic disorders in populations vulnerable to early-life chemical exposures. Collectively, this study not only illustrates the gut microbiome's critical role in shaping responses to environmental toxicants, such as PBDEs, but also highlights its relevance to the DOHaD paradigm and the growing need to integrate microbiome-informed mechanisms into environmental risk assessment.

**References**


Aghighi, Fatemeh, and Mahmoud Salami. 2024. "What We Need to Know about the Germ-Free Animal Models." *AIMS Microbiology* 10 (1): 107–47. https://doi.org/10.3934/microbiol.2024007.

Agus, Allison, Julien Planchais, and Harry Sokol. 2018. "Gut Microbiota Regulation of Tryptophan Metabolism in Health and Disease." *Cell Host & Microbe* 23 (6): 716–24. https://doi.org/10.1016/j.chom.2018.05.003.

Alaish, Samuel M., Alexis D. Smith, Jennifer Timmons, Jose Greenspon, Daniel Eyvazzadeh, Ebony Murphy, Terez Shea-Donahue, et al. 2013. "Gut Microbiota, Tight Junction Protein Expression, Intestinal Resistance, Bacterial Translocation and Mortality Following Cholestasis Depend on the Genetic Background of the Host." *Gut Microbes* 4 (4): 292–305. https://doi.org/10.4161/gmic.24706.

Alamshah, A., E. Spreckley, M. Norton, J. S. Kinsey-Jones, A. Amin, A. Ramgulam, Y. Cao, et al. 2017. "L-Phenylalanine Modulates Gut Hormone Release and Glucose Tolerance, and Suppresses Food Intake through the Calcium-Sensing Receptor in Rodents." *International Journal of Obesity (2005)* 41 (11): 1693–1701. https://doi.org/10.1038/ijo.2017.164.

Aleksunes, Lauren M., and Curtis D. Klaassen. 2012. "Coordinated Regulation of Hepatic Phase I and II Drug-Metabolizing Genes and Transporters Using AhR-, CAR-, PXR-, PPARα-, and Nrf2-Null Mice." *Drug Metabolism and Disposition: The Biological Fate of Chemicals* 40 (7): 1366–79. https://doi.org/10.1124/dmd.112.045112.

Alexeev, Erica E., Jordi M. Lanis, Daniel J. Kao, Eric L. Campbell, Caleb J. Kelly, Kayla D. Battista, Mark E. Gerich, et al. 2018. "Microbiota-Derived Indole Metabolites Promote Human and Murine Intestinal Homeostasis through Regulation of Interleukin-10 Receptor." *The American Journal of Pathology* 188 (5): 1183–94. https://doi.org/10.1016/j.ajpath.2018.01.011.

Alhouayek, Mireille, Pauline Bottemanne, Alexandros Makriyannis, and Giulio G. Muccioli. 2017. "N-Acylethanolamine-Hydrolyzing Acid Amidase and Fatty Acid Amide Hydrolase Inhibition Differentially Affect N-Acylethanolamine Levels and Macrophage Activation." *Biochimica Et Biophysica Acta. Molecular and Cell Biology of Lipids* 1862 (5): 474–84. https://doi.org/10.1016/j.bbalip.2017.01.001.

Altobelli, Emma, Paolo Matteo Angeletti, and Giovanni Latella. 2016. “Role of Urinary Biomarkers in the Diagnosis of Adenoma and Colorectal Cancer: A Systematic Review and Meta-Analysis.” *Journal of Cancer* 7 (14): 1984–2004. https://doi.org/10.7150/jca.16244.

Angrish, Nupur, Neha Lalwani, and Garima Khare. 2023. “In Silico Virtual Screening for the Identification of Novel Inhibitors against Dihydrodipicolinate Reductase (DapB) of Mycobacterium Tuberculosis, a Key Enzyme of Diaminopimelate Pathway.” *Microbiology Spectrum* 11 (6): e0135923. https://doi.org/10.1128/spectrum.01359-23.

Azar, Naomi, Linda Booij, Gina Muckle, Tye E. Arbuckle, Jean R. Séguin, Elizabeth Asztalos, William D. Fraser, Bruce P. Lanphear, and Maryse F. Bouchard. 2021. “Prenatal Exposure to Polybrominated Diphenyl Ethers (PBDEs) and Cognitive Ability in Early Childhood.” *Environment International* 146 (January):106296. https://doi.org/10.1016/j.envint.2020.106296.

Babalola, B. A., and A. A. Adeyi. 2018. “Levels, Dietary Intake and Risk of Polybrominated Diphenyl Ethers (PBDEs) in Foods Commonly Consumed in Nigeria.” *Food Chemistry* 265 (November):78–84. https://doi.org/10.1016/j.foodchem.2018.05.073.

Bacanlı, Merve, Hatice Gül Anlar, Sevtap Aydın, Tuğbagül Çal, Nuray Arı, Ülkü Ündeğer Bucurgat, A. Ahmet Başaran, and Nurşen Başaran. 2017. “D-Limonene Ameliorates Diabetes and Its Complications in Streptozotocin-Induced Diabetic Rats.” *Food and Chemical Toxicology: An International Journal Published for the British Industrial Biological Research Association* 110 (December):434–42. https://doi.org/10.1016/j.fct.2017.09.020.

Bassols, Judit, Matteo Serino, Gemma Carreras-Badosa, Rémy Burcelin, Vincent Blasco-Baque, Abel Lopez-Bermejo, and José-Manuel Fernandez-Real. 2016. “Gestational Diabetes Is Associated with Changes in Placental Microbiota and Microbiome.” *Pediatric Research* 80 (6): 777–84. https://doi.org/10.1038/pr.2016.155.

Braniste, Viorica, Maha Al-Asmakh, Czeslawa Kowal, Farhana Anuar, Afrouz Abbaspour, Miklós Tóth, Agata Korecka, et al. 2014. “The Gut Microbiota Influences Blood-Brain Barrier Permeability in Mice.” *Science Translational Medicine* 6 (263): 263ra158. https://doi.org/10.1126/scitranslmed.3009759.

Brewer, C. Trent, and Taosheng Chen. 2016. “PXR Variants: The Impact on Drug Metabolism

and Therapeutic Responses." *Acta Pharmaceutica Sinica. B* 6 (5): 441–49. https://doi.org/10.1016/j.apsb.2016.07.002.

Brown, Dustin G., Sangeeta Rao, Tiffany L. Weir, Joanne O'Malia, Marlon Bazan, Regina J. Brown, and Elizabeth P. Ryan. 2016. "Metabolomics and Metabolic Pathway Networks from Human Colorectal Cancers, Adjacent Mucosa, and Stool." *Cancer & Metabolism* 4:11. https://doi.org/10.1186/s40170-016-0151-y.

Bui, Thi Phuong Nam, Louise Mannerås-Holm, Robert Puschmann, Hao Wu, Antonio Dario Troise, Bart Nijsse, Sjef Boeren, Fredrik Bäckhed, Dorothea Fiedler, and Willem M. deVos. 2021. "Conversion of Dietary Inositol into Propionate and Acetate by Commensal Anaerostipes Associates with Host Health." *Nature Communications* 12 (1): 4798. https://doi.org/10.1038/s41467-021-25081-w.

Cabral, Damien J., Jenna I. Wurster, Benjamin J. Korry, Swathi Penumutchu, and Peter Belenky. 2020. "Consumption of a Western-Style Diet Modulates the Response of the Murine Gut Microbiome to Ciprofloxacin." *mSystems* 5 (4): e00317-20. https://doi.org/10.1128/mSystems.00317-20.

Cade, Sara E., Li-Jung Kuo, and Irvin R. Schultz. 2018. "Polybrominated Diphenyl Ethers and Their Hydroxylated and Methoxylated Derivatives in Seafood Obtained from Puget Sound, WA." *The Science of the Total Environment* 630 (July):1149–54. https://doi.org/10.1016/j.scitotenv.2018.02.301.

Carlson, Adlei B., and Gregory P. Kraus. 2025. "Physiology, Cholinergic Receptors." In *StatPearls*. Treasure Island (FL): StatPearls Publishing. http://www.ncbi.nlm.nih.gov/books/NBK526134/.

Carroll, Patrick A., Daniel Diolaiti, Lisa McFerrin, Haiwei Gu, Danijel Djukovic, Jianhai Du, Pei Feng Cheng, et al. 2015a. "Deregulated Myc Requires MondoA/Mlx for Metabolic Reprogramming and Tumorigenesis." *Cancer Cell* 27 (2): 271–85. https://doi.org/10.1016/j.ccell.2014.11.024.

———. 2015b. "Deregulated Myc Requires MondoA/Mlx for Metabolic Reprogramming and Tumorigenesis." *Cancer Cell* 27 (2): 271–85. https://doi.org/10.1016/j.ccell.2014.11.024.

Chek, Min Fey, Sun Yong Kim, Tomoyuki Mori, Hisayuki Kojima, and Toshio Hakoshima. 2021. "Crystal Structure of N-Terminal Degron-Truncated Human Glutamine Synthetase." *Acta Crystallographica. Section F, Structural Biology Communications* 77

(Pt 11): 427–34. https://doi.org/10.1107/S2053230X21010748.

Chen, Lu, Yuxuan Yang, Siyu Sun, Yuan Xie, Cailong Pan, Maining Li, Chen Li, et al. 2022. "Indolepropionic Acid Reduces Obesity-Induced Metabolic Dysfunction through Colonic Barrier Restoration Mediated via Tuft Cell-Derived IL-25." *The FEBS Journal* 289 (19): 5985–6004. https://doi.org/10.1111/febs.16470.

Cheng, Jie, Yatrik M. Shah, and Frank J. Gonzalez. 2012. "Pregnane X Receptor as a Target for Treatment of Inflammatory Bowel Disorders." *Trends in Pharmacological Sciences* 33 (6): 323–30. https://doi.org/10.1016/j.tips.2012.03.003.

Chia, J.-H., T.-S. Wu, T.-L. Wu, C.-L. Chen, C.-H. Chuang, L.-H. Su, H.-J. Chang, et al. 2018. "Clostridium Innocuum Is a Vancomycin-Resistant Pathogen That May Cause Antibiotic-Associated Diarrhoea." *Clinical Microbiology and Infection: The Official Publication of the European Society of Clinical Microbiology and Infectious Diseases* 24 (11): 1195–99. https://doi.org/10.1016/j.cmi.2018.02.015.

Chiu, Yu-Han, Jorge E. Chavarro, Barbra A. Dickerman, JoAnn E. Manson, Kenneth J. Mukamal, Kathryn M. Rexrode, Eric B. Rimm, and Miguel A. Hernán. 2021. "Estimating the Effect of Nutritional Interventions Using Observational Data: The American Heart Association's 2020 Dietary Goals and Mortality." *The American Journal of Clinical Nutrition* 114 (2): 690–703. https://doi.org/10.1093/ajcn/nqab100.

Cho, Byuri Angela, Seong-Keun Yoo, Young Shin Song, Su-Jin Kim, Kyu Eun Lee, Minho Shong, Young Joo Park, and Jeong-Sun Seo. 2018. "Transcriptome Network Analysis Reveals Aging-Related Mitochondrial and Proteasomal Dysfunction and Immune Activation in Human Thyroid." *Thyroid: Official Journal of the American Thyroid Association* 28 (5): 656–66. https://doi.org/10.1089/thy.2017.0359.

Clarke, Gerard, Roman M. Stilling, Paul J. Kennedy, Catherine Stanton, John F. Cryan, and Timothy G. Dinan. 2014. "Minireview: Gut Microbiota: The Neglected Endocrine Organ." *Molecular Endocrinology (Baltimore, Md.)* 28 (8): 1221–38. https://doi.org/10.1210/me.2014-1108.

Clarke, Siobhan F., Eileen F. Murphy, Kanishka Nilaweera, Paul R. Ross, Fergus Shanahan, Paul W. O'Toole, and Paul D. Cotter. 2012. "The Gut Microbiota and Its Relationship to Diet and Obesity: New Insights." *Gut Microbes* 3 (3): 186–202. https://doi.org/10.4161/gmic.20168.

Clayburgh, Daniel R., Le Shen, and Jerrold R. Turner. 2004. “A Porous Defense: The Leaky Epithelial Barrier in Intestinal Disease.” *Laboratory Investigation; a Journal of Technical Methods and Pathology* 84 (3): 282–91. https://doi.org/10.1038/labinvest.3700050.

Cryan, John F., and Timothy G. Dinan. 2012. “Mind-Altering Microorganisms: The Impact of the Gut Microbiota on Brain and Behaviour.” *Nature Reviews. Neuroscience* 13 (10): 701–12. https://doi.org/10.1038/nrn3346.

Cui, Julia Yue, and Curtis D. Klaassen. 2016. “RNA-Seq Reveals Common and Unique PXR- and CAR-Target Gene Signatures in the Mouse Liver Transcriptome.” *Biochimica Et Biophysica Acta* 1859 (9): 1198–1217. https://doi.org/10.1016/j.bbagrm.2016.04.010.

Cunningham, A. L., J. W. Stephens, and D. A. Harris. 2021. “Gut Microbiota Influence in Type 2 Diabetes Mellitus (T2DM).” *Gut Pathogens* 13 (1): 50. https://doi.org/10.1186/s13099-021-00446-0.

De, Arpan, Weijie Chen, Hao Li, Justin R. Wright, Regina Lamendella, Dana J. Lukin, Wendy A. Szymczak, et al. 2021. “Bacterial Swarmers Enriched During Intestinal Stress Ameliorate Damage.” *Gastroenterology* 161 (1): 211–24. https://doi.org/10.1053/j.gastro.2021.03.017.

DeBerardinis, Ralph J., and Craig B. Thompson. 2012. “Cellular Metabolism and Disease: What Do Metabolic Outliers Teach Us?” *Cell* 148 (6): 1132–44. https://doi.org/10.1016/j.cell.2012.02.032.

Dempsey, Joseph L., Dongfang Wang, Gunseli Siginir, Qiang Fei, Daniel Raftery, Haiwei Gu, and Julia Yue Cui. 2019. “Pharmacological Activation of PXR and CAR Downregulates Distinct Bile Acid-Metabolizing Intestinal Bacteria and Alters Bile Acid Homeostasis.” *Toxicological Sciences: An Official Journal of the Society of Toxicology* 168 (1): 40–60. https://doi.org/10.1093/toxsci/kfy271.

Di Domenico, Fabio, Eugenio Barone, Marzia Perluigi, and D. Allan Butterfield. 2017. “The Triangle of Death in Alzheimer’s Disease Brain: The Aberrant Cross-Talk Among Energy Metabolism, Mammalian Target of Rapamycin Signaling, and Protein Homeostasis Revealed by Redox Proteomics.” *Antioxidants & Redox Signaling* 26 (8): 364–87. https://doi.org/10.1089/ars.2016.6759.

Dong, Tien S., Kayti Luu, Venu Lagishetty, Farzaneh Sedighian, Shih-Lung Woo, Benjamin W. Dreskin, William Katzka, et al. 2021. “The Intestinal Microbiome Predicts Weight Loss

on a Calorie-Restricted Diet and Is Associated With Improved Hepatic Steatosis." *Frontiers in Nutrition* 8:718661. https://doi.org/10.3389/fnut.2021.718661.

Drissi, F., V. Merhej, E. Angelakis, A. El Kaoutari, F. Carrière, B. Henrissat, and D. Raoult. 2014. "Comparative Genomics Analysis of Lactobacillus Species Associated with Weight Gain or Weight Protection." *Nutrition & Diabetes* 4 (2): e109. https://doi.org/10.1038/nutd.2014.6.

Eghlimi, Ryan, Xiaojian Shi, Jonathan Hrovat, Bowei Xi, and Haiwei Gu. 2020. "Triple Negative Breast Cancer Detection Using LC-MS/MS Lipidomic Profiling." *Journal of Proteome Research* 19 (6): 2367–78. https://doi.org/10.1021/acs.jproteome.0c00038.

Ehrich, Mathias, John K. Field, Triantafillos Liloglou, George Xinarianos, Paul Oeth, Matthew R. Nelson, Charles R. Cantor, and Dirk van den Boom. 2006. "Cytosine Methylation Profiles as a Molecular Marker in Non-Small Cell Lung Cancer." *Cancer Research* 66 (22): 10911–18. https://doi.org/10.1158/0008-5472.CAN-06-0400.

Elshorbagy, Amany K., Maria Valdivia-Garcia, Helga Refsum, and Nancy Butte. 2012. "The Association of Cysteine with Obesity, Inflammatory Cytokines and Insulin Resistance in Hispanic Children and Adolescents." *PloS One* 7 (9): e44166. https://doi.org/10.1371/journal.pone.0044166.

Fisher, John T., Sandra G. Vincent, Jesus Gomeza, Masahisa Yamada, and Jürgen Wess. 2004. "Loss of Vagally Mediated Bradycardia and Bronchoconstriction in Mice Lacking M2 or M3 Muscarinic Acetylcholine Receptors." *FASEB Journal: Official Publication of the Federation of American Societies for Experimental Biology* 18 (6): 711–13. https://doi.org/10.1096/fj.03-0648fje.

Flannigan, Kyle L., Kristoff M. Nieves, Holly E. Szczepanski, Alex Serra, Joshua W. Lee, Laurie A. Alston, Hena Ramay, Sridhar Mani, and Simon A. Hirota. 2023. "The Pregnane X Receptor and Indole-3-Propionic Acid Shape the Intestinal Mesenchyme to Restrain Inflammation and Fibrosis." *Cellular and Molecular Gastroenterology and Hepatology* 15 (3): 765–95. https://doi.org/10.1016/j.jcmgh.2022.10.014.

Flaveny, Colin A., Iain A. Murray, and Gary H. Perdew. 2010. "Differential Gene Regulation by the Human and Mouse Aryl Hydrocarbon Receptor." *Toxicological Sciences: An Official Journal of the Society of Toxicology* 114 (2): 217–25. https://doi.org/10.1093/toxsci/kfp308.

Fortin, Geneviève. 2011. “L-Carnitine and Intestinal Inflammation.” *Vitamins and Hormones* 86:353–66. https://doi.org/10.1016/B978-0-12-386960-9.00015-0.

Fouces, Roberto, Encarnación Mellado, Bruno Díez, and José Luis Barredo. 1999. “The Tylosin Biosynthetic Cluster from Streptomyces Fradiae: Genetic Organization of the Left Region.” *Microbiology (Reading, England)* 145 ( Pt 4) (April):855–68. https://doi.org/10.1099/13500872-145-4-855.

Frank, Filipp, Eric A. Ortlund, and Xu Liu. 2021. “Structural Insights into Glucocorticoid Receptor Function.” *Biochemical Society Transactions* 49 (5): 2333–43. https://doi.org/10.1042/BST20210419.

Fu, Zidong Donna, and Julia Yue Cui. 2017. “Remote Sensing between Liver and Intestine: Importance of Microbial Metabolites.” *Current Pharmacology Reports* 3 (3): 101–13. https://doi.org/10.1007/s40495-017-0087-0.

Fu, Zidong Donna, Felcy Pavithra Selwyn, Julia Yue Cui, and Curtis D. Klaassen. 2016. “RNA Sequencing Quantification of Xenobiotic-Processing Genes in Various Sections of the Intestine in Comparison to the Liver of Male Mice.” *Drug Metabolism and Disposition: The Biological Fate of Chemicals* 44 (6): 842–56. https://doi.org/10.1124/dmd.115.068270.

Gao, Hui, Xueyan Wan, Boya Xiao, Kaichao Yang, Yafei Wang, Cheng Zhang, Pei Li, et al. 2021. “Impacts of PBDE-47 Exposure before, during and after Pregnancy on the Maternal Gut Microbiome and Its Association with Host Metabolism.” *Ecotoxicology and Environmental Safety* 222 (October):112530. https://doi.org/10.1016/j.ecoenv.2021.112530.

Gao, Kan, Chun-Long Mu, Aitak Farzi, and Wei-Yun Zhu. 2020. “Tryptophan Metabolism: A Link Between the Gut Microbiota and Brain.” *Advances in Nutrition (Bethesda, Md.)* 11 (3): 709–23. https://doi.org/10.1093/advances/nmz127.

Giebel, Nicholas L., Jeffrey D. Shadley, D. Gail McCarver, Kenneth Dorko, Roberto Gramignoli, Stephen C. Strom, Ke Yan, Pippa M. Simpson, and Ronald N. Hines. 2016. “Role of Chromatin Structural Changes in Regulating Human CYP3A Ontogeny.” *Drug Metabolism and Disposition: The Biological Fate of Chemicals* 44 (7): 1027–37. https://doi.org/10.1124/dmd.116.069344.

Gomez, Matthew V., Moumita Dutta, Alexander Suvorov, Xiaojian Shi, Haiwei Gu, Sridhar

Mani, and Julia Yue Cui. 2021. “Early Life Exposure to Environmental Contaminants (BDE-47, TBBPA, and BPS) Produced Persistent Alterations in Fecal Microbiome in Adult Male Mice.” *Toxicological Sciences: An Official Journal of the Society of Toxicology* 179 (1): 14–30. https://doi.org/10.1093/toxsci/kfaa161.

Gong, Jinhua, Yun Shen, Hongcheng Zhang, Man Cao, Muyun Guo, Jianquan He, Bangzhou Zhang, and Chuanxing Xiao. 2022. “Gut Microbiota Characteristics of People with Obesity by Meta-Analysis of Existing Datasets.” *Nutrients* 14 (14): 2993. https://doi.org/10.3390/nu14142993.

Gooding, Jessica R., Mette V. Jensen, Xiaoqing Dai, Brett R. Wenner, Danhong Lu, Ramamani Arumugam, Mourad Ferdaoussi, Patrick E. MacDonald, and Christopher B. Newgard. 2015. “Adenylosuccinate Is an Insulin Secretagogue Derived from Glucose-Induced Purine Metabolism.” *Cell Reports* 13 (1): 157–67. https://doi.org/10.1016/j.celrep.2015.08.072.

Gryp, Tessa, Raymond Vanholder, Mario Vaneechoutte, and Griet Glorieux. 2017. “P-Cresyl Sulfate.” *Toxins* 9 (2): 52. https://doi.org/10.3390/toxins9020052.

Gu, Haiwei, Patrick A. Carroll, Jianhai Du, Jiangjiang Zhu, Fausto Carnevale Neto, Robert N. Eisenman, and Daniel Raftery. 2016. “Quantitative Method to Investigate the Balance between Metabolism and Proteome Biomass: Starting from Glycine.” *Angewandte Chemie (International Ed. in English)* 55 (50): 15646–50. https://doi.org/10.1002/anie.201609236.

Gu, Haiwei, Ping Zhang, Jiangjiang Zhu, and Daniel Raftery. 2015a. “Globally Optimized Targeted Mass Spectrometry: Reliable Metabolomics Analysis with Broad Coverage.” *Analytical Chemistry* 87 (24): 12355–62. https://doi.org/10.1021/acs.analchem.5b03812.

———. 2015b. “Globally Optimized Targeted Mass Spectrometry: Reliable Metabolomics Analysis with Broad Coverage.” *Analytical Chemistry* 87 (24): 12355–62. https://doi.org/10.1021/acs.analchem.5b03812.

Guseva, Natalya V., Oskar W. Rokhlin, Rebecca A. Glover, and Michael B. Cohen. 2011. “TOFA (5-Tetradecyl-Oxy-2-Furoic Acid) Reduces Fatty Acid Synthesis, Inhibits Expression of AR, Neuropilin-1 and Mcl-1 and Kills Prostate Cancer Cells Independent of P53 Status.” *Cancer Biology & Therapy* 12 (1): 80–85. https://doi.org/10.4161/cbt.12.1.15721.

Hanus, L., A. Gopher, S. Almog, and R. Mechoulam. 1993. “Two New Unsaturated Fatty Acid Ethanolamides in Brain That Bind to the Cannabinoid Receptor.” *Journal of Medicinal Chemistry* 36 (20): 3032–34. https://doi.org/10.1021/jm00072a026.

Hardman, M. J., and R. K. Scopes. 1988. “The Kinetics of Glucose-Fructose Oxidoreductase from Zymomonas Mobilis.” *European Journal of Biochemistry* 173 (1): 203–9. https://doi.org/10.1111/j.1432-1033.1988.tb13985.x.

He, Feng, Xiaoli Ru, and Tao Wen. 2020. “NRF2, a Transcription Factor for Stress Response and Beyond.” *International Journal of Molecular Sciences* 21 (13): 4777. https://doi.org/10.3390/ijms21134777.

He, Hailang, Xiaojian Shi, Alex Lawrence, Jonathan Hrovat, Cassidy Turner, Julia Yue Cui, and Haiwei Gu. 2020. “2,2’,4,4’-Tetrabromodiphenyl Ether (BDE-47) Induces Wide Metabolic Changes Including Attenuated Mitochondrial Function and Enhanced Glycolysis in PC12 Cells.” *Ecotoxicology and Environmental Safety* 201 (September):110849. https://doi.org/10.1016/j.ecoenv.2020.110849.

Heinken, Almut, Dmitry A. Ravcheev, Federico Baldini, Laurent Heirendt, Ronan M. T. Fleming, and Ines Thiele. 2019. “Systematic Assessment of Secondary Bile Acid Metabolism in Gut Microbes Reveals Distinct Metabolic Capabilities in Inflammatory Bowel Disease.” *Microbiome* 7 (1): 75. https://doi.org/10.1186/s40168-019-0689-3.

Huang, Yinghui, Jie Zhou, Shaobo Wang, Jiachuan Xiong, Yin Chen, Yong Liu, Tangli Xiao, et al. 2020. “Indoxyl Sulfate Induces Intestinal Barrier Injury through IRF1-DRP1 Axis-Mediated Mitophagy Impairment.” *Theranostics* 10 (16): 7384–7400. https://doi.org/10.7150/thno.45455.

Huang, Zhi-Bin, Zhen Hu, Chen-Xin Lu, Si-Dan Luo, Yu Chen, Zhi-Peng Zhou, Jing-Juan Hu, Fang-Ling Zhang, Fan Deng, and Ke-Xuan Liu. 2022. “Gut Microbiota-Derived Indole 3-Propionic Acid Partially Activates Aryl Hydrocarbon Receptor to Promote Macrophage Phagocytosis and Attenuate Septic Injury.” *Frontiers in Cellular and Infection Microbiology* 12:1015386. https://doi.org/10.3389/fcimb.2022.1015386.

Hubbard, Troy D., Iain A. Murray, and Gary H. Perdew. 2015. “Indole and Tryptophan Metabolism: Endogenous and Dietary Routes to Ah Receptor Activation.” *Drug Metabolism and Disposition: The Biological Fate of Chemicals* 43 (10): 1522–35. https://doi.org/10.1124/dmd.115.064246.

Hwang, In Koo, Ki-Yeon Yoo, Hua Li, Ok Kyu Park, Choong Hyun Lee, Jung Hoon Choi, Young-Gil Jeong, et al. 2009. “Indole-3-Propionic Acid Attenuates Neuronal Damage and Oxidative Stress in the Ischemic Hippocampus.” *Journal of Neuroscience Research* 87 (9): 2126–37. https://doi.org/10.1002/jnr.22030.

Inoue, Tetsuyoshi, Ryuji Shingaki, Shotaro Hirose, Kaori Waki, Hirotada Mori, and Kazuhiro Fukui. 2007. “Genome-Wide Screening of Genes Required for Swarming Motility in Escherichia Coli K-12.” *Journal of Bacteriology* 189 (3): 950–57. https://doi.org/10.1128/JB.01294-06.

Islam, M. A., R. Bekele, J. H. J. Vanden Berg, Y. Kuswanti, O. Thapa, S. Soltani, F. X. R. van Leeuwen, I. M. C. M. Rietjens, and A. J. Murk. 2015. “Deconjugation of Soy Isoflavone Glucuronides Needed for Estrogenic Activity.” *Toxicology in Vitro: An International Journal Published in Association with BIBRA* 29 (4): 706–15. https://doi.org/10.1016/j.tiv.2015.01.013.

Jasbi, Paniz, Natalie M. Mitchell, Xiaojian Shi, Thomas E. Grys, Yiping Wei, Li Liu, Douglas F. Lake, and Haiwei Gu. 2019. “Coccidioidomycosis Detection Using Targeted Plasma and Urine Metabolic Profiling.” *Journal of Proteome Research* 18 (7): 2791–2802. https://doi.org/10.1021/acs.jproteome.9b00100.

Jasbi, Paniz, Xiaojian Shi, Ping Chu, Natalie Elliott, Haley Hudson, Douglas Jones, Geidy Serrano, et al. 2021. “Metabolic Profiling of Neocortical Tissue Discriminates Alzheimer’s Disease from Mild Cognitive Impairment, High Pathology Controls, and Normal Controls.” *Journal of Proteome Research* 20 (9): 4303–17. https://doi.org/10.1021/acs.jproteome.1c00290.

Jones, Roshonda B., Tanya L. Alderete, Jeniffer S. Kim, Joshua Millstein, Frank D. Gilliland, and Michael I. Goran. 2019. “High Intake of Dietary Fructose in Overweight/Obese Teenagers Associated with Depletion of Eubacterium and Streptococcus in Gut Microbiome.” *Gut Microbes* 10 (6): 712–19. https://doi.org/10.1080/19490976.2019.1592420.

Kahalehili, Heather M., Nolan K. Newman, Jamie M. Pennington, Siva K. Kolluri, Nancy I. Kerkvliet, Natalia Shulzhenko, Andrey Morgun, and Allison K. Ehrlich. 2020. “Dietary Indole-3-Carbinol Activates AhR in the Gut, Alters Th17-Microbe Interactions, and Exacerbates Insulitis in NOD Mice.” *Frontiers in Immunology* 11:606441.

https://doi.org/10.3389/fimmu.2020.606441.

Kalliomäki, Marko, Maria Carmen Collado, Seppo Salminen, and Erika Isolauri. 2008. "Early Differences in Fecal Microbiota Composition in Children May Predict Overweight." *The American Journal of Clinical Nutrition* 87 (3): 534–38. https://doi.org/10.1093/ajcn/87.3.534.

Karbownik, M., R. J. Reiter, J. J. Garcia, J. Cabrera, S. Burkhardt, C. Osuna, and A. Lewiński. 2001. "Indole-3-Propionic Acid, a Melatonin-Related Molecule, Protects Hepatic Microsomal Membranes from Iron-Induced Oxidative Damage: Relevance to Cancer Reduction." *Journal of Cellular Biochemistry* 81 (3): 507–13.

Kim, Jung-whan, and Chi V. Dang. 2006. "Cancer's Molecular Sweet Tooth and the Warburg Effect." *Cancer Research* 66 (18): 8927–30. https://doi.org/10.1158/0008-5472.CAN-06-1501.

Kim, Sarah, Sora Choi, Moumita Dutta, Jeffrey O. Asubonteng, Marianne Polunas, Michael Goedken, Frank J. Gonzalez, Julia Yue Cui, and Maxwell A. Gyamfi. 2021. "Pregnane X Receptor Exacerbates Nonalcoholic Fatty Liver Disease Accompanied by Obesity- and Inflammation-Prone Gut Microbiome Signature." *Biochemical Pharmacology* 193 (November):114698. https://doi.org/10.1016/j.bcp.2021.114698.

Kim, Sarah, Hao Li, Yan Jin, Jasmine Armad, Haiwei Gu, Sridhar Mani, and Julia Y. Cui. 2023. "Maternal PBDE Exposure Disrupts Gut Microbiome and Promotes Hepatic Proinflammatory Signaling in Humanized PXR-Transgenic Mouse Offspring over Time." *Toxicological Sciences: An Official Journal of the Society of Toxicology* 194 (2): 209–25. https://doi.org/10.1093/toxsci/kfad056.

Kiyosawa, Naoki, Joshua C. Kwekel, Lyle D. Burgoon, Edward Dere, Kurt J. Williams, Colleen Tashiro, Brock Chittim, and Timothy R. Zacharewski. 2008. "Species-Specific Regulation of PXR/CAR/ER-Target Genes in the Mouse and Rat Liver Elicited by o, p'-DDT." *BMC Genomics* 9 (October):487. https://doi.org/10.1186/1471-2164-9-487.

Kliewer, Steven A., Bryan Goodwin, and Timothy M. Willson. 2002. "The Nuclear Pregnane X Receptor: A Key Regulator of Xenobiotic Metabolism." *Endocrine Reviews* 23 (5): 687–702. https://doi.org/10.1210/er.2001-0038.

Konstantinov, Alexandre, Gilles Arsenault, Brock Chittim, Alan McAlees, Robert McCrindle, Dave Potter, Colleen Tashiro, and Brian Yeo. 2008. "Identification of the Minor

Components of Great Lakes DE-71 Technical Mix by Means of 1H NMR and GC/MS." *Chemosphere* 73 (1 Suppl): S39-43. https://doi.org/10.1016/j.chemosphere.2007.12.035.

Koppel, Nitzan, Vayu Maini Rekdal, and Emily P. Balskus. 2017. "Chemical Transformation of Xenobiotics by the Human Gut Microbiota." *Science (New York, N.Y.)* 356 (6344): eaag2770. https://doi.org/10.1126/science.aag2770.

Kozlova, Elena V., Bhuvaneswari D. Chinthirla, Pedro A. Pérez, Nicholas V. DiPatrizio, Donovan A. Argueta, Allison L. Phillips, Heather M. Stapleton, et al. 2020. "Maternal Transfer of Environmentally Relevant Polybrominated Diphenyl Ethers (PBDEs) Produces a Diabetic Phenotype and Disrupts Glucoregulatory Hormones and Hepatic Endocannabinoids in Adult Mouse Female Offspring." *Scientific Reports* 10 (1): 18102. https://doi.org/10.1038/s41598-020-74853-9.

Kozlova, Elena V., Maximillian E. Denys, Jonathan Benedum, Matthew C. Valdez, Dave Enriquez, Anthony E. Bishay, Bhuvaneswari D. Chinthirla, et al. 2022. "Developmental Exposure to Indoor Flame Retardants and Hypothalamic Molecular Signatures: Sex-Dependent Reprogramming of Lipid Homeostasis." *Frontiers in Endocrinology* 13:997304. https://doi.org/10.3389/fendo.2022.997304.

Laue, Hannah E., Kasey J. M. Brennan, Virginie Gillet, Nadia Abdelouahab, Brent A. Coull, Marc G. Weisskopf, Heather H. Burris, Wei Zhang, Larissa Takser, and Andrea A. Baccarelli. 2019. "Associations of Prenatal Exposure to Polybrominated Diphenyl Ethers and Polychlorinated Biphenyls with Long-Term Gut Microbiome Structure: A Pilot Study." *Environmental Epidemiology (Philadelphia, Pa.)* 3 (1): e039. https://doi.org/10.1097/EE9.0000000000000039.

Liliemark, J. 1997. "The Clinical Pharmacokinetics of Cladribine." *Clinical Pharmacokinetics* 32 (2): 120–31. https://doi.org/10.2165/00003088-199732020-00003.

Lim, Ji-Sun, Duk-Hee Lee, and David R. Jacobs. 2008. "Association of Brominated Flame Retardants with Diabetes and Metabolic Syndrome in the U.S. Population, 2003-2004." *Diabetes Care* 31 (9): 1802–7. https://doi.org/10.2337/dc08-0850.

Lim, Joe, Moumita Dutta, Joseph L. Dempsey, Hans-Joachim Lehmler, James MacDonald, Theo Bammler, Cheryl Walker, et al. 2021. "Neonatal Exposure to BPA, BDE-99, and PCB Produces Persistent Changes in Hepatic Transcriptome Associated With Gut Dysbiosis in Adult Mouse Livers." *Toxicological Sciences: An Official Journal of the Society of*

*Toxicology* 184 (1): 83–103. https://doi.org/10.1093/toxsci/kfab104.

Little, Mallory, Moumita Dutta, Hao Li, Adam Matson, Xiaojian Shi, Gabby Mascarinas, Bruk Molla, et al. 2022. "Understanding the Physiological Functions of the Host Xenobiotic-Sensing Nuclear Receptors PXR and CAR on the Gut Microbiome Using Genetically Modified Mice." *Acta Pharmaceutica Sinica. B* 12 (2): 801–20. https://doi.org/10.1016/j.apsb.2021.07.022.

Liu, Wen-Chih, Yasuhiko Tomino, and Kuo-Cheng Lu. 2018. "Impacts of Indoxyl Sulfate and P-Cresol Sulfate on Chronic Kidney Disease and Mitigating Effects of AST-120." *Toxins* 10 (9): 367. https://doi.org/10.3390/toxins10090367.

Liu, Xuemei, Bingyong Mao, Jiayu Gu, Jiaying Wu, Shumao Cui, Gang Wang, Jianxin Zhao, Hao Zhang, and Wei Chen. 2021. "Blautia-a New Functional Genus with Potential Probiotic Properties?" *Gut Microbes* 13 (1): 1–21. https://doi.org/10.1080/19490976.2021.1875796.

Lo, Raymond, and Jason Matthews. 2012. "High-Resolution Genome-Wide Mapping of AHR and ARNT Binding Sites by ChIP-Seq." *Toxicological Sciences: An Official Journal of the Society of Toxicology* 130 (2): 349–61. https://doi.org/10.1093/toxsci/kfs253.

Lopes, Guiomar S., Alice T. Ferreira, Maria Etsuko Oshiro, Irina Vladimirova, Neide H. Jurkiewicz, Aron Jurkiewicz, and Soraya S. Smaili. 2006. "Aging-Related Changes of Intracellular Ca2+ Stores and Contractile Response of Intestinal Smooth Muscle." *Experimental Gerontology* 41 (1): 55–62. https://doi.org/10.1016/j.exger.2005.10.004.

Louis, Petra, Georgina L. Hold, and Harry J. Flint. 2014. "The Gut Microbiota, Bacterial Metabolites and Colorectal Cancer." *Nature Reviews Microbiology* 12 (10): 661–72. https://doi.org/10.1038/nrmicro3344.

Luan, Guangxiang, Fangfang Tie, Zhenzhen Yuan, Gang Li, Jie He, Zhenhua Wang, and Honglun Wang. 2017. "Hypaphorine, an Indole Alkaloid Isolated from Caragana Korshinskii Kom., Inhibites 3T3-L1 Adipocyte Differentiation and Improves Insulin Sensitivity in Vitro." *Chemistry & Biodiversity* 14 (7). https://doi.org/10.1002/cbdv.201700038.

Luca, G. de, P. de Philip, M. Rousset, J. P. Belaich, and Z. Dermoun. 1998. "The NADP-Reducing Hydrogenase of Desulfovibrio Fructosovorans: Evidence for a Native Complex with Hydrogen-Dependent Methyl-Viologen-Reducing Activity." *Biochemical and*

*Biophysical Research Communications* 248 (3): 591–96. https://doi.org/10.1006/bbrc.1998.9022.

Lv, Ye, Yi-Yang Luo, Hui-Wen Ren, Cheng-Jie Li, Zhi-Xin Xiang, and Zhi-Lin Luan. 2022. "The Role of Pregnane X Receptor (PXR) in Substance Metabolism." *Frontiers in Endocrinology* 13:959902. https://doi.org/10.3389/fendo.2022.959902.

Ma, Xiaochao, Yatrik Shah, Connie Cheung, Grace L. Guo, Lionel Feigenbaum, Kristopher W. Krausz, Jeffrey R. Idle, and Frank J. Gonzalez. 2007. "The PREgnane X Receptor Gene-Humanized Mouse: A Model for Investigating Drug-Drug Interactions Mediated by Cytochromes P450 3A." *Drug Metabolism and Disposition: The Biological Fate of Chemicals* 35 (2): 194–200. https://doi.org/10.1124/dmd.106.012831.

Maglich, Jodi M., Derek J. Parks, Linda B. Moore, Jon L. Collins, Bryan Goodwin, Andrew N. Billin, Catherine A. Stoltz, et al. 2003. "Identification of a Novel Human Constitutive Androstane Receptor (CAR) Agonist and Its Use in the Identification of CAR Target Genes." *The Journal of Biological Chemistry* 278 (19): 17277–83. https://doi.org/10.1074/jbc.M300138200.

Mardinoglu, Adil, Saeed Shoaie, Mattias Bergentall, Pouyan Ghaffari, Cheng Zhang, Erik Larsson, Fredrik Bäckhed, and Jens Nielsen. 2015. "The Gut Microbiota Modulates Host Amino Acid and Glutathione Metabolism in Mice." *Molecular Systems Biology* 11 (10): 834. https://doi.org/10.15252/msb.20156487.

Martinez, Fernando D., and Stefano Guerra. 2018. "Early Origins of Asthma. Role of Microbial Dysbiosis and Metabolic Dysfunction." *American Journal of Respiratory and Critical Care Medicine* 197 (5): 573–79. https://doi.org/10.1164/rccm.201706-1091PP.

Martinez-Outschoorn, Ubaldo E., Maria Peiris-Pagés, Richard G. Pestell, Federica Sotgia, and Michael P. Lisanti. 2017. "Cancer Metabolism: A Therapeutic Perspective." *Nature Reviews. Clinical Oncology* 14 (1): 11–31. https://doi.org/10.1038/nrclinonc.2016.60.

Matsumoto, I., and T. Kuhara. 1996. "A New Chemical Diagnostic Method for Inborn Errors of Metabolism by Mass Spectrometry-Rapid, Practical, and Simultaneous Urinary Metabolites Analysis." *Mass Spectrometry Reviews* 15 (1): 43–57. https://doi.org/10.1002/(SICI)1098-2787(1996)15:1<43::AID-MAS3>3.0.CO;2-B.

Meech, Robyn, Dong Gui Hu, Ross A. McKinnon, Siti Nurul Mubarokah, Alex Z. Haines, Pramod C. Nair, Andrew Rowland, and Peter I. Mackenzie. 2019. "The UDP-

Glycosyltransferase (UGT) Superfamily: New Members, New Functions, and Novel Paradigms." *Physiological Reviews* 99 (2): 1153–1222. https://doi.org/10.1152/physrev.00058.2017.

Mefferd, Chrisabelle C., Shrikant S. Bhute, Jacqueline R. Phan, Jacob V. Villarama, Dung M. Do, Stephanie Alarcia, Ernesto Abel-Santos, and Brian P. Hedlund. 2020. "A High-Fat/High-Protein, Atkins-Type Diet Exacerbates Clostridioides (Clostridium) Difficile Infection in Mice, Whereas a High-Carbohydrate Diet Protects." *mSystems* 5 (1): e00765-19. https://doi.org/10.1128/mSystems.00765-19.

Mercer, Kelly E., Laxmi Yeruva, Lindsay Pack, James L. Graham, Kimber L. Stanhope, Sree V. Chintapalli, Umesh D. Wankhade, et al. 2020. "Xenometabolite Signatures in the UC Davis Type 2 Diabetes Mellitus Rat Model Revealed Using a Metabolomics Platform Enriched with Microbe-Derived Metabolites." *American Journal of Physiology. Gastrointestinal and Liver Physiology* 319 (2): G157–69. https://doi.org/10.1152/ajpgi.00105.2020.

Moffett, John R., Brian Ross, Peethambaran Arun, Chikkathur N. Madhavarao, and Aryan M. A. Namboodiri. 2007. "N-Acetylaspartate in the CNS: From Neurodiagnostics to Neurobiology." *Progress in Neurobiology* 81 (2): 89–131. https://doi.org/10.1016/j.pneurobio.2006.12.003.

Mohandas, Sundhar, and Balasubramaniyan Vairappan. 2017. "Role of Pregnane X-Receptor in Regulating Bacterial Translocation in Chronic Liver Diseases." *World Journal of Hepatology* 9 (32): 1210–26. https://doi.org/10.4254/wjh.v9.i32.1210.

Moore, John T., Linda B. Moore, Jodi M. Maglich, and Steve A. Kliewer. 2003. "Functional and Structural Comparison of PXR and CAR." *Biochimica Et Biophysica Acta* 1619 (3): 235–38. https://doi.org/10.1016/s0304-4165(02)00481-6.

Morgan, Edward T., Joseph L. Dempsey, Sylvie M. Mimche, Tracey J. Lamb, Supriya Kulkarni, Julia Yue Cui, Hyunyoung Jeong, and Angela L. Slitt. 2018. "Physiological Regulation of Drug Metabolism and Transport: Pregnancy, Microbiome, Inflammation, Infection, and Fasting." *Drug Metabolism and Disposition: The Biological Fate of Chemicals* 46 (5): 503–13. https://doi.org/10.1124/dmd.117.079905.

Morganti, S., G. P. Ceda, M. Saccani, B. Milli, D. Ugolotti, R. Prampolini, M. Maggio, G. Valenti, and G. Ceresini. 2005. "Thyroid Disease in the Elderly: Sex-Related Differences

in Clinical Expression." *Journal of Endocrinological Investigation* 28 (11 Suppl Proceedings): 101–4.

Osawa, Yosuke, Hiromitsu Kanamori, Ekihiro Seki, Masato Hoshi, Hirofumi Ohtaki, Yoichi Yasuda, Hiroyasu Ito, et al. 2011. "L-Tryptophan-Mediated Enhancement of Susceptibility to Nonalcoholic Fatty Liver Disease Is Dependent on the Mammalian Target of Rapamycin." *The Journal of Biological Chemistry* 286 (40): 34800–808. https://doi.org/10.1074/jbc.M111.235473.

Ostrov, David A., Aimon Alkanani, Kristen A. McDaniel, Stephanie Case, Erin E. Baschal, Laura Pyle, Sam Ellis, et al. 2018. "Methyldopa Blocks MHC Class II Binding to Disease-Specific Antigens in Autoimmune Diabetes." *The Journal of Clinical Investigation* 128 (5): 1888–1902. https://doi.org/10.1172/JCI97739.

Pacyniak, Erik K., Xingguo Cheng, Michael L. Cunningham, Kevin Crofton, Curtis D. Klaassen, and Grace L. Guo. 2007. "The Flame Retardants, Polybrominated Diphenyl Ethers, Are Pregnane X Receptor Activators." *Toxicological Sciences: An Official Journal of the Society of Toxicology* 97 (1): 94–102. https://doi.org/10.1093/toxsci/kfm025.

Patsouris, David, Janardan K. Reddy, Michael Müller, and Sander Kersten. 2006. "Peroxisome Proliferator-Activated Receptor Alpha Mediates the Effects of High-Fat Diet on Hepatic Gene Expression." *Endocrinology* 147 (3): 1508–16. https://doi.org/10.1210/en.2005-1132.

Peer, Cody J., Andrew K. L. Goey, Tristan M. Sissung, Sheryl Erlich, Min-Jung Lee, Yusuke Tomita, Jane B. Trepel, et al. 2016. "UGT1A1 Genotype-Dependent Dose Adjustment of Belinostat in Patients with Advanced Cancers Using Population Pharmacokinetic Modeling and Simulation." *Journal of Clinical Pharmacology* 56 (4): 450–60. https://doi.org/10.1002/jcph.627.

Pekala, Jolanta, Bozena Patkowska-Sokoła, Robert Bodkowski, Dorota Jamroz, Piotr Nowakowski, Stanisław Lochyński, and Tadeusz Librowski. 2011. "L-Carnitine--Metabolic Functions and Meaning in Humans Life." *Current Drug Metabolism* 12 (7): 667–78. https://doi.org/10.2174/138920011796504536.

Pietron, Wojciech, Marek Pajurek, Szczepan Mikolajczyk, Sebastian Maszewski, Malgorzata Warenik-Bany, and Jadwiga Piskorska-Pliszczynska. 2019. "Exposure to PBDEs Associated with Farm Animal Meat Consumption." *Chemosphere* 224 (June):58–64.

https://doi.org/10.1016/j.chemosphere.2019.02.067.

Qi, Yunpeng, Haiwei Gu, Yunlong Song, Xin Dong, Aijun Liu, Ziyang Lou, Guorong Fan, and Yifeng Chai. 2013. "Metabolomics Study of Resina Draconis on Myocardial Ischemia Rats Using Ultraperformance Liquid Chromatography/Quadrupole Time-of-Flight Mass Spectrometry Combined with Pattern Recognition Methods and Metabolic Pathway Analysis." *Evidence-Based Complementary and Alternative Medicine: eCAM* 2013:438680. https://doi.org/10.1155/2013/438680.

Qin, Junjie, Yingrui Li, Zhiming Cai, Shenghui Li, Jianfeng Zhu, Fan Zhang, Suisha Liang, et al. 2012. "A Metagenome-Wide Association Study of Gut Microbiota in Type 2 Diabetes." *Nature* 490 (7418): 55–60. https://doi.org/10.1038/nature11450.

Renzelli, Valerio, Marco Gallo, Lelio Morviducci, Giampiero Marino, Alberto Ragni, Enzo Tuveri, Antongiulio Faggiano, et al. 2023. "Polybrominated Diphenyl Ethers (PBDEs) and Human Health: Effects on Metabolism, Diabetes and Cancer." *Cancers* 15 (17): 4237. https://doi.org/10.3390/cancers15174237.

Roh, Eun, Soo Heon Kwak, Hye Seung Jung, Young Min Cho, Youngmi Kim Pak, Kyong Soo Park, Seong Yeon Kim, and Hong Kyu Lee. 2015. "Serum Aryl Hydrocarbon Receptor Ligand Activity Is Associated with Insulin Resistance and Resulting Type 2 Diabetes." *Acta Diabetologica* 52 (3): 489–95. https://doi.org/10.1007/s00592-014-0674-z.

Rohm, Theresa V., Daniel T. Meier, Jerrold M. Olefsky, and Marc Y. Donath. 2022. "Inflammation in Obesity, Diabetes, and Related Disorders." *Immunity* 55 (1): 31–55. https://doi.org/10.1016/j.immuni.2021.12.013.

Roudier, Emilie, and Anne Perrin. 2009. "Considering the Role of Pyruvate in Tumor Cells during Hypoxia." *Biochimica Et Biophysica Acta* 1796 (2): 55–62. https://doi.org/10.1016/j.bbcan.2009.02.003.

Rynkowska, Aleksandra, Jan Stępniak, and Małgorzata Karbownik-Lewińska. 2021. "Melatonin and Indole-3-Propionic Acid Reduce Oxidative Damage to Membrane Lipids Induced by High Iron Concentrations in Porcine Skin." *Membranes* 11 (8): 571. https://doi.org/10.3390/membranes11080571.

Sauer, Uwe. 2006. "Metabolic Networks in Motion: 13C-Based Flux Analysis." *Molecular Systems Biology* 2:62. https://doi.org/10.1038/msb4100109.

Schindler, J. F., K. B. Berst, and B. V. Plapp. 1998. "Inhibition of Human Alcohol

Dehydrogenases by Formamides." *Journal of Medicinal Chemistry* 41 (10): 1696–1701. https://doi.org/10.1021/jm9707380.

Schirmer, Melanie, Martin Stražar, Julian Avila-Pacheco, Daniel F. Rojas-Tapias, Eric M. Brown, Emily Temple, Amy Deik, et al. 2024. "Linking Microbial Genes to Plasma and Stool Metabolites Uncovers Host-Microbial Interactions Underlying Ulcerative Colitis Disease Course." *Cell Host & Microbe* 32 (2): 209-226.e7. https://doi.org/10.1016/j.chom.2023.12.013.

Schwabe, Robert F., and Christian Jobin. 2013. "The Microbiome and Cancer." *Nature Reviews. Cancer* 13 (11): 800–812. https://doi.org/10.1038/nrc3610.

Scoville, David K., Cindy Yanfei Li, Dongfang Wang, Joseph L. Dempsey, Daniel Raftery, Sridhar Mani, Haiwei Gu, and Julia Yue Cui. 2019. "Polybrominated Diphenyl Ethers and Gut Microbiome Modulate Metabolic Syndrome-Related Aqueous Metabolites in Mice." *Drug Metabolism and Disposition: The Biological Fate of Chemicals* 47 (8): 928–40. https://doi.org/10.1124/dmd.119.086538.

Selwyn, Felcy Pavithra, Julia Yue Cui, and Curtis D. Klaassen. 2015. "RNA-Seq Quantification of Hepatic Drug Processing Genes in Germ-Free Mice." *Drug Metabolism and Disposition: The Biological Fate of Chemicals* 43 (10): 1572–80. https://doi.org/10.1124/dmd.115.063545.

Seow, Wei Jie, Xiao-Ou Shu, Jeremy K. Nicholson, Elaine Holmes, Douglas I. Walker, Wei Hu, Qiuyin Cai, et al. 2019. "Association of Untargeted Urinary Metabolomics and Lung Cancer Risk Among Never-Smoking Women in China." *JAMA Network Open* 2 (9): e1911970. https://doi.org/10.1001/jamanetworkopen.2019.11970.

Shah, Yatrik M., Xiaochao Ma, Keiichirou Morimura, Insook Kim, and Frank J. Gonzalez. 2007. "Pregnane X Receptor Activation Ameliorates DSS-Induced Inflammatory Bowel Disease via Inhibition of NF-kappaB Target Gene Expression." *American Journal of Physiology. Gastrointestinal and Liver Physiology* 292 (4): G1114-1122. https://doi.org/10.1152/ajpgi.00528.2006.

Shen, Ming-Che, Xiangmin Zhao, Gene P. Siegal, Renee Desmond, and Robert W. Hardy. 2014. "Dietary Stearic Acid Leads to a Reduction of Visceral Adipose Tissue in Athymic Nude Mice." *PloS One* 9 (9): e104083. https://doi.org/10.1371/journal.pone.0104083.

Shi, Xiaojian, Shuai Wang, Paniz Jasbi, Cassidy Turner, Jonathan Hrovat, Yiping Wei, Jingping

Liu, and Haiwei Gu. 2019. “Database-Assisted Globally Optimized Targeted Mass Spectrometry (dGOT-MS): Broad and Reliable Metabolomics Analysis with Enhanced Identification.” *Analytical Chemistry* 91 (21): 13737–45. https://doi.org/10.1021/acs.analchem.9b03107.

Shi, Xiaojian, Bowei Xi, Paniz Jasbi, Cassidy Turner, Yan Jin, and Haiwei Gu. 2020. “Comprehensive Isotopic Targeted Mass Spectrometry: Reliable Metabolic Flux Analysis with Broad Coverage.” *Analytical Chemistry* 92 (17): 11728–38. https://doi.org/10.1021/acs.analchem.0c01767.

Sierkstra, L. N., H. H. Silljé, J. M. Verbakel, and C. T. Verrips. 1993. “The Glucose-6-Phosphate-Isomerase Reaction Is Essential for Normal Glucose Repression in Saccharomyces Cerevisiae.” *European Journal of Biochemistry* 214 (1): 121–27. https://doi.org/10.1111/j.1432-1033.1993.tb17903.x.

Sittipo, Panida, Jae-Won Shim, and Yun Kyung Lee. 2019. “Microbial Metabolites Determine Host Health and the Status of Some Diseases.” *International Journal of Molecular Sciences* 20 (21): 5296. https://doi.org/10.3390/ijms20215296.

Soga, Tomoyoshi, Masahiro Sugimoto, Masashi Honma, Masayo Mori, Kaori Igarashi, Kasumi Kashikura, Satsuki Ikeda, et al. 2011. “Serum Metabolomics Reveals γ-Glutamyl Dipeptides as Biomarkers for Discrimination among Different Forms of Liver Disease.” *Journal of Hepatology* 55 (4): 896–905. https://doi.org/10.1016/j.jhep.2011.01.031.

Sookoian, Silvia, Gustavo O. Castaño, Adriana L. Burgueño, Tomas Fernández Gianotti, María Soledad Rosselli, and Carlos Jose Pirola. 2010. “The Nuclear Receptor PXR Gene Variants Are Associated with Liver Injury in Nonalcoholic Fatty Liver Disease.” *Pharmacogenetics and Genomics* 20 (1): 1–8. https://doi.org/10.1097/FPC.0b013e328333a1dd.

Spanogiannopoulos, Peter, Elizabeth N. Bess, Rachel N. Carmody, and Peter J. Turnbaugh. 2016. “The Microbial Pharmacists within Us: A Metagenomic View of Xenobiotic Metabolism.” *Nature Reviews. Microbiology* 14 (5): 273–87. https://doi.org/10.1038/nrmicro.2016.17.

Spruiell, Krisstonia, Ricardo M. Richardson, John M. Cullen, Emmanuel M. Awumey, Frank J. Gonzalez, and Maxwell A. Gyamfi. 2014. “Role of Pregnane X Receptor in Obesity and Glucose Homeostasis in Male Mice.” *The Journal of Biological Chemistry* 289 (6):

3244–61. https://doi.org/10.1074/jbc.M113.494575.

Staudinger, J. L., B. Goodwin, S. A. Jones, D. Hawkins-Brown, K. I. MacKenzie, A. LaTour, Y. Liu, et al. 2001. "The Nuclear Receptor PXR Is a Lithocholic Acid Sensor That Protects against Liver Toxicity." *Proceedings of the National Academy of Sciences of the United States of America* 98 (6): 3369–74. https://doi.org/10.1073/pnas.051551698.

Sugiyama, K., S. Okuyama, M. Imoto, K. Okumura, K. Takagi, and T. Satake. 1986. "Clinical Evaluation of Serum 3 Beta-Hydroxy-5-Cholenoic Acid in Hepatobiliary Diseases." *Gastroenterologia Japonica* 21 (6): 608–16. https://doi.org/10.1007/BF02774489.

Sun, Haijian, Xuexue Zhu, Weiwei Cai, and Liying Qiu. 2017. "Hypaphorine Attenuates Lipopolysaccharide-Induced Endothelial Inflammation via Regulation of TLR4 and PPAR-γ Dependent on PI3K/Akt/mTOR Signal Pathway." *International Journal of Molecular Sciences* 18 (4): 844. https://doi.org/10.3390/ijms18040844.

Takato, Tamae, Kai Iwata, Chiaki Murakami, Yuko Wada, and Fumio Sakane. 2017. "Chronic Administration of Myristic Acid Improves Hyperglycaemia in the Nagoya-Shibata-Yasuda Mouse Model of Congenital Type 2 Diabetes." *Diabetologia* 60 (10): 2076–83. https://doi.org/10.1007/s00125-017-4366-4.

Tian, Mengyuan, Shujuan Ma, Yiping You, Sisi Long, Jiayue Zhang, Chuhao Guo, Xiaolei Wang, and Hongzhuan Tan. 2021. "Serum Metabolites as an Indicator of Developing Gestational Diabetes Mellitus Later in the Pregnancy: A Prospective Cohort of a Chinese Population." *Journal of Diabetes Research* 2021:8885954. https://doi.org/10.1155/2021/8885954.

Townsend, Danyelle M., Kenneth D. Tew, and Haim Tapiero. 2003. "The Importance of Glutathione in Human Disease." *Biomedicine & Pharmacotherapy = Biomedecine & Pharmacotherapie* 57 (3–4): 145–55. https://doi.org/10.1016/s0753-3322(03)00043-x.

Tuomainen, Marjo, Jaana Lindström, Marko Lehtonen, Seppo Auriola, Jussi Pihlajamäki, Markku Peltonen, Jaakko Tuomilehto, Matti Uusitupa, Vanessa D. de Mello, and Kati Hanhineva. 2018. "Associations of Serum Indolepropionic Acid, a Gut Microbiota Metabolite, with Type 2 Diabetes and Low-Grade Inflammation in High-Risk Individuals." *Nutrition & Diabetes* 8 (1): 35. https://doi.org/10.1038/s41387-018-0046-9.

Turyk, Mary E., Henry A. Anderson, Dyan Steenport, Carol Buelow, Pamela Imm, and Lynda Knobeloch. 2010. "Longitudinal Biomonitoring for Polybrominated Diphenyl Ethers

(PBDEs) in Residents of the Great Lakes Basin." *Chemosphere* 81 (4): 517–22. https://doi.org/10.1016/j.chemosphere.2010.07.037.

Vander Heiden, Matthew G., Lewis C. Cantley, and Craig B. Thompson. 2009. "Understanding the Warburg Effect: The Metabolic Requirements of Cell Proliferation." *Science (New York, N.Y.)* 324 (5930): 1029–33. https://doi.org/10.1126/science.1160809.

Venkatesh, Madhukumar, Subhajit Mukherjee, Hongwei Wang, Hao Li, Katherine Sun, Alexandre P. Benechet, Zhijuan Qiu, et al. 2014a. "Symbiotic Bacterial Metabolites Regulate Gastrointestinal Barrier Function via the Xenobiotic Sensor PXR and Toll-like Receptor 4." *Immunity* 41 (2): 296–310. https://doi.org/10.1016/j.immuni.2014.06.014.

———. 2014b. "Symbiotic Bacterial Metabolites Regulate Gastrointestinal Barrier Function via the Xenobiotic Sensor PXR and Toll-like Receptor 4." *Immunity* 41 (2): 296–310. https://doi.org/10.1016/j.immuni.2014.06.014.

Viberg, Henrik, Anders Fredriksson, and Per Eriksson. 2004. "Investigations of Strain and/or Gender Differences in Developmental Neurotoxic Effects of Polybrominated Diphenyl Ethers in Mice." *Toxicological Sciences: An Official Journal of the Society of Toxicology* 81 (2): 344–53. https://doi.org/10.1093/toxsci/kfh215.

Vickers, Alison E. M., Robyn L. Fisher, and John R. Sinclair. 2010. "Glutathione Modulation and Oxidative Stress in Human Liver Slices." *Current Drug Discovery Technologies* 7 (3): 154–69. https://doi.org/10.2174/157016310793180530.

Vojta, Aleksandar, Paula Dobrinić, Vanja Tadić, Luka Bočkor, Petra Korać, Boris Julg, Marija Klasić, and Vlatka Zoldoš. 2016. "Repurposing the CRISPR-Cas9 System for Targeted DNA Methylation." *Nucleic Acids Research* 44 (12): 5615–28. https://doi.org/10.1093/nar/gkw159.

Vrzalová, Aneta, Petra Pečinková, Peter Illés, Soňa Gurská, Petr Džubák, Martin Szotkowski, Marián Hajdúch, Sridhar Mani, and Zdeněk Dvořák. 2022. "Mixture Effects of Tryptophan Intestinal Microbial Metabolites on Aryl Hydrocarbon Receptor Activity." *International Journal of Molecular Sciences* 23 (18): 10825. https://doi.org/10.3390/ijms231810825.

Walsh, Kelly R., Sara J. Haak, Torsten Bohn, Qingguo Tian, Steven J. Schwartz, and Mark L. Failla. 2007. "Isoflavonoid Glucosides Are Deconjugated and Absorbed in the Small Intestine of Human Subjects with Ileostomies." *The American Journal of Clinical*

*Nutrition* 85 (4): 1050–56. https://doi.org/10.1093/ajcn/85.4.1050.

Wang, Shuang, Liangzhi Xiong, Zhihua Ruan, Xiaofang Gong, Yanrong Luo, Chengyi Wu, Yu Wang, Hui Shang, and Jingyi Chen. 2023. "Indole-3-Propionic Acid Alleviates Sepsis-Associated Acute Liver Injury by Activating Pregnane X Receptor." *Molecular Medicine (Cambridge, Mass.)* 29 (1): 65. https://doi.org/10.1186/s10020-023-00658-x.

Wei, P., J. Zhang, M. Egan-Hafley, S. Liang, and D. D. Moore. 2000. "The Nuclear Receptor CAR Mediates Specific Xenobiotic Induction of Drug Metabolism." *Nature* 407 (6806): 920–23. https://doi.org/10.1038/35038112.

Wei, Yiping, Paniz Jasbi, Xiaojian Shi, Cassidy Turner, Jonathon Hrovat, Li Liu, Yuri Rabena, Peggy Porter, and Haiwei Gu. 2021. "Early Breast Cancer Detection Using Untargeted and Targeted Metabolomics." *Journal of Proteome Research* 20 (6): 3124–33. https://doi.org/10.1021/acs.jproteome.1c00019.

Wikoff, William R., Andrew T. Anfora, Jun Liu, Peter G. Schultz, Scott A. Lesley, Eric C. Peters, and Gary Siuzdak. 2009. "Metabolomics Analysis Reveals Large Effects of Gut Microflora on Mammalian Blood Metabolites." *Proceedings of the National Academy of Sciences of the United States of America* 106 (10): 3698–3703. https://doi.org/10.1073/pnas.0812874106.

Windham, Gayle C., Susan M. Pinney, Andreas Sjodin, Raymond Lum, Richard S. Jones, Larry L. Needham, Frank M. Biro, Robert A. Hiatt, and Lawrence H. Kushi. 2010. "Body Burdens of Brominated Flame Retardants and Other Persistent Organo-Halogenated Compounds and Their Descriptors in US Girls." *Environmental Research* 110 (3): 251–57. https://doi.org/10.1016/j.envres.2010.01.004.

Wlodarska, Marta, Chengwei Luo, Raivo Kolde, Eva d'Hennezel, John W. Annand, Cortney E. Heim, Philipp Krastel, et al. 2017. "Indoleacrylic Acid Produced by Commensal Peptostreptococcus Species Suppresses Inflammation." *Cell Host & Microbe* 22 (1): 25-37.e6. https://doi.org/10.1016/j.chom.2017.06.007.

Won, Sung-Min, Siyu Chen, Seo Yeon Lee, Kyung Eun Lee, Kye Won Park, and Jung-Hoon Yoon. 2020. "Lactobacillus Sakei ADM14 Induces Anti-Obesity Effects and Changes in Gut Microbiome in High-Fat Diet-Induced Obese Mice." *Nutrients* 12 (12): 3703. https://doi.org/10.3390/nu12123703.

Wong, Chyn Boon, Azusa Tanaka, Tetsuya Kuhara, and Jin-Zhong Xiao. 2020. "Potential

Effects of Indole-3-Lactic Acid, a Metabolite of Human Bifidobacteria, on NGF-Induced Neurite Outgrowth in PC12 Cells." *Microorganisms* 8 (3): 398. https://doi.org/10.3390/microorganisms8030398.

Wu, Shaohong, Hao He, Ge-Xiu Liu, Xiao-Peng Li, Shun Yao, Huan-Xing Su, Xiang Li, Zi Ren, Haitao Zeng, and Jinli Liao. 2020. "Elevated GTP Cyclohydrolase I Pathway in Endothelial Progenitor Cells of Overweight Premenopausal Women." *Cardiology Research and Practice* 2020:5914916. https://doi.org/10.1155/2020/5914916.

Xie, Wen, and John Y. L. Chiang. 2013. "Nuclear Receptors in Drug Metabolism and Beyond." *Drug Metabolism Reviews* 45 (1): 1–2. https://doi.org/10.3109/03602532.2013.754577.

Xu, Jing, Wangyang Qian, Juying Li, Xiaofei Zhang, Jian He, and Deyang Kong. 2019. "Polybrominated Diphenyl Ethers (PBDEs) in Soil and Dust from Plastic Production and Surrounding Areas in Eastern of China." *Environmental Geochemistry and Health* 41 (5): 2315–27. https://doi.org/10.1007/s10653-019-00247-0.

Xu, Xiuxiu, Siyuan Sun, Ling Liang, Chenxi Lou, Qijin He, Maojuan Ran, Lu Zhang, et al. 2021. "Role of the Aryl Hydrocarbon Receptor and Gut Microbiota-Derived Metabolites Indole-3-Acetic Acid in Sulforaphane Alleviates Hepatic Steatosis in Mice." *Frontiers in Nutrition* 8:756565. https://doi.org/10.3389/fnut.2021.756565.

Xue, Jinsong, Qingqing Xiao, Min Zhang, Dan Li, and Xiaofei Wang. 2023. "Toxic Effects and Mechanisms of Polybrominated Diphenyl Ethers." *International Journal of Molecular Sciences* 24 (17): 13487. https://doi.org/10.3390/ijms241713487.

Yan, Liang, Yiting Wang, Jingyang Liu, Yali Nie, Xiao-Bo Zhong, Quancheng Kan, and Lirong Zhang. 2017. "Alterations of Histone Modifications Contribute to Pregnane X Receptor-Mediated Induction of CYP3A4 by Rifampicin." *Molecular Pharmacology* 92 (2): 113–23. https://doi.org/10.1124/mol.117.108225.

Yao, Weifeng, Haiwei Gu, Jiangjiang Zhu, Gregory Barding, Haibo Cheng, Beihua Bao, Li Zhang, Anwei Ding, and Wei Li. 2014. "Integrated Plasma and Urine Metabolomics Coupled with HPLC/QTOF-MS and Chemometric Analysis on Potential Biomarkers in Liver Injury and Hepatoprotective Effects of Er-Zhi-Wan." *Analytical and Bioanalytical Chemistry* 406 (28): 7367–78. https://doi.org/10.1007/s00216-014-8169-x.

Zachariou, M., and R. K. Scopes. 1986. "Glucose-Fructose Oxidoreductase, a New Enzyme Isolated from Zymomonas Mobilis That Is Responsible for Sorbitol Production." *Journal*

*of Bacteriology* 167 (3): 863–69. https://doi.org/10.1128/jb.167.3.863-869.1986.

Zhang, Binbin, Minjie Jiang, Jianan Zhao, Yu Song, Weidong Du, and Junping Shi. 2022. "The Mechanism Underlying the Influence of Indole-3-Propionic Acid: A Relevance to Metabolic Disorders." *Frontiers in Endocrinology* 13:841703. https://doi.org/10.3389/fendo.2022.841703.

Zhang, Zhan, Shushu Li, Lu Liu, Li Wang, Xue Xiao, Zhenzhen Sun, Xichen Wang, et al. 2016. "Environmental Exposure to BDE47 Is Associated with Increased Diabetes Prevalence: Evidence from Community-Based Case-Control Studies and an Animal Experiment." *Scientific Reports* 6 (June):27854. https://doi.org/10.1038/srep27854.

Zhao, Xue-Ying, Jian-Wei Wang, Yue Yin, Kai Li, Miao Zhang, and Fu-Ping Yan. 2019. "Effect of Tong Xie Yao Fang on Endogenous Metabolites in Urine of Irritable Bowel Syndrome Model Rats." *World Journal of Gastroenterology* 25 (34): 5134–51. https://doi.org/10.3748/wjg.v25.i34.5134.

Zhao, Ze-Hua, Feng-Zhi Xin, Yaqian Xue, Zhimin Hu, Yamei Han, Fengguang Ma, Da Zhou, et al. 2019. "Indole-3-Propionic Acid Inhibits Gut Dysbiosis and Endotoxin Leakage to Attenuate Steatohepatitis in Rats." *Experimental & Molecular Medicine* 51 (9): 1–14. https://doi.org/10.1038/s12276-019-0304-5.

Zhou, Ziheng, Hanrui Yin, Yajie Guo, Yuanyuan Fang, Feixiang Yuan, Shanghai Chen, and Feifan Guo. 2021. "A Fifty Percent Leucine-Restricted Diet Reduces Fat Mass and Improves Glucose Regulation." *Nutrition & Metabolism* 18 (1): 34. https://doi.org/10.1186/s12986-021-00564-1.

Zhuang, Yijing, Weidong Chen, Fen Yao, Yuanchun Huang, Shuqin Zhou, Haiyan Li, Zijie Zhang, Congyi Cai, Yi Gao, and Qing Peng. 2016. "Short-Term Pretreatment of Sub-Inhibitory Concentrations of Gentamycin Inhibits the Swarming Motility of Escherichia Coli by Down-Regulating the Succinate Dehydrogenase Gene." *Cellular Physiology and Biochemistry: International Journal of Experimental Cellular Physiology, Biochemistry, and Pharmacology* 39 (4): 1307–16. https://doi.org/10.1159/000447835.

Zolfaghar, Irandokht, David J. Evans, and Suzanne M. J. Fleiszig. 2003. "Twitching Motility Contributes to the Role of Pili in Corneal Infection Caused by Pseudomonas Aeruginosa." *Infection and Immunity* 71 (9): 5389–93. https://doi.org/10.1128/IAI.71.9.5389-5393.2003.